12

I-ARA-93-U-60

FINAL TECHNICAL REPORT

Analytical Study of

BEAM HANDLING AND EMITTANCE CONTROL

Submitted to

OFFICE OF NAVAL RESEARCH
N00014-88-C-0542

by

AUSTIN RESEARCH ASSOCIATES
Austin, Texas

December 1993

James R. Thompson and M. L. Sloan
Co-Principal Investigators

I-ARA-93-U-60

FINAL TECHNICAL REPORT

Analytical Study of

BEAM HANDLING AND EMITTANCE CONTROL

Submitted to

OFFICE OF NAVAL RESEARCH

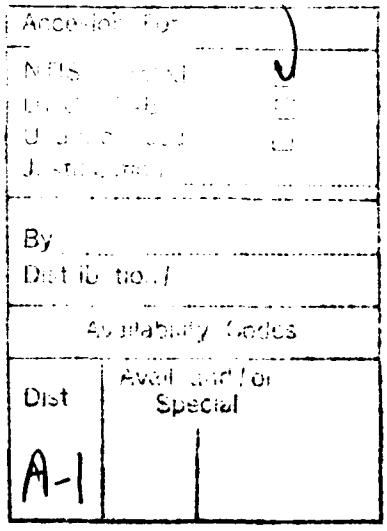

by

AUSTIN RESEARCH ASSOCIATES
Austin, Texas

December 1993

James R. Thompson and M. L. Sloan
Co-Principal Investigators

BEAM HANDLING AND EMITTANCE CONTROL

TABLE OF CONTENTS

TABLE OF CONTENTS (Continued)

BEAM HANDLING AND EMITTANCE CONTROL

1. INTRODUCTION

This is the final report on research conducted by Austin Research Associates on the subject of beam handling and emittance control in high current accelerators. This research was performed under ONR Contract N00014-88-C-0542 during 1988-1993.

Because this research has been conducted over an extended period of time, some of it has been reported previously in technical reports and conference proceedings. In this final report we have attempted to pull all of this previously published material together with new research results which are described here for the first time to produce a unified summary of this research effort. As an aid to the interested reader, we have also included (where specifically noted) a small amount of research conducted prior to this contract, which motivated some of the subsequent contract research.

The format of this final report is that the technical material is presented in a number of largely self-contained technical appendices. Some of these appendices are the previously published reports, while others contain the fresh research results, and a few contain only slides and figures which describe some aspects of the research. These appendices are presented roughly chronologically in the order that research was conducted, with the more recent research near the end. As it happens, the subject matter of the early appendices pertains especially to beam quality issues which are most important at the low energy end of an accelerator, while later appendices concern issues of more importance at higher beam energy. In order to keep this report summary concise, we seek here only to provide a road map to the technical appendices, and to highlight the salient results which were obtained from this research.

2. MOTIVATION FOR RESEARCH

The thrust of our research at Austin Research Associates on beam handling and emittance control has been to explore how one might design high current electron

accelerators, with the preservation of high beam quality designated as the primary design consideration. As the testbed for this research, we have considered high current, induction linacs in the parameter class of the ETA/ATA accelerators at LLNL, but with improvements to the accelerator gap design and other features to permit a very significant increase in the deliverable beam brightness. Our approach for beam quality control has centered on the use of solenoidal magnetic focusing through such induction accelerators, together with gently-shaped (adiabatic) acceleration gaps. To the accelerator designer, this approach offers several tools for the control of beam quality. The strength and axial variation in the solenoidal magnetic field may be designed, as may the length and shape of the acceleration gaps, the loading of the gaps, and the axial spacing from gap to gap. This research has shown that each of these design features may individually be optimized to contribute to improved beam quality control, and by exploiting these features in concert it appears feasible to produce high current, high energy electron beams possessing breakthrough beam quality and brightness. Consequently, applications which have been heretofore technologically unachievable may for the first time become possible. One such application is the production of high performance free electron lasers at very short wavelengths, extending down to the optical (< 1 μm) regime. It is the opening of such new technologies which has been the promise of this research on beam handling and emittance control.

Appendix A contains several slides regarding beam quality and the motivating need for superior beam quality for the application of driving a high performance free electron laser (FEL). There has existed an historical technological barrier to the achievement of high performance free electron lasers at very short wavelengths, which may be qualitatively explained as follows (and for which quantitative scaling laws are indicated in Appendix A). To achieve high performance, high beam current is needed in order to produce high laser gain with high efficiency and high power output. Moreover, to achieve very short laser wavelengths, high beam particle energy is needed. The thorny problem is that the beam emittance requirements become much more demanding at high energy, while at the same time the achievable

emittance worsens as either the beam current or the final beam energy (or number of acceleration gaps) is increased. The net result has been a very disappointing inability to demonstrate high performance FELs in the high-gain Compton regime at wavelengths below about a millimeter, as is evidenced from the results of the ATA PALADIN experiments. It is this technological barrier which this research has attempted to overcome.

At least theoretically, our attempt appears to have been successful, in that techniques have been discovered which appear to allow the actual achievement of the deliverable beam quality which is required for high performance FELs at wavelengths from the millimeter to the micron regime.

3. SOURCE REGION BEAM EMITTANCE

Appendix B contains slides regarding sources of beam quality degradation and emittance growth, and some particular results obtained under previous contracts regarding source region beam emittance, which were motivational for the research under this contract.

It is well known that phase-mixed beam emittance tends to be like entropy: it increases monotonically down the accelerator. The beam quality likewise tends to degrade monotonically, so that the best possibility is to preserve whatever beam quality exists at a particular point. Consequently, when seeking to control beam quality, one must first concentrate upon the source region, since one is stuck with whatever emittance growth occurs there--apart from the resort of downstream aperturing of beam current to reduce the remaining emittance. (Such downstream current aperturing is commonly undertaken out of desperation and is generally unsatisfactory since it immediately reduces the potential performance obtainable from the beam. Aperturing can also degrade the quality of the transmitted beam. In this contract, we presume that the desired beam current is generated by the source diode and then preserved down the accelerator.)

The second slide in Appendix B summarizes scaling laws reported by various researchers[1,2] which suggest that with care, diodes may be designed to produce MeV,

kA electron beams with normalized emittance below 10^{-2} rad-cm. The next five slides in Appendix B review prior studies which revealed the danger of sharp electrical corners in the diode region for producing large beam sausaging excitations, due to image charge concentrations near the corners. Likewise smoothly tapered anode and cathode structures were shown to produce much cooler beams. Smooth foilless diodes immersed in solenoidal magnetic fields were generally found capable of producing good quality beams.

Theoretical analysis of the beam excitations received in a field-immersed diode showed that these excitations were proportional to the axial Fourier transform of the radial electromagnetic forces acting upon the electrons, evaluated at the cyclotron wave number of the focusing magnetic guide field. Consequently, much cooler beams can result if the guide field is increased to the point that the focusing gyrolength is reduced below the transverse force gradient lengths of the diode--since then phase cancellations of the perturbing forces can occur. This theoretical prediction was verified computationally. The final slide in Appendix B suggests a scaling law for the realizable, normalized beam emittance, which indicates that very low emittance may be obtained from a radially small but strongly field-immersed diode. The field may be subsequently flared out to reduce the beam current density somewhat for the beam transport through downstream acceleration gaps.

This prior research taught us the lessons that smooth electrical boundaries, which vary axially only slowly (adiabatically) are desirable, as is radial focusing strong enough that phase cancellation of transverse perturbations can occur. In turn, we have applied these lessons during this contract to produce accelerator gap designs which afford minimum emittance growth during the lengthy multi-gap acceleration which is required to reach the electron beam energies of tens to hundreds of MeV that are needed for many high performance applications.

4. CONTRACT RESEARCH ISSUES

The central question addressed under this contract has been how to design a multi-gap high energy electron accelerator so as to maintain the good beam quality

available from the injector, despite high beam current, during the lengthy transport and acceleration required to attain the high output beam energy? A major culprit afflicting many high energy, high current electron accelerators has been the severe erosion of beam brightness during high current transport through multiple accelerator gaps due to failure to simultaneously control beam breakup kinking and beam sausaging, driven by current-dependent interactions at the acceleration gaps. Another problem has been the use of different focusing techniques near the beam source, injector, through the accelerator, and during extraction from the accelerator and insertion into an FEL wiggler (for example). Emittance growth often occurs during the multiple handoffs between different focusing fields.

Therefore we have concentrated this contract research upon the twin tasks of minimizing beam sausaging excitations and beam kinking excitations, while attempting to maintain uniform focusing throughout the accelerator to avoid emittance growth during the handoffs between different focusing fields. Because of our previous success in achieving high quality foilless diode designs with strong solenoidal beam focusing in the diode region, we decided to pursue an accelerator design predicated upon the use of solenoidal magnetic focusing. Although we envisioned that the source cathode would likely be field immersed to harvest the benefit of strong focusing at the source in achieving high quality beam injectors, the accelerator cavity design techniques appear in retrospect to also be applicable in the case that the source cathode is shielded.

Beam "sausaging" refers to axisymmetric $m = 0$ beam excitations which are commonly excited near acceleration gaps by radial space-charge forces associated with axial concentrations of image charges in the electrical walls of the accelerator. This sausaging is relatively more severe near the front, or low-energy end of the accelerator where the beam is least stiff, and since it is related to space charge effects, it is naturally more severe at high current levels. Because the beam becomes relatively immune to further sausaging as it gains energy, the special techniques to control sausaging are primarily required only at the low-energy end of the accelerator, and may be abandoned at higher energy acceleration gaps in favor of

techniques pertinent to beam quality control in the high energy regime. Sausaging excitations in the beam source region are evident in the third slide of Appendix B.

Beam "kinking" refers to the asymmetric m = 1 beam kink displacements which arise from instabilities acting upon the beam. The most troublesome is the cumulative beam breakup (BBU) instability, which is a kink excitation that results from coupling the negative energy beam cyclotron mode with the cavity modes of the acceleration cavities, and cumulates to progressively higher levels of beam excitation as the beam passes through successive acceleration gaps. Since the raw growth rate of the BBU instability is independent of the beam energy, it--unlike the sausaging excitations--is troublesome throughout the accelerator. Since it arises as an instability, it commonly manifests toward the high energy end of the accelerator, and since the growth is exponential, the BBU instability may lead to complete disruption of the beam if it is not adequately controlled. Finally, since the BBU amplification scales upward with the beam current, it is particularly significant for high performance applications requiring high beam currents. If not adequately controlled, the BBU instability will effectively limit the amount of beam current which may be accelerated to high energy to unacceptably low levels. It is the demonstration of novel techniques for controlling beam breakup which is perhaps the most significant achievement of this research.

Control of beam sausaging and beam kinking are each necessary to the achievement of the demanding goals of high delivered beam quality. Moreover, there must be compatibility between the design techniques employed against these two problems. Since beam sausaging is essentially a disruption of beam equilibrium, we chose to examine this problem first. Then, within the framework of the design techniques established for control of beam sausaging, we attacked the more challenging problem of BBU kinking excitations. The result of this research has been the development of a series of accelerator cavity design techniques which in concert permit adequate control of both sausaging and kinking, so that the desired high beam quality may be delivered from the accelerator. These techniques are briefly listed below and are discussed in more detail later as the research is further described.

5. ACCELERATOR DESIGN APPROACH

Use of solenoidal magnetic transport through long, small radius acceleration gaps permits emittance control by a combination of techniques:

(1) Carefully designed, solenoidal field-immersed diodes allow extraction of high current beams at low emittance;

(2) Smoothly shaped, impedance matched gaps minimize the concentration of image charges and avoid abrupt kicks when beam electrons firsst enter the gap;

(3) Long gaps permit the possibility of phase cancellation within a gap for both sausaging and kinking modes;

(4) Tuning of the solenoidal magnetic field within the gaps can compensate image charge perturbations;

(5) Small radius gaps with a re-entrant TEM coax power feed structure allow electromagnetic isolation of the induction cavity drive structure;

(6) Re-entrant gap geometry permits resistive loading of cavity kink mode fields with minimal disruption of the symmetrical acceleration drive fields;

(7) Optimized (resonant) gap-to-gap spacing may allow phase cancellation of perturbations for both sausaging and kinking modes;

(8) Supplemental, inter-gap focusing enhances the effectiveness of resonant gap-to-gap spacing for BBU suppression;

(9) Use of a single solenoidal focusing system from the beam source to the post-accelerator application (e.g., FEL wiggler) avoids emittance growth during multiple handoffs.

The development of these accelerator design techniques resulted from the application of extensive theoretical analysis together with detailed numerical simulation of the behavior of the acceleration cavities. For this purpose, several simulation codes were developed and utilized. Three of the most significant codes, DRIFTER, EIGENMODE and BREAKUP, are briefly described in Appendix C. The code DRIFTER was used extensively in simulations of the control of beam sausaging,

driven by space charge fields in the acceleration gaps. The codes EIGENMODE and BREAKUP were likewise used extensively in studies of the control of BBU kinking amplification in the acceleration cavities. The ability of all of these codes to accept non-uniform geometrical cavities and to handle conductive and resistive wall materials was an indispensable component of this research.

6. SUPPRESSION OF BEAM SAUSAGING/EMITTANCE GROWTH

Our research on methods of suppression of the axisymmetric $m = 0$ beam sausaging excitations are thoroughly described in Appendix D. The tools which were employed in this analysis were the two-dimensional (r,z), steady state, electromagnetic, relativistic particle simulations with DRIFTER, together with theoretical analysis based largely upon a beam "envelope equation,"[3,4,5,6] which describes the axial behavior of the radial beam envelope in terms of the electric and magnetic potentials and their gradients with respect to the axial z-coordinate.

What was discovered in this phase of the research was that a variety of techniques are individually capable of contributing modest improvements to control of the sausaging emittance growth, and that in combination truly significant improvements are possible. These design techniques include Items (2), (3), (4) and (7) from the previous list of accelerator design techniques. Below we elaborate briefly on the nature of the improvements offered by these techniques.

- Smoothly shaped gaps minimize the perturbations from a concentration of image charges.

Square corners have commonly appeared in anode designs and in acceleration cavity designs, because of the ease of manufacturing such cavity shapes. However, image charges tend to collect near such corners and hence they are notorious for exciting beam sausaging. The effects of such square corner designs may be clearly seen in the third slide of Appendix B and in Figure 1 of Appendix D. Doing nothing but rounding off the corners--particularly the downstream corner--commonly reduces the emittance growth by a factor of two or so. This corner smoothing, plus the desire to convert

from the radial power feed geometry (c.f., Appendix D, Figure 1) to a re-entrant TEM power feed structure [per the accelerator design technique (6) discussed later], leads directly to the generic "low emittance" acceleration gap geometry illustrated below in Figure 1.

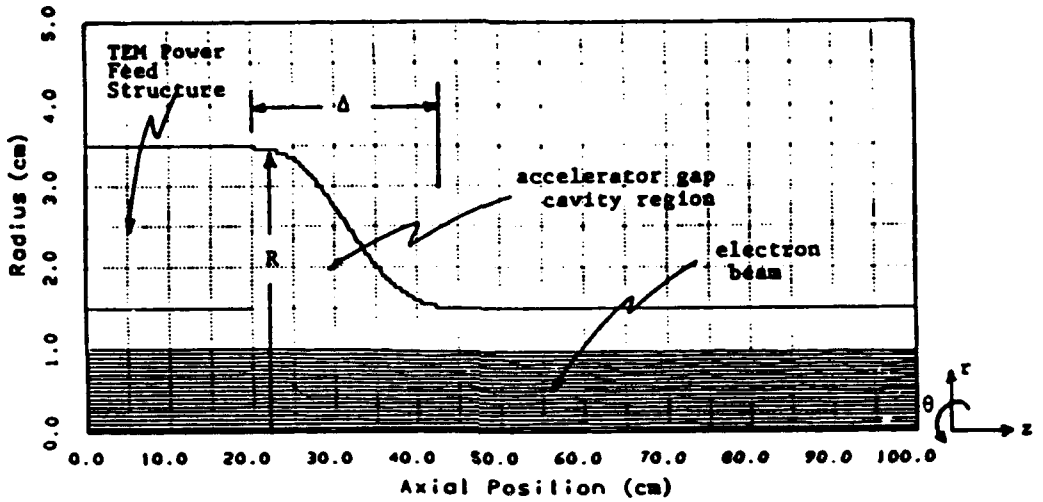

Figure 1. Low emittance acceleration gap geometry.

- Impedance matched gaps do not subject the beam electrons to δ-function kicks when they first enter the gaps.

As may be seen mathematically from Equations (8), (18) and (20) of Appendix D, it is possible to match the radial geometry of the gap to the applied accelerating potential and the beam current in such a way that the accelerating potentials are felt smoothly rather than suddenly by electrons entering the gap. The incremental beam space charge potential associated with the larger gap wall radius is matched to the gap axial potential variation.

- Long gaps permit the possibility of phase cancellation of perturbing forces within a gap.

Typical gap lengths L (or Δ in Figure 1) are much larger than beam or cavity radii. If the gap length is also larger than the inverse focusing wave number (i.e., the cyclotron wave number for strong solenoidal focusing), the phase cancellation of the perturbing forces can occur within a cycle of the focusing dynamics which can occur during the gap transit. This is because the gap excitations may again be expressed as a Fourier transform of the perturbing fields, evaluated at the focusing wave number, as seen in Equations (11) through (17) of Appendix D. When $kL > 1$, the excitations diminish, as suggested by Equations (25) and (26) for one particular gap shape. In principle there may even be choices of gap length for which the phase cancellation is complete during a transit and the sausaging excitation is nulled; however, these gap lengths for complete nulling tend to be rather long [e.g., $kL = 4\pi$ for the gap shape of Equations (19) and (21) of Appendix D].

- Optimized gap-to-gap spacings may also allow phase cancellation of perturbing forces.

Here the physics of the phase cancellation is the same as that for a single gap, although the required gap-to-gap spacing D is more affordable (i.e., $kD = \pi, 3\pi, \ldots$]. Such phase cancellation in Gap 2 of the excitations produced in Gap 1 is feasible, because there will typically not be much phase mixing of the excitations during the transit from Gap 1 to Gap 2. In such a case, the potential emittance growth may actually be reversed to a large extent, as illustrated in Figure 11 of Appendix D.

- Tuning of the solenoidal field within the gaps can compensate image charge perturbations.

This is a powerful but somewhat complex technique of emittance control which exploits the tunability which solenoidal magnetic transport affords. Programmed magnetic perturbations are introduced within the acceleration gap in such a manner that the magnetic Lorentz force perturbations just exactly offset the gap force

perturbations. The required tuning is illustrated in Equation (38) and Figure 12 of Appendix D.

It may also be seen from the analysis of Appendix D that the amount of emittance growth due to gap excitations of sausaging declines down the accelerator as γ increases and the beam becomes "stiff." This is important, because it means that some of these sophisticated techniques of emittance control may be profitably employed at the front end of the accelerator, where the beam is most vulnerable to disruption, but need not be used throughout the accelerator.

The combined effect of these emittance control techniques is illustrated for a pair of low energy gaps in Figure 2, where emittance growth is seen to be reduced by a factor of 72, and brightness is increased by a factor of 5000--in comparison with the corresponding pair of ordinary radial feed acceleration gaps.

7. HISTORICAL REVIEW OF SOME PRIOR BBU INVESTIGATIONS

Since there has been a large amount of previous research on the BBU instability, extending over decades, we briefly digress to review certain aspects of the earlier work in order that the apparently novel BBU control techniques which we have developed under this contract might be better placed into context.

The phenomenon of beam breakup, representing a $m = 1$ kink mode displacement of the beam centroid excited in an acceleration cavity, first appeared about 1957. This $m = 1$ mode is most dangerous, since the self-consistent electromagnetic fields for this mode are finite near the cavity axis where the beam propagates.

Historically it was observed that the BBU instability afflicted accelerator operation if the current exceeded a certain critical but rather low threshold--a level so low that effects of beam self-space charge fields were still negligible. Many of the earliest detailed observations[7,8] of BBU were made on the SLAC 2-mile electron accelerator, where BBU effects manifested at current levels of a few tens of milliamperes. Consequently, the BBU instability has long been recognized as a major problem afflicting accelerators of even modestly high currents. At small

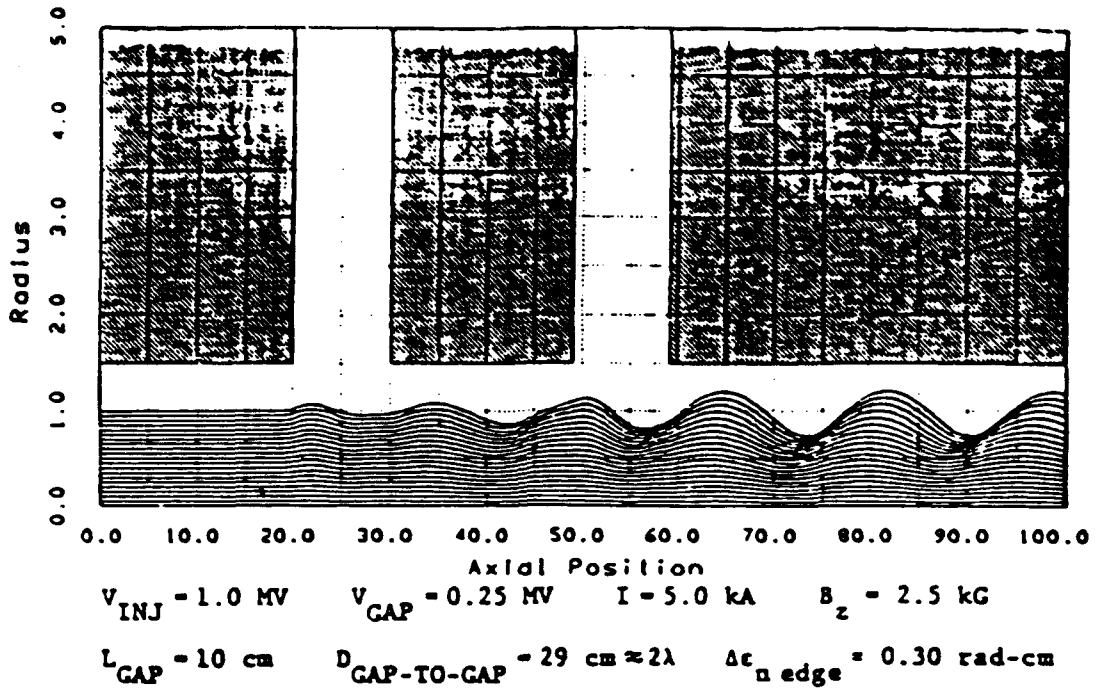

Transport of a high current beam past two ordinary radial feed acceleration gaps showing usual beam quality degradation.

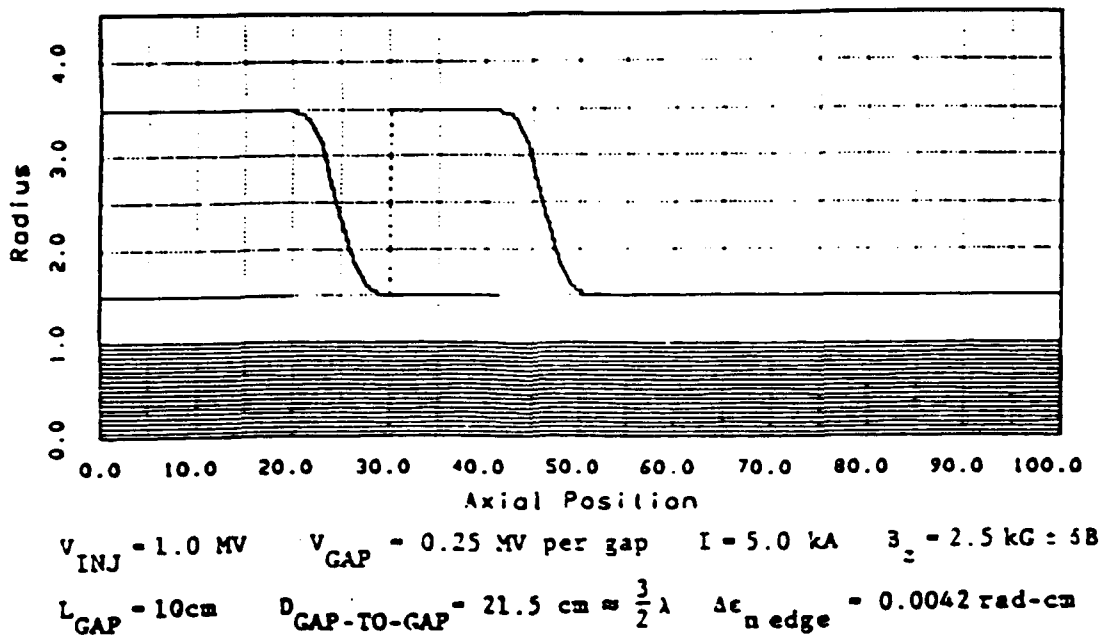

Transport of a high current beam past two contoured, impedance matched, magnetically tuned gaps, with optimized gap spacing. Combined techniques of emittance control reduce emittance growth by a factor of 72 and increase brightness by a factor of 5000.

Figure 2. Successful design for emittance control of beam sausaging.

amplitude, a BBU excitation represents an effective increase in the beam emittance, while at large amplitude it may deflect the beam into the accelerator walls, causing partial or total loss of the beam.

Beam breakup was first observed at very low current levels for which only weak focusing was required. In the initial paper[7] of Panofsky and Bander on BBU, focusing was completely neglected until the end of the paper, and then was introduced in the spirit of a weak correction. It was recognized immediately that focusing was helpful, however, and led to an increase in the current level at which BBU disruption occurred. The type of focusing first considered was linear quadrupole focusing, typical of long high-energy accelerators such as SLAC. Several approximations appropriate to low current, weakly focused, long multi-gap accelerators were employed in the early BBU analysis, and to a large extent they have been retained in much of the more recent analysis as well. These include the neglect of space charge forces and the use of a short gap, or thin lens, or impulse approximation in the calculation of the deflection suffered by the electron beam in crossing an acceleration cavity. Under this approximation, the beam displacement is assumed not to vary during the transit across a single cavity, while the transverse momentum receives an increment treated as an impulsive kick. Also under this approximation, transverse focusing--when included at all--is neglected during the beam transit across the acceleration cavity and is only retained and assumed to apply in the drift space between acceleration cavities. This local decoupling of the focusing from the beam-cavity interaction is, of course, entirely within the spirit of traditional accelerator transport calculations, in which a lattice or matrix formalism is often adopted and different elements of the transport are assumed to occur sequentially. Moreover, for some accelerators the decoupling may even be physically correct, since the focusing elements may in fact occur only in the drift space between acceleration cavities. In addition, even when focusing is physically applied within a cavity as well as between cavities, if the focusing is so weak that the betatron wavelength is many times the cavity length (as may well

be the case for very low beam current), then the neglect of focusing during the cavity transit may be a good approximation.

It has been recognized[8] for at least twenty years that there are several avenues available to reduce the growth of BBU excitations to a tolerable level. None of these is a panacea, however; complete stabilization is rarely possible and at sufficient current level BBU rears its ugly head. The BBU control techniques fall generally into the categories of rf cure and focusing. The rf cures include "Q-spoiling," which may mean lowering the Q of the cavity through impedance loading, or otherwise selectively coupling power out of the BBU TEM modes. In addition, rf cures may involve "detuning" by introducing a spread in the cavity resonant frequencies from cavity to cavity. Feedback stabilization has also been examined, but is generally regarded as prohibitively difficult. Focusing has been regarded as a brute force technique, but with significant cost attached so that complete reliance upon focusing is normally unaffordable. Another possibility is to introduce a spread in the betatron frequency to achieve a detuning effect, similar to that resulting from a spread in cavity frequencies. Which of these control techniques is most effective for a particular machine is a question which has received much attention over the years, and only recently has some understanding of this question emerged from a careful examination of the scaling laws embodied in a model BBU master equation.

In the 1970s, Neil and co-authors considered[9,10] the case of BBU excitation upon high current (kA) electron beams in linear induction accelerators. In the latter paper,[10] the case of solenoidal magnetic focusing in a high current induction linac was explored--which is the same configuration that we have been investigating at Austin Research Associates. However, Neil, Hall and Cooper continued to employ the thin lens impulse approximation in which the acceleration gap deflections are locally decoupled from the solenoidal focusing, with each of these effects incorporated into a transport matrix formalism. The solenoidal focusing matrix M_F was evaluated for the case of a magnetically shielded beam source for which the canonical momentum P_θ is zero, and the effect of

electromagnetic self-forces were also neglected. Because of their desire to achieve the simplifying result that M_F not vary from one focusing segment to the next, Neil, Hall and Cooper also assumed in effect that P_θ continued to remain zero as the beam propagated through successive acceleration cells. The justification for this assumption--other than simplifying the analysis--appears elusive since the BBU fields will alter the canonical momentum of the beam in the acceleration gaps. (Our own BBU analysis has avoided this assumption as well as the short gap, impulse assumption.) Neil and Cooper concluded[9] that for kiloampere current accelerated to a few MeV in the short, fat, Q=50 acceleration cavities of the Astron injector, stabilization of BBU is quite difficult. Even with fairly strong focusing (e.g., betatron wavelength ~ meter), both finite Q effects and a significant spread in betatron frequency was required. Neil, Hall and Cooper concluded that for an ATA class accelerator (i.e., 2 kA, 100 MeV, 800 MHz cavity frequency) and a solenoidal field strength of 4 kG, it was still necessary to strive to reduce Q to around 20 and employ other BBU control mechanisms as well (e.g., detuning).

In 1988, R. B. Miller, et al.[11] proposed an entirely new technique for control of cumulative BBU in a high current linear induction accelerator. This is to introduce a short section of coaxial transmission line between the cavity structure and the accelerating gap region in order to cut off communication between the induction cavity drive structure and the accelerating gap region. The small radius TEM power feed structure embodied in the adiabatic acceleration gap shown in Figure 1 carries this same advantage, and in this respect our own research is related to that of Miller, et al. Unfortunately, our investigations showed that coupling can still occur between the beam and resonances associated with the gap region geometry itself, at higher frequency than the modes of the induction cavity structure. It is this high frequency cumulative BBU instability that we have investigated at Austin Research Associate under this contract.

During 1988-1989, Y. Y. Lau, together with D. G. Colombant, published several papers[12,13,14,15] in which there was an attempt to reconcile the various results obtained in previous analysis (e.g., Panofsky and Bander,[7] Neil, Hall and

Cooper,[10] and Chao, Richter and Yao[16]) by careful examination of the scaling laws embodied in a model BBU master equation (i.e., the "standard model"). This research is very enlightening and yielded a useful classification scheme[15] for cumulative BBU under which

(a) the Panofsky and Bander regime of weak focal strength, low current, and long pulse length falls into Type A,

(b) the Neil, Hall and Cooper regime of strong focusing field, high beam current and moderate pulse length falls into Type B, and

(c) the Chao, Richter and Yao regime of moderate focal strength, short pulse length, moderate current, and long propagation distance falls into Type C.

It was concluded that BBU of Type C may be more readily stabilized by focusing techniques (e.g., betatron spreads); Type A may be more readily stabilized by rf cure techniques (e.g., lowering Q, cavity frequency spreads); while Type B is a more difficult regime requiring both rf cure and external focusing.

It may be noted that the ATA experiments also fell within the difficult Type B regime, and indeed, extraordinary measures were found necessary to control BBU. In addition to striving for Q as low as 4, it was deemed necessary to introduce strong ion focusing at the moderate and high energy end of ATA, provided by an ion channel generated along the beam path by a laser.[17] This resulted in a complex transport system in which the beam was generated at a magnetically shielded cathode, introduced to a solenoidal magnetic field and accelerated to 6 MeV, then passed to the ion focusing channel and accelerated to 50 MeV, then handed to the Paladin FEL focusing system. Although BBU control was thereby improved, such a complex beam transport system was incapable of providing good emittance control, and emittance growth during acceleration of at least a factor of ten was reported.[18]

The results of the Lau and Colombant papers, while consistent with those obtained individually by the various prior authors and while introducing no new

methods of BBU control, nevertheless provide a satisfying unity of perspective to predictions obtained under the "standard model."

This standard model may be expressed mathematically as Equation (3) of Reference 15, where the focusing term appears as $\gamma k_\beta^2 x$. This model is based upon the approximations developed in the prior References 7, 10 and 16. As described earlier, these approximations include the short gap impulse approximation and the local decoupling of the focusing effect from the BBU cavity deflections within a single acceleration gap.

8. SUPPRESSION OF BEAM BREAKUP

At Austin Research Associates, our investigations under this contract have not included these approximations embodied in the standard model of cumulative BBU control; rather, our investigation of BBU has been performed for the case in which solenoidal focusing is applied within as well as between acceleration gaps. Our studies of BBU kinking suppression have also been based upon the use of long, adiabatic *acceleration* gaps of the type shown in Figure 1, which were shown to be appropriate for avoidance of beam sausaging and the preservation of high brightness. Consequently, we have not adopted the short gap-thin lens-impulse approximation, nor have we assumed $P\theta$ constant across the acceleration gap.

The investigations of beam breakup suppression which we have completed under this contract are documented in Appendices E, F, G, H and I of this final report. Using the low emittance acceleration gap geometry of Figure 1, we were able to discover several design techniques which appear to offer the prospect for adequate suppression of the cumulative BBU throughout the entire accelerator, despite multi-kiloampere current levels and final beam energy of tens to hundreds of MeV. Given the all-too-slim arsenal of techniques effective in BBU control at very high current, we consider these achievements under this contract to be very significant. These techniques for BBU control include Items (3), (5), (6), (7) and (8) from the previous general list of accelerator design techniques. It will be seen that there is significant overlap between these BBU control techniques and the

beam sausaging control techniques, although the latter are primarily needed at the low energy end of the accelerator. It will also be seen that several of the BBU control techniques manifest their primary usefulness at different energy ranges along the accelerator. Below we will elaborate further on the nature of the improvements offered by each of the BBU control techniques, and will indicate where these are discussed in more detail in the appendices.

The mathematical attack on BBU control, within the context of long, adiabatic cavity gaps with intra-gap solenoidal focusing, was first laid out in Appendix E, published[19] in 1990. The seeds for all of the successful design techniques for BBU suppression may be found in that report, although the successes were not confirmed until later work was completed. Preliminary tests of the design code RESONANT (a precursor of EIGENMODE) and BREAKUP were also described in this report.

- Small radius gaps with a re-entrant TEM coax power feed structure allow electromagnetic isolation of the induction cavity drive structure.

Conventional induction acceleration cavities have very short axial gaps of large radial extent which are coupled into a large ferrite drive structure. These are typified by the ETA/ATA acceleration modules which are described in the extensive ATA literature.[20,21] These conventional cavities are illustrated in Figures 1 of References 20 and 21, and in Figures 1 and 2 of Appendix G and Figure 2 of Appendix F. By contrast, a small radius gap with the re-entrant TEM coax power feed structure is illustrated in Figure 1 (previously), as well as Figure 1 of Appendices E, F and H. It was noted in the historical review that Miller[11] proposed this coax geometry in 1988 for the purpose of cutting off communication between the induction cavity drive structure and the acceleration gap cavity. (About the same time we had independently discovered this re-entrant geometry during our work on emittance control.) The details of this isolation are discussed in Appendix H, where the cutoff frequency is ~700 MHz for the optimized cavities considered. There was initially hope that this disruption of

beam coupling to the ferrite cavity modes would be of major benefit in BBU suppression. Unfortunately, our simulations (c.f., Appendix E, Figures 2 through 4) immediately revealed a surviving BBU interaction in which the beam is coupled to the higher frequency (i.e., GHz) modes of the smaller radius coax feed structure and/or the acceleration cavity. Nevertheless, the isolation of the larger ferrite drive structure and the corresponding reduction of the BBU problem to the coupling between the beam and coax/cavity modes was helpful in achieving some reduction in the BBU gain, as discussed further below.

- Re-entrant gap geometry permits resistive loading of the cavity kink mode fields with minimal disruption of the symmetrical acceleration drive fields.

As mentioned previously, one method which has long been used for BBU control involves impedance loading, or "Q-spoiling" of the cavity. However, this is a process that is extremely tricky to accomplish well, and only modest results are often attainable. One problem is that the symmetric drive fields which accomplish the beam acceleration must propagate down the feed lines to the acceleration gap at the beam axis, and if these fields encounter resistive materials at positions where the fields have large amplitude, then significant power may be dumped into the load and the fields available for acceleration will be modified. In conventional cavities, both the $m = 0$ drive fields and the $m = 1$ BBU fields have large Ez fields, zero E_θ and Er fields in the radial feed lines. Therefore, the loading material must be "hidden" from the drive fields in the large ferrite drive structure. In contrast, the coax re-entrant gap feed structure provides a very natural method of resistive loading of the BBU $m = 1$ modes without any adverse effect on the $m = 0$ driving fields. This is possible because in the coax region the $m = 0$ drive fields are entirely E_r, while the $m = 1$ BBU modes in the coax structure exhibit significant components of both E_θ and E_z. Therefore, the coax structure can be loaded with resistive structures of finite conductivity in the θ and/or z direction to provide effective Q spoiling of the $m = 1$ BBU modes without any effect on the $m = 0$ drive fields. Such loading moreover provides

further isolation of the induction ferrite drive apparatus from the gap region even for frequencies above the m = 1 coax cutoff through resistive damping of the modes as they traverse the coax feed.

Even with these advantages, it remains quite difficult to arrive at an optimum resistive loading design. One difficulty is that the introduction of resistive material can permit a resistive wall instability under some circumstances, which can compete with the BBU instability. Even worse is the frequent result that loading the cavity to better control one mode can often create conditions whereby beam coupling to a different cavity mode is actually enhanced, a circumstance described as a "marshmallow" effect.

Fortunately, it was possible to exploit the versatility of the design codes EIGENMODE and BREAKUP to survey the possibilities and determine an optimum cavity loading configuration. The details of this optimization process are illustrated for a particular adiabatic gap design in Appendix H. The result of this tedious process of optimization is that the BBU gain per gap can typically be reduced by about a factor of two from what it would be in a conventional radial feed gap having the same beam current, focusing field, acceleration potential, and inner wall radius. This improvement is illustrated by the coefficient reduction between Equations (4) and (5) of Appendix F. Although this may sound like a modest improvement, a 50 percent reduction in the growth rate of an exponentially growing instability is really quite significant. It would permit twice as much current to be accelerated, for example.

- Long adiabatic gaps permit phase cancellation of BBU excitations during the electron acceleration across the gap.

The physics of this intra-gap BBU phase cancellation is very similar to the analogous reduction of the sausaging excitations. The possibility of this cancellation was noted in the original analysis of Appendix E [i.e., Item 6 following Equation (32)]. Such intra-gap phase cancellation permits a major suppression of BBU amplification at those low and moderate electron energies for

which it is feasible to keep the inverse focusing wave number less than the gap length. In effect, the onset of BBU growth may be postponed to that point in the accelerator where the inverse gyrowave number has increased to the cavity length, and even beyond that point there will be some residual gain reduction due to phase cancellation. This important result is one which cannot be obtained within the usual short gap, or impulse approximation. Detailed analysis of this intra-gap phase cancellation is presented in Appendices F and H, and BBU gain simulations confirming the effect are described in Appendices F, G and H. The mathematical expression of this phase cancellation effect is presented on the following slides: Figures 3 and 4.

It may be seen that the cumulative BBU gain per gap G is proportional to the square magnitude of a complex overlap integral of the electron beam negative energy $m = 1$ displacement mode with the electric fields on axis of the unstable cavity resonance. If the gap is so narrow that the fields $\mathbf{E}$ and $\exp i(\omega + \Omega)z/c$ do not vary significantly across the gap, then there cannot be phase cancellation and one obtains the usual narrow gap gain in which G is proportional to gap length L (as well as to I_b/B_z and other parameters). On the other hand, for wide gaps the gain is very significantly reduced as indicated by the wide-gap gain expression on Figure 4, which corresponds to Equation (3) of Appendix F. The gain per gap is reduced by the factor $1 + k^2 \ell^2$, where $k = \Omega/c$ is the focusing cyclotron wave number and ℓ is the axial length of the cavity eigenmode--normally near the gap length L. The dramatic BBU gain suppression occurs when $k\ell > 1$, or $\gamma < Bz\ (kG)\ \ell\ (cm)/1.7$. An expression for the cumulative BBU amplification may also be obtained, in which the phase cancellation appears as an Arctan term on Figure 4, corresponding to Equation (8) of Appendix F. This cumulative effect is often quite significant, as indicated by the results of Table 1 of Appendix F for an ATA-comparable accelerator design.

BEAM BREAKUP AMPLIFICATION

TOTAL AMPLIFICATION = $(1 + G_1)(1 + G_2) \ldots (1 + G_{Nc})$

N_c = NUMBER OF CAVITIES

G_J = BBU GAIN IN THE jth GAP

$$G = 8\pi \frac{I_b}{mc^3/e} \frac{Qc^3}{\omega^2 \Omega \gamma} \frac{\left| \int_0^L dz \left[\partial_r E_z - (\partial_z - i\omega) E_r\right]_{r=0} \exp\left[-i(\omega+\Omega) z/c\right] \right|^2}{\int d^3x \ |\mathbf{E}|^2}$$

$$\Omega = \frac{eB_z}{\gamma mc} = \text{RELATIVISTIC CYCLOTRON FREQUENCY}$$

$$\omega = \text{FREQUENCY OF CAVITY RESONANCE}$$

$$Q = \frac{\omega \int d^3x |E|^2}{\int d^3x \ 4\pi\sigma |E|^2} = \text{RESONANT CAVITY QUALITY FACTOR}$$

$$G\,(\text{Narrow Gap Limit}) = \alpha \frac{I_b\,(kA)}{B_z\,(kG)} \quad (\text{Independent of } \gamma)$$

$$\alpha\,(L^3 \text{ Notation}) = K\,\omega\,(Z_\perp/Q)\,Q$$

Figure 3

BEAM BREAKUP AMPLIFICATION

ARBITRARY GAP WIDTH $\left(\frac{\Omega \ell}{c} = \frac{B_z \ell}{1.7\gamma} \right)$

ℓ = AXIAL LENGTH OF CAVITY EIGENMODE

$$G_{wide} = \frac{G_{narrow}}{1 + \frac{\Omega^2 \ell^2}{c^2}} = \alpha \frac{I_b}{B_z} \frac{\gamma^2}{\gamma^2 + (B_z \ell / 1.7)^2}$$

NOTE GAIN REDUCTION WHEN $\gamma < \frac{B_z\,(kG)\,\ell\,(cm)}{1.7}$

$$\text{CUMULATIVE AMLIFICATION} = \exp \; N_c \, \alpha \frac{I_b}{B_z} \left[1 - \frac{\Omega_f \ell}{c} \text{ Arc tan } \frac{c}{\Omega_f \ell} \right]$$

N_c = NUMBER OF CAVITIES

$$\Omega_f = \frac{B_z \ell}{1.7 \gamma_f}$$

γ_f = FINAL γ ATTAINED

NOTE THAT IF $\Omega_f \ell / c > 0.43$, THE CUMULATIVE NUMBER OF BBU E-FOLDINGS IS REDUCED BY OVER A FACTOR OF TWO.

Figure 4

- **Optimized (resonant) gap-to-gap spacing may allow phase cancellation of BBU excitations via enhanced coupling of a competing positive energy beam mode.**

The possibility of using certain resonant gap-to-gap spacings to obtain a reduction in BBU amplification was also noted in the original analysis of Appendix E [i.e., Item 4 following Equation (32)]. These resonant spacings are $\Omega L_G = 0, 2\pi, 4\pi, \ldots$, where Ω is the relativistic cyclotron focusing frequency and L_G is the gap-to-gap spacing. The reason that this resonant spacing permits reduced amplification is that it causes the positive energy beam ballistic mode to be tightly coupled into the beam-cavity interaction, together with the usual negative energy beam cyclotron mode. Consequently a competition between these modes occurs, with the positive energy mode absorbing energy from the cavity as the negative energy mode is driving energy into the cavity. Under favorable circumstances, the net result may be little or no BBU growth. The details of the reduced BBU amplification due to resonant gap-to-gap spacing are presented in Appendix I. In Figure 1 of Appendix I, the net BBU gain per gap is illustrated in the vicinity of the resonance at $\Omega L_G \approx 4\pi$, for different mixtures of the destabilizing cyclotron mode and the stabilizing ballistic mode. It is clear that it is desirable to have a larger component of the stabilizing eigenmode component $|S|$, and that it is necessary for the gap-to-gap spacing to be fairly tightly controlled if the reduced growth is to be obtained.

The reduction in BBU amplification accruing from resonant gap-to-gap spacing is of greatest value at moderate and high electron energy, where the effectiveness of the wide gap phase cancellations has diminished appreciably. However, in this case in which the individual gaps are relatively narrow, the overlap integrals for the positive and negative energy modes tend to have comparable magnitudes, as is evident from Equation (5) of Appendix I when $\Omega \Delta < 1$. Therefore in this important regime of moderate and high electron energy, in order to realize appreciable BBU suppression, it is necessary to achieve the desired gap-to-gap spacing within the very small tolerances which exist

around the resonant spacings. Figure 3 of Appendix I is an overview of these acceptable "notches" within which the accelerator may operate at reduced BBU amplification. Unfortunately, the tolerances corresponding to these resonant notches are so tight that successful achievement of appreciable BBU suppression by this method might prove impractical--if it were not for the following significant discovery.

- Supplemental, inter-gap focusing enhances the feasibility of BBU suppression by resonant gap-to-gap spacing.

It was discovered that if a strong focusing lens is inserted in the drift space between acceleration gaps, it has the significant benefit of widening the tolerance of the resonant spacing notches and correspondingly reducing the BBU amplification for gap-to-gap spacings near the desired values. These effects are also described further in Appendix I. Unlike the previous analysis which is relevant and important at the lower energy acceleration cavities, this resonant spacing plus supplemental focusing technique, which is useful for higher energy cavities, contains all of the traditional thin lens-short gap-impulse approximations of conventional high energy accelerator transport. Hence the usual matrix transport theory applies.

The physical reason that supplemental focusing lens are useful in BBU suppression is that they "reset" the mix of positive energy to negative energy beam eigenmodes between the cavities--making it more difficult for the negative energy component to gain dominance and exponentiate from cavity to cavity. There is a new danger that if the gap-to-gap spacing is set incorrectly, there is now the possibility of a new "focusing transport" instability due to the strong focusing lenses. However, there is no reason that the accelerator gap spacings may not be set properly to harvest the reduced BBU amplification. The expanded notches resulting from the supplemental focusing may be seen in Figures 4 and 5 of Appendix I, where the desirable operating regions are where the gain per gap is reduced below the raw BBU value [i.e., $g \approx 0.1$ for the examples]. As the

supplemental focusing is increased, there is greater reduction in the BBU gain, but some tightening of the width of the operational notches.

Eventually, toward the high energy end of the accelerator, only the lowest notch will be accessible, because $\Omega L_G = \Omega_0 L_G/\gamma$ cannot practically be made to exceed one. [Here $c = 1$ units are employed.] In this final, high-energy operational regime, the BBU gain is indicated by Equation (14) and Figure 7 of Appendix I. Even in this most difficult accelerator regime, it appears practical to achieve over 50 percent reduction in the raw BBU gain per gap by a modest investment in supplemental focusing. As noted earlier, such a reduction in gain per gap, when compounded over perhaps more than a hundred gaps, will allow a truly significant reduction in cumulative BBU amplification.

It is important to step back and recognize how these various beam quality control techniques--both for sausaging emittance control and BBU suppression--harmonize with one another. At the beam source and in the first few lowest energy acceleration cavities, the design emphasis should be primarily upon controlling sausaging. There the strong field immersion and the smooth, impedance matched, wide (adiabatic) acceleration gaps--perhaps with designed magnetic tuning--can preserve the beam quality until the beam acquires some stiffness. At the same time, the re-entrant geometry with optimized impedance loading will be favorable for BBU control, and the width of the gaps will be decisive in effectively postponing the onset of BBU growth. A bit further down the accelerator, attention to gap-to-gap spacing can further control beam sausaging while the beam acquires even more stiffness. Meanwhile, the relatively wider than usual gaps will still provide some phase cancellation of sausaging and of BBU gain. Finally, at the high energy end of the accelerator, when the beam's stiffness has given it some immunity against sausaging, it is appropriate to design resonant gap-to-gap spacing plus supplemental strong focusing to control BBU growth further. These latter two techniques are not ideal for sausaging, since the strong focusing might provide some $m = 0$ excitation and the integral gyrolength spacing for BBU suppression is not compatible with the half-integral spacing

desired for phase cancellation of sausaging. However, given the beam stiffness, the trade-off of strong BBU suppression for weak excitation of sausaging is likely to be beneficial. The net cumulative result of the incremental benefits of all of these various design techniques appears to offer the prospect of major improvements (i.e., orders of magnitude) in deliverable beam brightness from very long, high energy and high current induction linear accelerators.

9. PRACTICAL ENGINEERING PACKAGING CONSIDERATIONS

Although the effectiveness of these low emittance, wide gap acceleration cavity designs has not been disputed when various aspects of the designs have been described,[19,22,23] criticism was raised by LLNL personnel that such gap designs might be incompatible with engineering constraints dictated by limitations on the size, shape, and placement of the drive ferrites and the desirability to maintain as short an accelerator as possible.

In order to address these concerns head-on and demonstrate that such accelerating structures can be configured consistent with practical engineering considerations, we undertook the challenge of conceptually retrofitting an ATA narrow gap drive structure with an adiabatic, high-brightness design. This task was successfully accomplished and is described in Appendix G. The retrofit involves only the interior of the 6-inch diameter vacuum drift space and does not alter in any way the guide magnetic field coil geometry, ferrite core structure, power coupling, loading of the ferrite cavity, or any other aspects of the ATA drive structure exterior to the 6-inch beam line.

Even under the constraints of this retrofit, which in no way constitutes an optimum design, the superior beam breakup suppression characteristics of the high brightness adiabatic accelerating gap structures are demonstrably maintained--as shown by simulation results reported in Appendix G.

For purposes of comparison, it may be noted that the retrofitted cavity design of Appendix G is somewhat smaller than the cavity design of Appendix F, with the smaller design having a slightly larger BBU gain per gap as expected. In

Appendix F, the results of gap optimization studies were reported for that larger gap. Subsequently, gap optimization studies were repeated for the smaller gap design, and these are the ones described in detail in Appendix H.

10. EMITTANCE CONTROL DURING BEAM INJECTION INTO A FREE ELECTRON LASER WIGGLER

One final task which was undertaken under this contract involved studies of the process of optimizing the injection of a high quality beam into an FEL wiggler in such a way as to minimize emittance growth during the injection. We have already noted the design consideration that the use of a single solenoidal focusing system from the beam source to the post-accelerator application (e.g., FEL wiggler) avoids emittance growth during multiple handoffs. Since it would not be feasible to remove a beam which had been born in a solenoidal field-immersed cathode from the field prior to injection into the wiggler, we also examined the suitability of introducing a solenoidal field into such a FEL wiggler, to be driven by a high current, high energy electron beam.

This task was addressed periodically throughout this contract; however, it was given lower priority than the other tasks which related to the beam quality control in the accelerator cavities per se. Unfortunately (or fortunately, depending on one's perspective), in the final year of the contract we discovered the prospect for the significant further suppression of BBU gain by resonant gap-to-gap spacing plus supplemental focusing, and we elected to concentrate our efforts upon this task in lieu of completing the investigation of solenoidal injection into a FEL. Consequently, we have not included in this final report our preliminary but unfinished calculations upon this task.

Our tentative conclusion is that there do not appear to be any undue difficulties related to such injection, or to the presence of a solenoidal field in the wiggler. Because of the separation of wave numbers $k_c << k_w << k_s$, where k_c, k_w, k_s are the relativistic cyclotron, wiggler and laser wave numbers, the focusing betatron dynamics is well removed from the resonance which occurs at $k_c \approx \beta_z k_w$.

Consequently, the FEL may be operated well into the familiar regime of Group I orbits[24] in which the guide field B_z does not appreciably influence the FEL dynamics. Given the presence of the guide field, it did appear desirable to have a helical wiggler rather than a linear wiggler, although perhaps a combination roughly equivalent to a helical wiggler--such as a linear wiggler plus curved pole piece focusing--would have also sufficed. We did not complete a determination of whether it is preferable to have wiggler focusing or solenoidal focusing dominant for the betatron dynamics in the wiggler, and likewise we did not determine the optimum final values of the wiggler magnetic field B_w versus the solenoidal magnetic field B_z. It did appear that the transitional turn-on of the wiggler magnetic field and axial variation in the solenoidal field should occur adiabatically with respect to the betatron period in order to minimize the beam excitations during injection. Overall, we remain confident that injection into an FEL can almost certainly be accomplished without appreciable loss of beam quality, although confirmation of this expectation would require completion of the calculations and simulations which we had only initiated.

In summary, we are pleased with the results which have been achieved during our investigations of beam handling and emittance control under this contract. We feel that the stage has now been set for future experimental development of these techniques for advancing high quality, high brightness electron beam technology.

11. LIST OF REFERENCES

1. C. W. Roberson and P. Sprangle, Physics of Fluids B 1 (1989), p. 26.

2. Y. Y. Lau, J. Appl. Phys. 61, 36 (1987).

3. P. T. Kirstein, G. S. Kino, and W. E. Waters, Space Charge Flow (McGraw-Hill, New York, 1967), Chap. 3.

4. A. Septier, Applied Charged Particle Optics (Academic Press, New York, 1983).

5. E. P. Lee and R. K. Cooper, Part. Accel. 7, 83 (1976).

6. G. J. Caporaso, A. G. Cole, and J. K. Boyd, IEEE Trans. Nucl. Sci. NS-32, 2605 (1985).

7. W. K. H. Panofsky and M. Bander, Rev. Sci. Instrum. 39, 206 (1968).

8. R. Helm and G. Loew, Linear Accelerators, Eds. P. M. Lapostolle and A. L. Septier (North-Holland, Amsterdam, 1970), Ch. B.1.4.

9. V. K. Neil and R. K. Cooper, Part. Accel. 1, 111 (1970).

10. V. K. Neil, L. S. Hall, and R. K. Cooper, Part. Accel. 9, 213 (1979).

11. R. B. Miller, B. M. Marder, P. D. Coleman, and R. E. Clark, J. Appl. Phys. 63 (4), 997 (1988).

12. Y. Y. Lau, Naval Research Laboratory Report No. 6237 (1988).

13. D. G. Colombant and Y. Y. Lau, Appl. Phys. Lett. 53, 2602 (1988).

14. D. G. Colombant and Y. Y. Lau, Appl. Phys. Lett. 55, 27 (1989).

15. Y. Y. Lau, Phys. Rev. Lett. 63, 1141 (1989).

16. A. W. Chao, B. Richter, and C. Y. Yao, Nucl. Instrum. Methods 178, 1 (1980).

17. G. J. Caporaso, F. Rainer, W. E. Martin, D. S. Prono, and A. G. Cole, Phys. Rev. Lett. 57, 1591 (1986).

18. J. L. Miller, "High Power Induction Free-Electron Laser," Proc. SPIE, High Power and Solid State Lasers II, Vol. 1040, 152 (1989).

19. M. L. Sloan and James R. Thompson, Proc. SPIE, Intense Microwave and Particle Beams, Vol. 1226, 447 (1990).

20. R. J. Briggs, et al., IEEE Trans. NS-28, 3360 (1981).

21. D. S. Prono, "Recent Progress of the Advanced Test Accelerator," IEEE Trans. Nuc. Sci., Vol. NS-32, 3144 (1985).

22. J. R. Thompson, M. L. Sloan, J. R. Uglum, and B. N. Moore, Proc. SPIE, Microwave and Particle Beam Sources and Directed Energy Concepts, Vol. 1601, 454 (1989).

23. M. L. Sloan, J. R. Thompson, and C. S. Kueny, Proc. 9th International Conference on High-Power Particle Beams, Vol. I, 305 (1992).

24. Reference 1, p. 21.

APPENDIX A

BEAM QUALITY REQUIREMENTS FOR A HIGH PERFORMANCE FREE ELECTRON LASER

Briefing Slides

BEAM QUALITY

IDEAL:

(1) ALL BEAM PARTICLES SHOULD HAVE NEGLIGIBLE TRANSVERSE ENERGY IN THE ACCELERATOR (I.E., LOW $\perp$ EMITTANCE).

(2) THEY SHOULD HAVE NEGLIGIBLE VARIATION IN LONGITUDINAL ENERGY (I.E., LOW EMITTANCE).

(3) THERE SHOULD BE A HIGH CURRENT OF PARTICLES.

(4) THE BEAM CROSS SECTION SHOULD BE VERY SMALL (I.E., HIGH CURRENT DENSITY).

(5) THE BEAM CENTROID SHOULD MOVE ALONG THE DESIGN TRAJECTORY, DOWN THE CENTER OF THE ACCELERATOR

$$\varepsilon_n\,(edge) \;=\; \gamma\beta_\perp\; x_\perp$$

$$B_n \;=\; \frac{\pi^2\; I_b}{\gamma^2\,\beta^2\,V_4\,(x_\perp,\beta_\perp)} \;=\; \frac{2I_b}{\varepsilon_n^2\,(edge)} \;=\; \frac{2I_b}{9\,\varepsilon_n^2\,(RMS)}$$

$$\left(\quad \bar{B}_n \;=\; \frac{B_n}{\pi^2}\right)$$

HOW IS BEAM QUALITY IMPORTANT FOR A HIGH PERFORMANCE FREE ELECTRON LASER?

- UNLESS THERE IS A TIGHT RESONANCE BETWEEN THE AXIAL VELOCITY OF ALL ELECTRONS AND THE PHASE VELOCITY OF THE PONDERMOTIVE WAVE, THERE WILL NOT BE EFFICIENT, HIGH-GAIN WAVEGROWTH AND THERE WILL NOT BE A HIGH FRACTION OF ELECTRONS TRAPPED IN THE PONDERMOTIVE WELL.

- WITHOUT GOOD LINEAR GAIN, AN FEL OSCILLATOR MAY NOT START, AND AN FEL AMPLIFIER MAY REQUIRE A LONG WIGGLER, WITH INCREASED VULNERABILITY TO SIDEBAND MODE DISRUPTION AND POWER SPECTRUM BROADENING.

- NONLINEAR POWER AMPLIFICATION IN THE VARIABLE PARAMETER WIGGLER IS ENTIRELY DEPENDENT UPON A HIGH TRAPPING EFFICIENCY IN THE PONDERMOTIVE WELL.

- FEL GAINS AND POWER OUTPUTS ALSO SCALE AS $I_b^n r_b^{-m}$, PLACING A PREMIUM ON HIGH BEAM CURRENT AND CURRENT DENSITY.

HIGH PERFORMANCE FEL OPERATION REQUIRES

- A small spread in β_z
- High beam currents (I_b)

or, Low emittance (ε_n)

High beam brightness $\left(B_n = \frac{2I_b}{\varepsilon_n^2}\right)$

TO GET HIGH LEVELS OF

- Linear gain
- Saturated power
- Trapping efficiency
- Nonlinear gain
- Output laser power

$$\beta_z^2 = 1 - \gamma^{-2} - \beta_\perp^2$$

$$= 1 - \gamma_c^{-2} + \underbrace{\frac{2\nu r^2}{\gamma_c^3 r_b^2}}_{\substack{\text{Space Charge} \\ \text{Radial Spread}}} - \underbrace{\frac{\varepsilon_n^2 r^2}{\gamma^2 r_b^4}}_{\substack{\text{Paraxial Thermal} \\ \text{Radial Spread}}}$$

WHAT IS DIFFICULT ABOUT PRESERVING HIGH BEAM QUALITY IN HIGH CURRENT, HIGH ENERGY ACCELERATORS TO PRODUCE FEL BEAM DRIVERS?

Lawson-Penner: $\varepsilon_n \sim .3\, I_b^{1/2}(kA)$ *rad-cm*

ε_n | *achievable*

-- QUALITATIVELY CORRECT IN PREDICTION THAT EMITTANCE TENDS TO INCREASE WITH BEAM CURRENT

REASONS:

- BEAM INSTABILITIES (BBU, IMAGE DISPLACEMENT, ...)
- LARGER BEAM SIZE REQUIRED
- BEAM SPACE CHARGE EFFECTS NEAR CATHODE
- STRONGER FOCUSING REQUIRED
- IMAGE SPACE CHARGE EFFECTS NEAR ACCELERATION CAVITY GAPS

ROBERSON-SPRANGLE FEL RADIATION OVERLAP:

$$\lambda = \frac{\lambda_w}{2\gamma^2} \approx \pi\varepsilon = \pi\frac{\varepsilon_n}{\gamma}$$

$$\varepsilon_n \sim \frac{1}{k_w\gamma}$$

ε_n | *needed*

-- QUALITATIVELY CORRECT IN PREDICTION THAT BEAM QUALITY REQUIREMENTS FOR EFFICIENT FEL INTERACTION ARE MORE DIFFICULT AT HIGHER BEAM ENERGY, SHORTER RADIATION WAVELENGTHS

FEL SCALING LAWS

$$\left(k - \frac{\omega}{c}\right)(k - k_-)\,(k - k_+) = -F\,\frac{\omega_b^2}{2\gamma_o c^2}\;k_w\,\frac{\beta_w^2}{\beta_z^2}$$

$$k_\pm = \frac{\omega}{v_z} - k_w \pm \frac{\omega_b}{\gamma_o^{1/2}\,\gamma_z\,v_z} \qquad \frac{\omega_b}{k_w c} = \frac{2\upsilon^{1/2}}{k_w r_b}$$

$$\Phi_{pond}(z,t) = \frac{e}{mc^2\gamma_o}\,A_w A_R\,\cos\left[(\mathrm{Re}\,k + k_w)\;z - \omega t\right]$$

$$v_{ph} = \frac{\omega}{R_e k + k_w} \qquad \Delta v_{z\,fluid} = v_z - v_{ph} > \Delta v_{z\,thermal}$$

BEAM PARAMETERS: $\omega_b,\ \gamma_o,\ \gamma_z = \left(1 - \beta_z^2\right)^{1/2}$

$$\gamma_o = \gamma_z\left[1 + a_w^2 + \frac{\varepsilon_n^2}{2r_b^2}\right]^{1/2} \qquad a_w = \gamma_o\beta_w = \frac{eA_w}{mc^2}$$

RESONANCE CONDITION: $\omega = \gamma_z^2\,\beta_z\,(1 + \beta_z)\,k_w c = \mathrm{Re}\,k\;c$

HIGH GAIN COMPTOM REGIME: $\beta_w > \left[16\,\dfrac{\upsilon}{F^2 k_w^2 r_b^2 \gamma_o \gamma_z^6}\right]^{1/4}$

(WEAK BEAM, STRONG WIGGLER, HIGH ENERGY
SHORT FEL WAVELENGTH)

FEL SCALING LAWS @ HIGH-GAIN COMPTON REGIME

$$\Delta\gamma_{FL.\,COMP.}|_{p_\perp} = \gamma_o \gamma_z^2 \left(1 - \frac{v_{ph}}{v_z}\right) = \left[\frac{F v a_w^2}{32 k_w^2 r_b^2}\right]^{\frac{1}{3}} > \frac{\gamma_z^2 \varepsilon_n^2}{4\sqrt{3}\,\gamma_o r_b^2}$$

$$\text{WIGGLER FOCUSING: } r_b^2 = \frac{2^{1/2}\varepsilon_n}{k_w a_w}$$

$$\Rightarrow \quad \varepsilon_n < \frac{(fv)^{1/4}\ (1 + a_w^2)^{\frac{3}{4}}}{2(3)^{\frac{3}{8}} k_w \gamma_o^{\frac{3}{4}}}$$

(FOR FLUID COMPTON FEL INTERACTION)

$$\text{LINEAR POWER GAIN}\left(\frac{dB}{\Delta z}\right) = (20 \log_{10} e)\ \text{Im}\,k$$

$$= (40\sqrt{3}\ \log_{10} e)\ k_w\ \frac{\Delta\gamma_{fluid}}{\gamma_o}$$

$$\propto (I_b/\varepsilon_n)^{\frac{1}{3}}$$

$$\text{SATURATED LASER POWER} \propto I_b^{4/3}/\varepsilon_n^{\frac{1}{3}}$$

CONCLUSION: IN THE HIGH ENERGY, HIGH GAIN COMPTON FEL REGIME, A COMBINATION OF HIGH CURRENT AND LOW EMITTANCE IS NECESSARY FOR HIGH PERFORMANCE.

INDUCTION LINAC DRIVEN FEL EXPERIMENTS

PARAMETERS	ETA ELF 1986	ATA PALLADIN PLANNED	ATA PALLADIN 1988	ATA "SUPER" PLANNED
Energy (MeV)	3.5	50	46	300
I_b(kA)	0.85	2	0.5	3
$\varepsilon_{n\ edge}$ (rad-cm)	.29	.14	.24	.055
r_b (cm)	.62	.44	.62	.19
λ_w (cm)	9.8	8	8	8
λ_s (cm)	0.87	1.06×10^{-3}	1.06×10^{-3}	10^{-4}
γ_z	2.9	61.4	61.4	200
$a_{w\ rms}$	2.52	1.26	1.09	2.76
B_w (kG)	3.72	2.38	1.96	3.69
Regime	Raman	Compton	Compton	Compton
$\Delta\ \gamma_{thermal}$	.04	.55	.85	.82
$\Delta\ \gamma_{fluid}$	.62	.40	.19	1.24
Linear Gain (dB/m)	34	5.4	1.8	5
$f_{trapped}$	75%	50%	< 1%	> 50%

BEAM QUALITY GOALS FOR FEL DRIVERS

PALADIN

50 MeV

2 kA

$\lambda_s = 10.6\ \mu m$

$\lambda_w = 8\ cm$

$r_b = 0.45\ cm$

$\varepsilon_n < 0.14$ Rad-cm

$B_n > 2 \times 10^5 \ \frac{A}{cm^2 - Rad^2}$

174 Acceleration Gaps

Accelerator Length 75 m

Wiggler Length 25 m

HIGH POWER, 1 μm FEL

300 MeV

3 kA

$\lambda_s = 1\ \mu m$

$\lambda_w = 8\ cm$

$r_b = 0.19\ cm$

$\varepsilon_n < 0.055$ Rad-cm

$B_n > 2 \times 10^6 \ \frac{A}{cm^2 - Rad^2}$

BEAM QUALITY GOALS FOR FEL DRIVERS

PALADIN

50 MeV

2 kA

$\lambda_s = 10.6\ \mu m$

$\lambda_w = 8\ cm$

$r_b = 0.45\ cm$

174 Acceleration Gaps

Accelerator Length 75 m

Wiggler Length 25 m

$\varepsilon_n < 0.14$ Rad-cm

$B_n > 2 \times 10^5 \ \frac{A}{cm^2 - Rad^2}$

HIGH POWER, 1 μm FEL

300 MeV

3 kA

$\lambda_s = 1\ \mu m$

$\lambda_w = 8\ cm$

$r_b = 0.19\ cm$

$\varepsilon_n < 0.055$ Rad-cm

$B_n > 2 \times 10^6 \ \frac{A}{cm^2 - Rad^2}$

APPENDIX B

SOURCE REGION BEAM EMITTANCE

Briefing Slides

POSSIBLE SOURCES OF POOR BEAM QUALITY

- HIGH CURRENT BEAM DIODE SOURCE

- BEAM TRANSPORT THRU MULTIPLE ACCELERATION GAPS

  -- Induced Sausaging Envelope Oscillations

  -- Amplification of Kinking Perturbations

     Beam Breakup Instability

     Image Displacement Instability

- BEAM HANDOFF INTO FEL

WHAT IS THE BEAM EMITTANCE OBTAINED AT THE SOURCE CATHODE?

TEMPERATURE: $\varepsilon_n = 2r_c(T/mc^2)^{1/2}$

$T = 0.1\,eV,\ r_c = \text{few cm} \Rightarrow \varepsilon_n = \text{few} \times 10^{-3}\,\text{rad-cm}$

SURFACE ROUGHNESS: $\varepsilon_n = 1.22\,(\gamma_o - 1)\left(\frac{h}{d}\right)^{3/5} \frac{h^{1/2}}{(h^2 + w^2)^{1/4}}\, r_b$

$\frac{h}{w} \sim 1 \qquad \frac{h}{d} \sim 10^{-3} \qquad r_b < 1\,cm$

$\Rightarrow \varepsilon_n = 10^{-3} \text{ -- } 10^{-2}\,\text{rad-cm}$

ANODE MESH SCATTERING: $\varepsilon_n = \frac{1}{2\sqrt{6}} \left(\frac{\gamma_o - 1}{\beta_o}\right)\frac{b}{d}\, r_b$

$\frac{b}{d} \sim \text{few} \times 10^{-2} \qquad r_b < 1\,cm$

$\Rightarrow \varepsilon_n = 10^{-3} \text{ -- } 10^{-2}\,\text{rad-cm}$

CONCLUSION: FOR MeV, kA DIODES, SOURCE EMITTANCE CAN BE HELD BELOW 10^{-2} RAD-CM WITH SOME CARE.

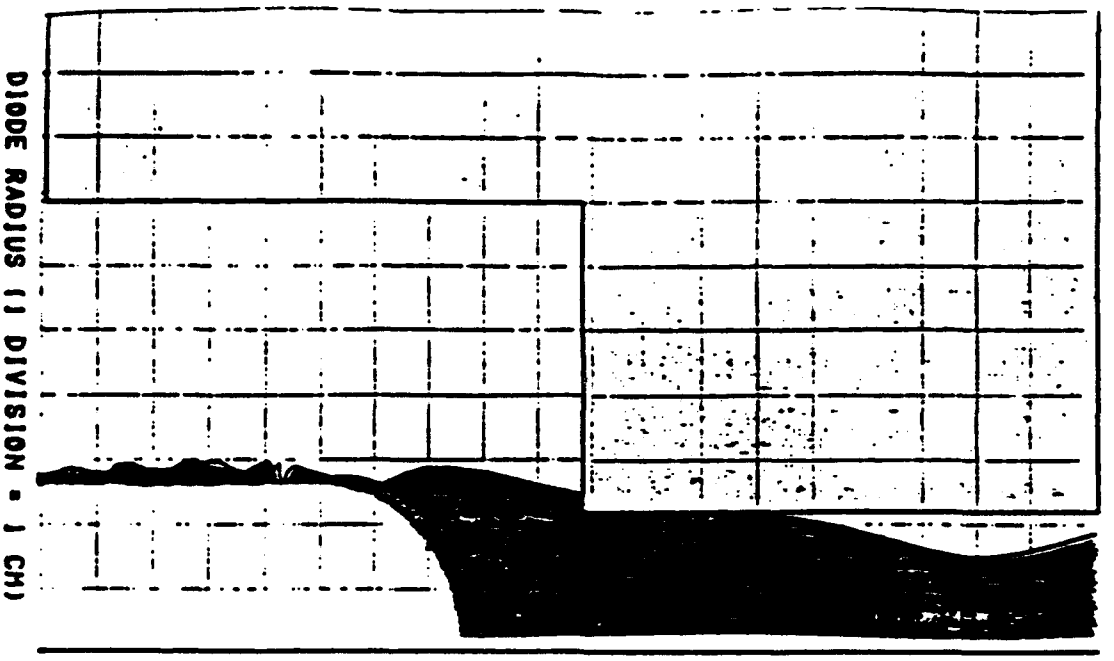

2.3 MV 11 KA 6.0 = BMAX(KG) 22 rad-mm = ε_n

(a) Square Anode Aperture

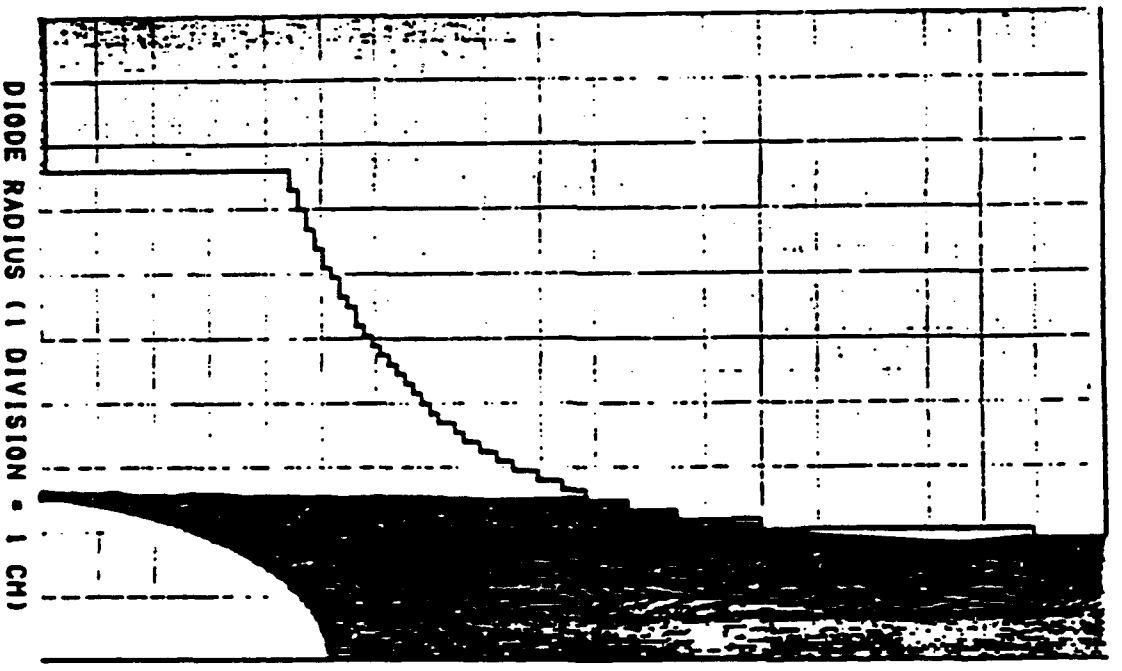

2.3 MV 12 kA 6.5 = BMAX(KG) 5.6 rad-mm = ε_n

(b) Exponentially Tapered Anode Aperture

Figure 2. An illustration of the improvement in beam quality which was achieved for a high current field emission diode by exponentially tapering the anode aperture.

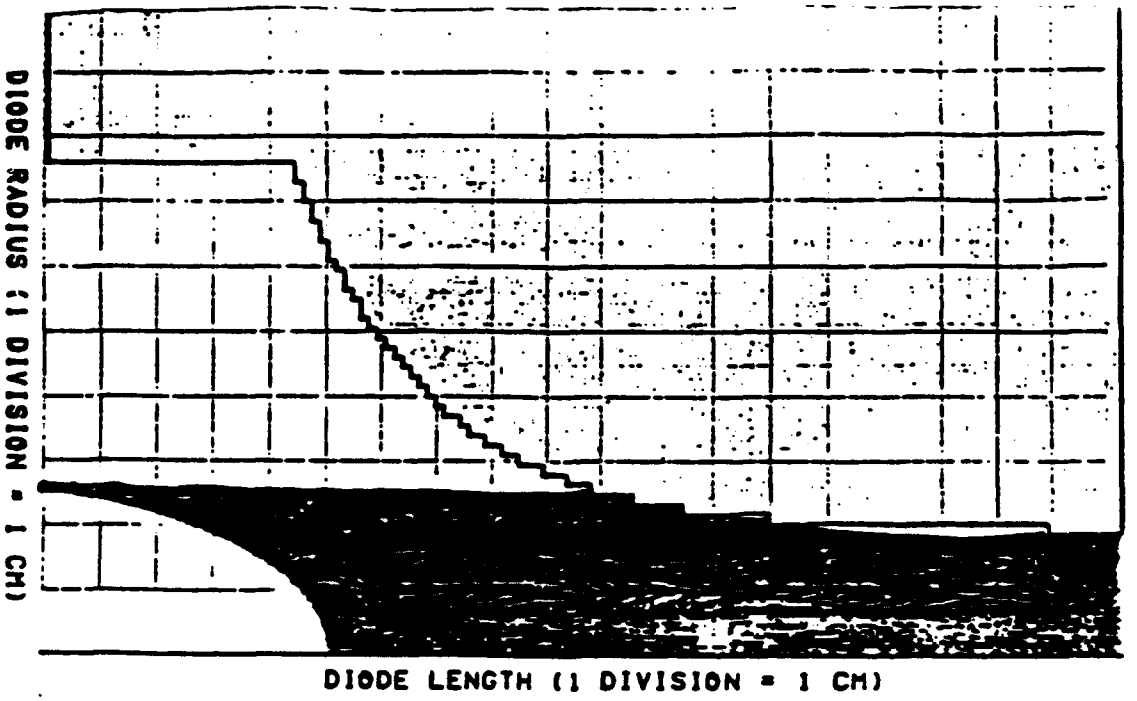

2.3 MV 12 kA 6.5 = BMAX(KG) 5.6 rad-mm = ε_n

(b) Exponentially Tapered Anode Aperture

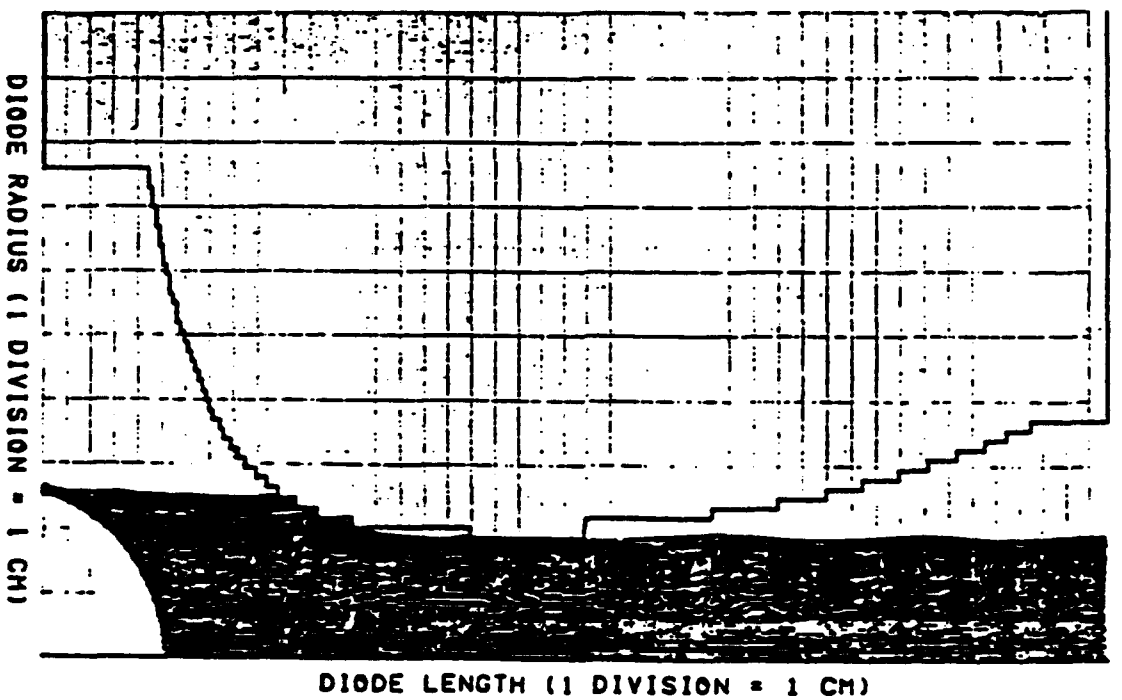

2.3 MV 15 kA 6.5 = BMAX(KG) 5.9 rad-mm = ε_n

(c) Tapered Anode Aperture, with Smooth Flaring

Figure 3. An illustration that the beam quality achieved for a high current field emission diode by smoothly tapering the anode aperture down, may be retained if the anode is later smoothly flared out.

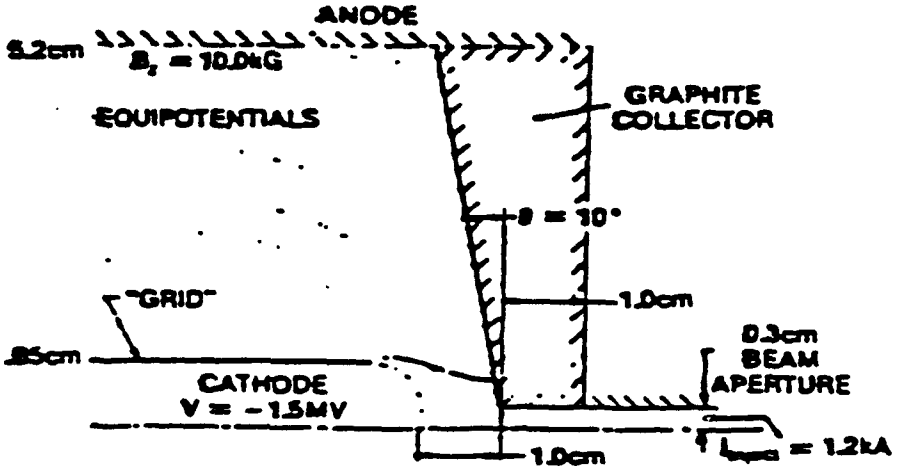

Fig. 3. The VEBA apertured diode with the calculated electron trajectories (only half of the trajectories are shown). Note the paraxial flow close to the axis between the cathode and anode, and the defocusing effect of the aperture.

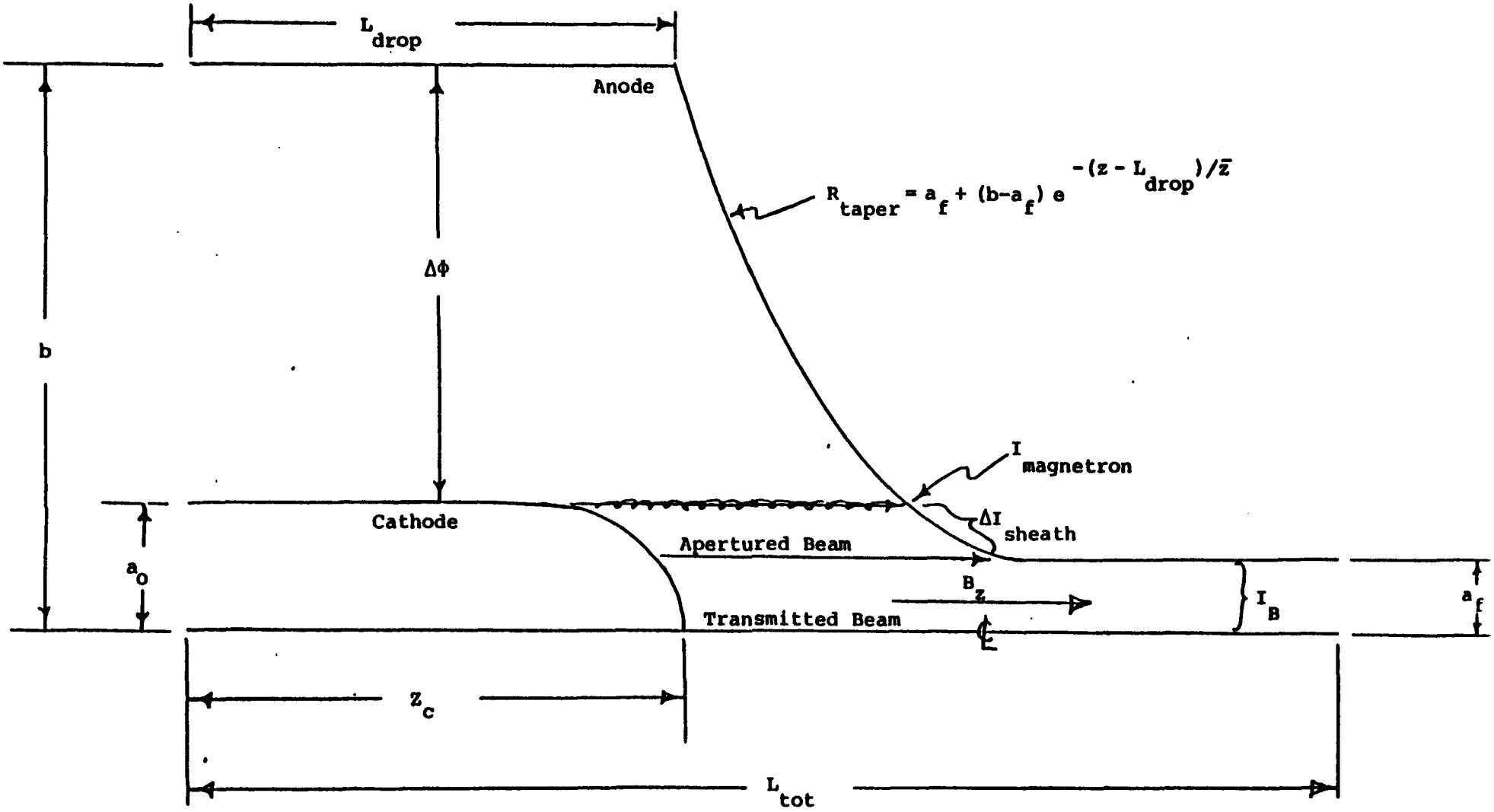

Figure 1. VEBA-like Foilless Diode Geometry

TABLE 1

PARAMETERS FOR BEAM QUALITY STUDIES
IN A MAGNETIZED, FOILLESS DIODE

	Low B_z, Smooth Anode Taper	High B_z, Smooth Anode Taper	High B_z, Sharp Anode Taper
$\Delta\Phi$	1.5 MV	1.5 MV	1.5 MV
$I_{magnetron}$	1.81 kA	0.47 kA	0.47 kA
ΔI_{sheath}	6.3 kA	8.0 kA	8.0 kA
I_B	1.2 kA	1.2 kA	1.2 kA
b	5.20 cm	5.20 cm	5.20 cm
a_o	0.85 cm	0.85 cm	0.85 cm
a_f	0.306 cm	0.306 cm	0.306 cm
L_{tot}	15.20 cm	15.20 cm	15.20 cm
L_{drop}	6.80 cm	6.80 cm	6.80 cm
z_c	6.60 cm	6.60 cm	5.64 cm
$\bar{z}$	0.51 cm	0.51 cm	0.034 cm
B_z	7.44 kG	15.0 kG	15.0 kG
$\langle\beta_\perp\rangle$	0.0221	0.0024	0.0605
$\gamma\langle\beta_\perp\rangle a_f$	27 mrad-cm	3 mrad-cm	73 mrad-cm
$\beta_z c/\Omega$	0.87 cm	0.43 cm	0.43 cm

Thus the transverse beam temperature is related to the Fourier transform of the forces acting upon the electrons in the diode region, evaluated at the gyrofrequency.

The transverse forces are given by

$$F_r = \frac{\gamma e}{m}(-E_r + \beta_z B_\phi) + \frac{p_\phi^2}{r} \simeq \frac{\gamma e}{m}(-E_r + \beta_z B_\phi)$$

$$F_\phi = -\frac{p_r p_\phi}{\gamma m} \simeq 0 \qquad \text{(A8)}$$

where the centrifugal and centripetal forces may be neglected in the strong magnetic field. Hence

$$\gamma\beta_\perp = \frac{1}{c}\left|\int_0^\infty d\tau\, F_r(\tau)\, e^{-i\Omega_0\tau}\right|$$

$$= \frac{e}{mc}\left|\int_0^\infty \frac{dz}{c\beta_z}(-E_r + \beta_z B_\phi)\, e^{-\left(\frac{i\Omega_0}{c}\int_0^z \frac{dz'}{\gamma\beta_z}\right)}\right| \qquad \text{(A9)}$$

It is apparent from Equation (A9) that large transverse velocity perturbations may result when the fields $E_r - \beta_z B_\phi$ have significant components on the same scale length as $\gamma\beta_z c/\Omega_0$. Likewise, increasing B_0 should significantly reduce $\beta_\perp$ by reducing the latter gyrolength below the transverse force gradient lengths.

MAGNETIC FIELD-IMMERSED DIODE DESIGN

$\varepsilon_n \approx 0.05$ rad-cm $\qquad B_n \approx 4 \times 10^6 \frac{A}{cm^2\ rad^2}$

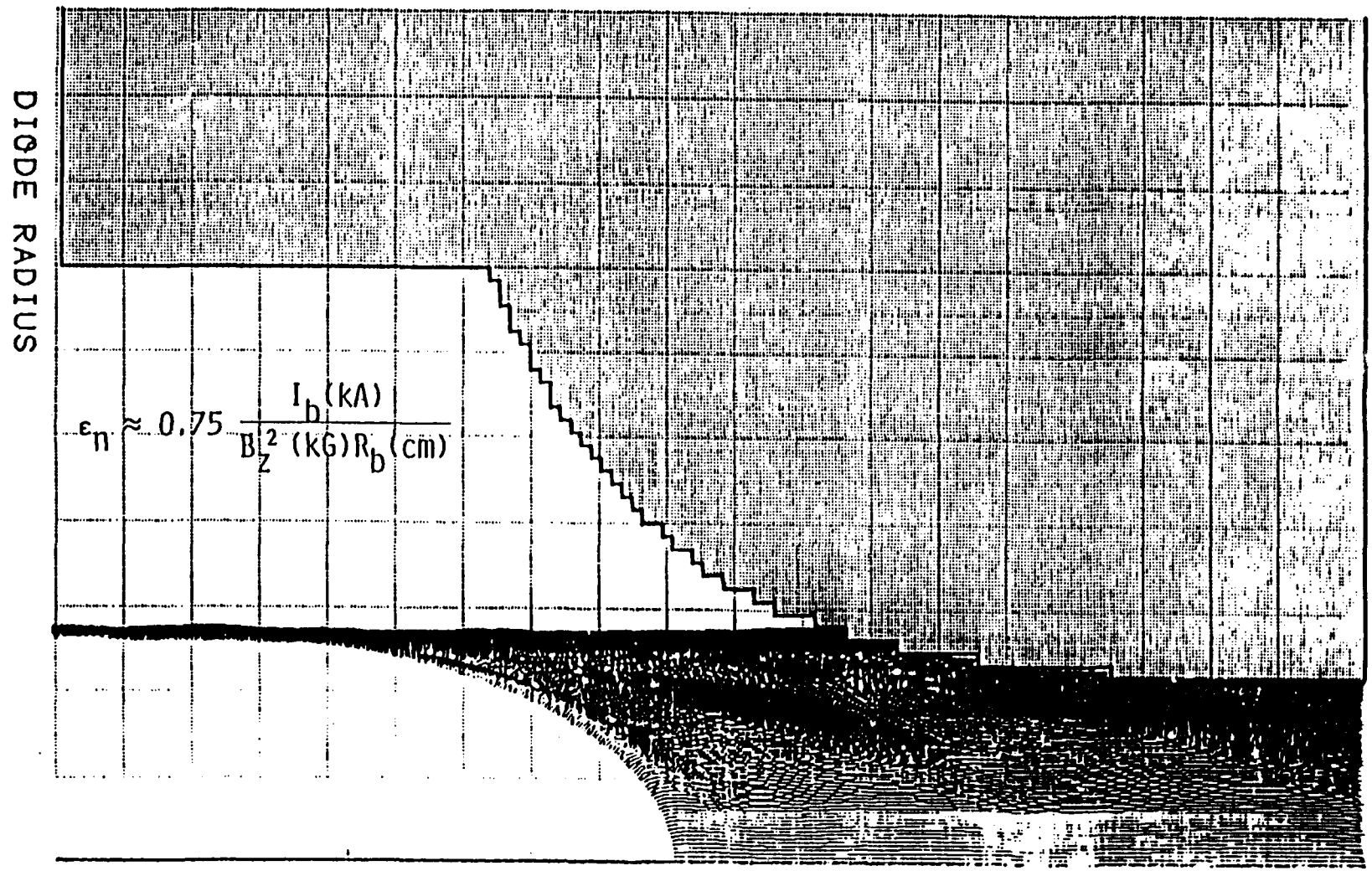

1.0 MV $\qquad$ 5.0 kA $\qquad$ $B_z = 13.6$ kG $\qquad$ $R_b = 0.43$ cm

APPENDIX C

A BRIEF DESCRIPTION OF THE ARA SIMULATION CODES

Three significant codes have been developed and utilized in the investigation of the properties of induction linac transport and handling of high current relativistic electron beams. These codes, DRIFTER, EIGENMODE, and BREAKUP, played critical roles in both developing and later confirming methods of attack suggested by analytical investigations for dealing with specific beam transport problems. Moreover, they provided a fundamental tool for investigations in those areas which for reasons of complexity are simply not amenable to direct analytical assault.

DRIFTER

The DRIFTER code is an axisymmetric, relativistic PIC, steady state transport code which follows the steady state propagation of a high density electron beam through an accelerator. This code is an outgrowth and refinement of an earlier code used for investigation of the high current electron beam behavior in an experimental charged particle beam research effort. Both relativistic, as well as non-relativistic motion can be simulated, allowing this code to provide information about the electron injection system as well as the actual acceleration section proper. The code allows for the employment of various transport elements, as well as variation in the size, shaping, and voltages applied to the drift tube walls in order to accurately simulate and gauge the effects of accelerator gap geometry. The nonlinear electron beam charge density and current are used to self-consistently calculate the beam self-potential and azimuthal magnetic field. The only field term which is not calculated self-consistently is the beam diamagnetic correction to the solenoidal guide field. Such corrections are neglected in the DRIFTER simulation.

The DRIFTER code has proven invaluable in examining the complex motion, subsequent heating (emittance growth), and sausaging motion acquired by relativistic electron beams in traversing various accelerator gap geometries, and provides confirmation of the very significant improvements in beam brightness afforded by the adiabatic acceleration gap geometries and judicial guide magnetic field profiling developed under this research effort.

EIGENMODE

The EIGENMODE code is not per se a full simulation code. Rather, it provides a detailed map of the electric and magnetic fields associated with the resonances of the induction accelerator gap geometry, as well as a determination of the resonant frequencies for each resonance. Such resonances play a fundamental role in the physics of the beam breakup instability.

Specifically, the EIGENMODE code determines the eigenmodes and eigenvalues of an axisymmetric, but otherwise arbitrary, cavity geometry. This geometry can be very complex, with the EIGENMODE code allowing a large number of internal structures (20 at present), comprised of conducting cylindrical segments, cones, annuli, rods of arbitrary orientation, and rings. The EIGENMODE code utilizes the electric field $\mathbf{E}(\mathbf{x}, t)$ as its fundamental variable, with the accompanying magnetic field easily calculated from the induction law

$$\dot{\boldsymbol{B}} = -\nabla \times \boldsymbol{E} \tag{1}$$

once $\mathbf{E}(\mathbf{x}, t)$ is determined.

Because the cavity is axisymmetric, the electric field can be Fourier resolved into azimuthal mode numbers

$$\mathbf{E}(x,t) = \boldsymbol{E}(R,z,t)e^{im\theta} \tag{2}$$

and each azimuthal mode m treated separately. The electric field is then specified on a staggered mesh in cylindrical R,Z coordinates. This staggered mesh provides not only centered differences for the electromagnetic fields, but at the same time allows proper specification of the electric field boundary conditions; namely only electric fields[1] on the conducting structures comprising the cavity structure are needed. Specification of the (often) discontinuous normal component of the electric field on the interior and boundary conducting surfaces is never required.

---

[1]For perfectly conducting cavity structures, the correct boundary conditions are that the tangential electric fields vanish on the conducting surfaces.

Once the cavity structure has been specified, the code calculates the cavity eigenmodes by undertaking a relaxation solution of the following non-physical equation governing the electric field **E**:

$$\dot{\mathbf{E}} = -\nabla \times (\nabla \times \boldsymbol{E}) \tag{3}$$

with initial data $\mathbf{E}_i$ (**x**) specified. The operator $\nabla \times \nabla \mathbf{x}$ is a Hermetian finite difference operator derived from the following quadratic finite difference variational form

$$\delta \int |\nabla \times \boldsymbol{E}|^2 \, d^3x \tag{4}$$

The use of such a Hermetian finite difference operator derived from a variational principle ensures that the eigenfrequencies are not only real, but second order accurate.

The manner in which this relaxation procedure provides information on the cavity eigenmodes can be demonstrated as follows:
The electric field of Equation (3) can, of course, be expanded in the eigenmodes of the cavity:

$$\mathbf{E}(\bar{x}, t) = \sum_{n=1}^{\infty} a_n(t) \; \mathbf{E}_n(x) \tag{5}$$

where $\mathbf{E}_n$ are the eigenmodes of the cavity structures

$$\nabla \times \nabla \times \boldsymbol{E}_n = \omega_n^2 \, \boldsymbol{E}_n \tag{6}$$

and where

$$\omega_1 < \omega_2 < \omega_3 \ldots \tag{7}$$

are the non-degenerate eigenfrequencies (resonant frequencies) of the cavity.

Using this expansion and the orthogonality property of the eigenmodes, the time behavior of the coefficients a_n is found from Equations (3), (5), (6), to be given by

$$\dot{a}_n = -\omega_n^2 a_n \qquad n = 1, 2, \ldots \tag{8}$$

These are immediately integrable, allowing the solution to the time development of the electric field E under Equation (5) to be expressed:

$$\mathbf{E}(x,t) = \sum_{n=1}^{\infty} a_n(0)\, e^{-\omega_n^2 t}\, E_n(x) \tag{9}$$

where $a_n(0)$ is the population of the nth eigenmode comprising the initial E field data load E_i. Not surprisingly, the solutions relax from the initial data to zero for large time. However, an examination of Equation (9) shows that as $t \to \infty$, the electric field solution is dominated by the lowest eigenmode with non-zero a_n, all higher eigenmodes damping more rapidly to zero. Therefore, by allowing the computer to mindlessly relaxation solve Equation (3) with an initial data load rich in eigenmodes (i.e., random noise load), after many iterations the electric field is completely dominated by the lowest order eigenmode.

$$\mathbf{E}(x,t) \to a_1\, e^{-\omega_1^2 t}\, E_1(x) \tag{10}$$

At this point, the lowest order eigenmode can then be read off directly from the E field spatial distribution and the eigenfrequency determined immediately from the time dependence of the solution.

Once the lowest order eigenmode has been determined, the electric field is re-initialized and a second relaxation solution carried out, except that the lowest eigenmode component of the initial data load is removed by application of a "scrubbing" operator to the initial data

$$\mathbf{E}_i'(x) = \nabla \times \nabla \times E_i(x) - \omega_1^2 E_i(x) \tag{11}$$

With the lowest eigenmode removed in $\mathbf{E}_1'$, the relaxation solution of Equation (3) now will asymptote to the next highest frequency eigenmode

$$\mathbf{E}(x,t) \rightarrow a_2 e^{-\omega_2^2 t} \mathbf{E}_2(x) \tag{12}$$

so that the second eigenmode and eigenfrequency may now be determined.

[Note, however, that since the scrubbing operation only reduces the lowest order eigenmode component to round off and since such roundoff error would eventually come to dominate the time asymptotic development of the electric field, since the first eigenmode has a smaller damping coefficient ($e^{-\omega_1^2 t}$) than the second eigenmode ($e^{-\omega_2^2 t}$, $\omega_2 > \omega_1$), periodic reapplication of the scrubbing operation is required to keep the lowest eigenmode suppressed.]

Once the second eigenmode and eigenfrequency are determined, one can similarly proceed to a determination of the third eigenmodes, except that scrubbing is now required of not only the lowest but the first eigenmode. Similarly for all higher eigenmodes, with scrubbing required of all lower eigenmodes to keep their contributions to the electric field suppressed.[2]

This procedure has provided extremely accurate determination of the eigenmodes and eigenfrequencies of even very complex cavities. Typically, six to eight eigenmodes can be determined within a very short period of time using modest computational resources. Eigenfrequencies are typically determined to one part in 10^9. Such an approach where all field components except the desired eigenmode $\mathbf{E}_n$ field are successfully damped away appears to provide a significant improvement over more conventional schemes which determine eigenmode structure and frequencies by shock excitation or source driving the cavity and subsequent decomposition of the resulting electric field structure into its related eigenmodes by Fourier transform in the time domain.

---

[2]In addition to the finite frequency eigenmodes, there is in fact an $\omega_0^2 = 0$ degenerate eigenmode characterized by $\mathbf{E}_0 = -\nabla\phi$ and associated with initial data loads that are not divergence free. Scrubbing of the initial data load and additional periodic scrubbing of this mode by the operator $\nabla \times \nabla \times$ during the relaxation procedure is also required.

The EIGENMODE code has provided crucial information about the m = 1 eigenmodes associated with BBU. In particular, examination of the electric field patterns of the particularly dangerous resonances, such as lower order TM resonances, has provided welcome guidance on the placement of Q spoiling materials within the cavity to attempt to eliminate or at least minimize BBU problems.

BREAKUP

The BREAKUP code provides a relativistic discrete cell simulation of the growth and saturation of the beam breakup instability driven by high current relativistic electron beams traversing an induction acceleration gap structure. This code utilizes the Hermetian $\nabla \times \nabla \times$ of the EIGENMODE code, as well as the cavity internal structure (i.e.., sheets, annuli, cones, etc.). However, in contrast to the EIGENMODE code, BREAKUP also allows the placement within and on the boundaries of the cavity of finite resistivity materials to provide Q spoiling of the cavity. Such resistive materials are characterized in Ohms/sq, with typical values for optimum loading ranging from 5-50 Ohms/sq.

Once the cavity and resistive loading structures are specified, the code allows for the selection of a band of frequencies (ω_0 - ω_1) to be examined. This band is further divided into (typically) 99 discrete frequencies and the incoming electron beam negative energy mode (the beam motion associated with BBU) modulated at these frequencies to provide coupling to the BBU modes. Maxwell's equation

$$\nabla \times \nabla \times \boldsymbol{E} = - \ddot{\boldsymbol{E}} - 4\pi \dot{\boldsymbol{J}}_b - 4\pi\sigma \dot{\boldsymbol{E}} \quad , \tag{13}$$

where $\mathbf{J_b}$ is the electron Beam BBU current driven at the discrete frequencies and $\sigma\mathbf{E}$ represents the currents induced in the resistive loading structures of the cavity, then allows the time development of the electric field to be followed for each discrete frequency until saturation, at which time gain factors for each frequency are determined and plotted. The results can then be compared to data from the EIGENMODE code to assess the role cavity resonances are playing in overall BBU behavior, to determine which resonances are most dangerous, and to determine how

best to configure resistive structures to mitigate BBU effects. Theoretically predicted behavior such as phase cancellation of BBU growth for strong solenoidal transport fields can also be confirmed and quantified through BREAKUP simulation studies.

APPENDIX D

BEAM HANDLING AND EMITTANCE CONTROL

James R. Thompson, M. L. Sloan, J. R. Uglum, and B. N. Moore, Proc. SPIE, Microwave and Particle Beam Sources and Directed Energy Concepts, Vol. 1061, 454 (1989).

Beam handling and emittance control

J. R. Thompson, M. L. Sloan, J. R. Uglum, and B. N. Moore

Austin Research Associates
1901 Rutland Drive, Austin, Texas 78758

ABSTRACT

Image charge electric fields can produce large cumulative erosion of the brightness of a high current electron beam during transport through successive high-gradient accelerating gaps. However, this erosion in beam brightness may be significantly reduced through the use of smoothly shaped, impedance-matched accelerating gaps with optimized gap-to-gap spacing. Moreover, for beams transported with solenoidal magnetic focusing, it is possible to spatially tune the solenoidal field within the accelerating gaps to compensate the image charge perturbations. Calculations suggest that with such techniques it is possible to deliver from a multi-gap accelerator, high current beams whose diode brightness is essentially preserved during transport and acceleration. If disruptive, high current beam kinking instabilities are also controlled, such high-brightness beams are uniquely capable of driving high performance FEL operation at wavelengths in the infrared and below.

1. INTRODUCTION

Advanced electron accelerators will emphasize high current (1 kA or more) concepts that can be scaled to energies of a few hundred megavolts--capabilities which are beyond anything now in existence. As such accelerators are developed, the evolution toward higher currents, higher particle energy, and higher acceleration gradients all conspire to make it more difficult to preserve the necessary beam quality and brightness (i.e., low emittance and energy spread at high current). These requirements are particularly stringent for free electron laser (FEL) devices, where to the extent possible all electrons should have the same axial velocity $\beta_z c$ to match the axial phase velocity of the FEL ponderomotive wave.

In particular, high performance FEL operation requires low emittance ($\varepsilon_n = x_\perp \gamma\beta_\perp$) and high beam brightness ($B_n = 2I_b/\varepsilon_n^2$) in order to obtain high levels of linear gain, saturated power, trapping efficiency, nonlinear gain, and output laser power. Furthermore, the required beam quality goals become more difficult to achieve as the FEL laser wavelength is reduced. For example, in the ongoing Livermore PALADIN FEL experiment,[1] an electron beam driver of 50 MeV, 2 kA, and 0.45 cm radius interacts with a wiggler of 8 cm wavelength to produce 10.6 μm radiation. The desired beam quality goals for an efficient, hydrodynamic FEL interaction are $\varepsilon_n < 0.14$ rad-cm and $B_n > 2 \times 10^5$ A/cm^2-rad^2. In comparison, a high power 1 μm FEL, driven by a 300 MeV, 3 kA, 0.2 cm radius electron beam in a similar wiggler, would have more difficult beam quality goals of $\varepsilon_n < 0.055$ rad-cm and $B_n > 2 \times 10^6$ A/cm^2-rad^2.

Unfortunately, even the milder PALADIN-like beam quality requirements for efficient high power FEL operation in the infrared have not yet been achieved experimentally for beams transported to the FEL.[2] A major culprit appears to be the erosion of beam brightness which occurs due to image charge effects or beam instability during transport through multiple acceleration gaps. Moreover, beam quality may be reduced in the operation of a high current beam diode source, or during beam handoff between different focusing fields, or during injection into the FEL.

We describe herein an analysis of beam handling and emittance control, using solenoidal magnetic transport of high current beams extracted from magnetic field-immersed diodes. The emittance control techniques include optimized geometric shaping and spacing of conducting acceleration gap structures, as well as magnetic tuning during beam acceleration. The unique advantages of this approach include the brighter diodes which are generally possible with magnetic field immersion, plus the large reduction in emittance growth during acceleration, which results from the magnetic tunability.

2. ANALYSIS OF EMITTANCE AND EMITTANCE GROWTH DURING SOLENOIDAL MAGNETIC TRANSPORT OF BEAMS FROM FIELD-IMMERSED CATHODES

There are a number of problems which can arise during the generation, transport, and acceleration of high current electron beams which have the potential for causing significant degradation of the beam quality. The category of problems which is addressed herein concerns sausaging envelope oscillations which may be induced upon a steady state, azimuthally symmetric, propagating electron beam. Another category of problems which has

been widely investigated, but which is not discussed herein, concerns the amplification of time dependent, $m = 1$ kinking perturbations during beam transport and acceleration. This category includes the beam breakup instability and the image displacement instability. However, the techniques which we describe for the control of sausaging oscillations are not inconsistent with the measures needed to control the kinking instabilities.

The tools which we have employed in the analysis of the steady state, $m = 0$ sausaging oscillations are two-dimensional (r,z), steady state, electromagnetic, relativistic particle simulations, together with theoretical analysis based largely upon a beam "envelope equation,"[3,4,5,6] which describes the axial behavior of the radial beam envelope in terms of the electric and magnetic potentials and their gradients with respect to the axial z coordinate. This work is an extension of preliminary calculations described previously.[7]

2.1 Emittance Control in Magnetic Field-Immersed Diodes

It is well recognized that emittance growth tends to be most severe at low beam energy. Consequently, emittance which is created in the diode itself can well be significant, if particular care is not taken in the diode design. One approach which has been shown[8,9,10] capable of producing very low emittance, high current beams is that of employing gently-shaped foilless anode-cathode structures which are immersed in a strong magnetic guide field. The anode taper is brought down to a radius somewhat less than that of the cathode shank, so that the hot shank-emitted electrons are apertured from the transmitted beam. One may employ a computational design procedure[8] which allows the desired output current density profile $J_z(r)$ to be specified, and the cathode shape needed to produce this profile may then be determined.

Analysis reveals that in such field-immersed diodes, emittance is created near the cathode surface, as the radial component of the electric field--not yet compensated by the $v_z B_\phi$ Lorentz forces--tends to drive electrons out across the axial guide field B_z. The electrons quickly acquire a slow azimuthal velocity $\beta_\phi c$, and approach the usual propagating equilibrium in which $\beta_\phi B_z$ pinch forces balance the outward $E_r - B_z B_\phi$ forces. The stronger the guide field B_z, the more quickly equilibrium is achieved, and the lower the acquired diode emittance becomes. A rough theoretical estimate, which has been found in fair agreement with diode simulation studies, is

$$\varepsilon_n \approx 0.75 \frac{I_b\,(kA)}{B_z^2\,(kG)\,r_b\,(cm)} \quad \text{rad-cm} \tag{1}$$

where I_b is the beam current transmitted within radius r_b.

It is apparent that the strong B_z dependence of Equation (1) can be exploited to reach the desired diode emittance by designing a small radius, high B_z diode, and subsequently expanding the beam along a $B_z r_b^2$ flux surface to the larger radius, smaller B_z values desired for beam transport. For example, a beam of $I_b = 5$ kA can be created in a field-immersed diode with $r_b = 0.43$ cm, $B_z = 13.6$ kG to have an emittance $\varepsilon_n \approx 0.05$ rad-cm, and brightness $B_n \approx 4 \times 10^6$ A/cm^2-rad^2. This beam quality would be adequate even for a high performance, high power, 1 μm FEL, and such a beam could be transported along a solenoidal magnetic flux surface of $B_z r_b^2 \approx 2.5$ kG-cm^2.

2.2 Emittance Control During Multi-Gap Acceleration

Experience with multi-gap induction accelerators (e.g., the Advanced Test Accelerator of the PALADIN experiment contains some 174 gaps) reveals that even when the diode emittance is fairly low, very significant emittance growth often occurs during the multi-gap acceleration. For example, Figure 1 shows the transport of a 5 kA, 1 cm beam of 1 MeV input energy, along a 2.5 kG B_z field through two square induction gaps of 0.25 MV each. The beam is found to gain normalized edge emittance of about $\Delta\varepsilon_n \approx 0.15$ rad-cm in each gap, and the gap spacing is such that the emittance adds coherently in this case. In the remainder of this paper, we develop the scaling laws which describe gap-excited emittance, and present strategies for minimizing such beam oscillations.

It should be remarked that such large, coherent envelope oscillations--largely cyclotron oscillations for immersed cathode, solenoidal transport--are detrimental to FEL performance even prior to phase mixing. Despite the fact that β_r and β_ϕ are out of phase such that $\beta_\perp^2$ is approximately uniform axially, there is a large radial spread in $\beta_\perp^2$ which is detrimental to a hydrodynamical FEL interaction.

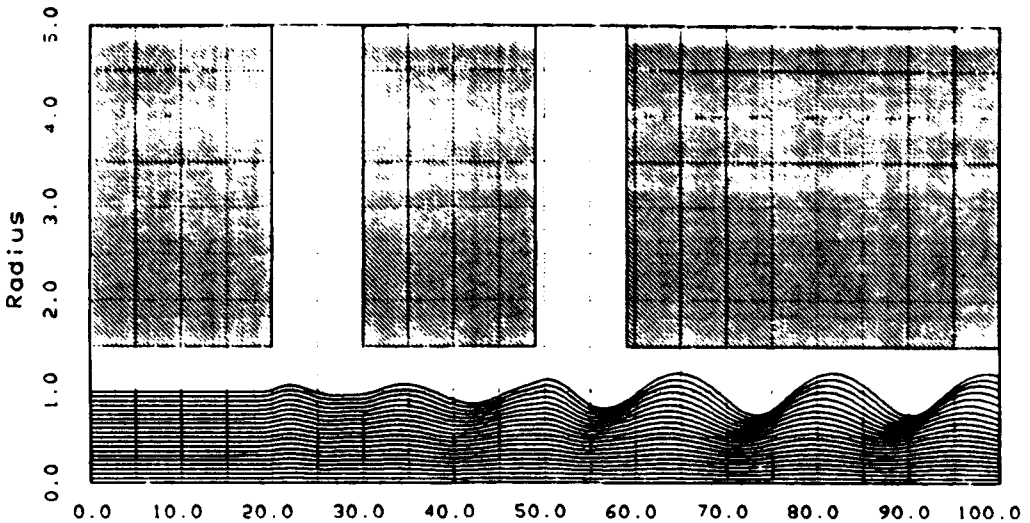

$V_{INJ} = 1.0$ MV $\quad V_{GAP} = 0.25$ MV $\quad I = 5.0$ kA $\quad B_z = 2.5$ kG

$L_{GAP} = 10$ cm $\quad D_{GAP\text{-}TO\text{-}GAP} = 29$ cm $\approx 2\lambda$ $\quad \varepsilon_{n\ edge} = 0.30$ rad-cm

Figure 1. Transport of a high current beam past two radial feed acceleration gaps.

The analysis of such envelope oscillations is based upon the beam envelope equation, obtained as follows. For steady state, azimuthally symmetric beam flow, the relativistic radial force equation

$$\frac{d}{dt}\gamma\beta_r = -\frac{e}{mc}\beta_\phi B_z - \frac{e}{mc}\left(E_r - B_z B_\phi\right) + \frac{c\gamma\beta_\phi^2}{r} \tag{2}$$

may be combined with the azimuthal canonical momentum constant

$$P_\phi = \gamma r \beta_\phi - \frac{eB_z}{mc^2}\frac{r^2}{2} \tag{3}$$

to eliminate β_ϕ. Maxwell's equations may then be used, under the paraxial approximation, to obtain E_r and B_ϕ in terms of the beam current, energy, and radius, such that Equation (2) is converted into the beam envelope equation

$$0 = \gamma^2\beta^2 r'' + \gamma\gamma' r' + \left(\frac{\gamma\gamma''}{2} + \frac{\Omega_o^2}{4c^2}\right) r - \frac{2I_b}{mc^3/e}\frac{1}{\gamma\beta r} - \frac{\left(P_\phi^2 + \varepsilon_n^2\right)}{r^3} \tag{4}$$

where $\Omega_o = eB_z/mc^2$, I_b is the magnitude of the beam current, $(\gamma-1)mc^2$ is the beam energy, $\beta c = \beta_z c$ is the beam velocity, $mc^3/e = 17$ kA, ε_n is the normalized beam thermal emittance, and in Equation (4), r is the radius of the beam envelope. The primes represent derivatives with respect to the axial z coordinate. It is assumed that the axial dependences of $B_z(z)$ and $\gamma(z)$ are known, and Equation (4) is then to be solved for $r(z)$. Knowledge of γ is equivalent to knowledge of the electric potential Φ since $\gamma - e\Phi/mc^2$ is constant for steady state flow.

In the paraxial approximation, it is presumed that γ, β_z, B_z, and the beam axial current density J_z are roughly uniform in r; P_ϕ, $\varepsilon_n \propto r^2$; and β_r, β_ϕ, E_r, $B_\phi \propto r$. Then Equation (2) is self-similar, such that $r_1(z)/r_2(z)$ is constant for the trajectories of particles at any radii r_1 and r_2.

In the envelope equation (4), the Ω_o^2 term represents a portion of the solenoidal magnetic focusing; the I_b term represents the net outward $E_r - \beta_z B_\phi$ force due to the self space charge of the beam; the P_ϕ^2 term represents a portion of the magnetic focusing and the outward centrifugal forces; the ε_n^2 term represents the outward pressure of existing thermal emittance; and the γ'' term represents radial electric fields other than the beam self radial field, typically produced by image charges which concentrate at the acceleration gaps. For slowly rotating, magnetically focused beams, the net self space charge forces represented by I_b are relatively weak; the greater danger for the excitation of envelope oscillations is posed by the γ'' radial image charge fields.

The relationship between the γ'' image charge forces and the geometry of the acceleration gap walls may be developed as in prior work.[7] Let $z = 0$ be the beginning of the acceleration gap, where a zero potential wall ends--corresponding to the 20 cm point in Figure 1. The total electric potential $\Phi(r,z)$ is decomposed into $\phi_o(r)$ plus $\phi_1(r,z)$, where $\phi_o(r)$ represents the unperturbed beam space charge [i.e., $\nabla_r^2 \phi_o(r) = -4\pi\rho$] and $\phi_1(r,z)$ is the remaining homogeneous part of the potential [i.e., $(\nabla_r^2 + \nabla_z^2)\,\phi_1(r,z) = 0$] needed to satisfy the boundary conditions on the acceleration gap wall $b(z)$, which are

$$\phi_1[r = b(z), z] = \begin{cases} -\phi_o[r = b(z) = b_o] = 0 & , z < 0 \\ \Delta\Phi - \phi_o[r = b(z)] = \Delta\Phi + \dfrac{mc^2}{e}\, 2\nu\, \ell n\, \dfrac{b_o}{b(z)} & , z > 0 \end{cases} \tag{5}$$

where $\Delta\Phi$ is the potential jump across the accelerating gaps, and $\nu = I_b/(\beta_z mc^3/e)$ is the Budker parameter. It is presumed that at the downstream end of the gap, $z = L$, $b(z = L) = b_o$.

Assuming that reasonably gentle axial variations occur in $b(z)$, and that $b/L \ll 1$, in the spirit of the paraxial approximation a power series solution for $\phi_1(r,z)$ may be developed in the form

$$\phi_1(r,z) = g(z) - \frac{r^2}{4}\, g''(z) + \ldots \tag{6}$$

and the application of the boundary conditions (5) leads to a solution for $\phi_1(r,z) = \phi_1[r,b(z)]$ valid for *arbitrary downstream* wall profiles $b(z)$:

$$\frac{e\phi_1(r,z)}{mc^2} = \begin{cases} 0 & , z < 0 \\ \Delta\gamma - 2\nu \left| \ell n\, \dfrac{b(z)}{b_o} + \left(1 - \dfrac{r^2}{b^2}\right)\left(\dfrac{bb'' - b'^2}{4}\right) + \ldots \right| & , z > 0 \end{cases} \tag{7}$$

where $\Delta\gamma = e\Delta\Phi/mc^2$. The leading z-dependent term of Equation (7) becomes

$$\delta\gamma(z) = \frac{e\phi_1(z)}{mc^2} = \begin{cases} 0 & , z < 0 \\ \Delta\gamma - 2\nu\, \ell n\, \dfrac{b(z)}{b_o} & , 0 < z < L \\ \Delta\gamma & , L < z \end{cases} \tag{8}$$

where $\gamma = \gamma_o(r) + \delta\gamma(z) + \ldots$, and the perturbing electric fields which correspond to the wall potential ϕ_1 may be expressed to lowest order as

$$\frac{e E_{1z}}{mc^2} = -\gamma' + \ldots = -\delta\gamma' + \ldots \tag{9}$$

$$\frac{e E_{1r}}{mc^2} = \frac{1}{2}\, r\, \gamma'' + \ldots = \frac{1}{2}\, r\, \delta\gamma'' + \ldots \tag{10}$$

It is these image charge fields $\tilde{E}_1$ which are a major source of gap-excited envelope oscillations, described by Equation (4). Equation (8) relates these fields to the gap geometry $b(z)$.

In order to quantify the amount of transverse beam perturbation induced by an accelerating gap, it is straightforward to perform a linearized perturbation analysis of the envelope equation. If the beam is presumed to be in a smooth, slowly rotating equilibrium at $z = -\infty$, with $\gamma = \gamma_o$, $r = r_o$, and if the magnetic field B_z remains uniform through the gap, and if the gap induces electric fields which perturb $\gamma = \gamma_o + \delta\gamma(z)$, then corresponding radial perturbations $r = r_o + \delta r(z)$ will occur which are described by the linearized envelope equation

$$\delta r'' + k^2 \delta r = S(z) \tag{11}$$

where

$$k^2 \equiv \frac{\Omega_o^2}{\gamma_o^2 \beta_o^2 c^2} - \frac{4I_b}{mc^3/e} \frac{1}{\gamma_o^3 \beta_o^3 r_o^2} \tag{12}$$

and

$$S(z) \equiv - \frac{r_o}{2\gamma_o \beta_o^2} \left[\delta\gamma'' + \frac{2I_b}{mc^3/e} \frac{1}{\gamma_o^3 \beta_o^3 r_o^2} \delta\gamma \right] \tag{13}$$

The envelope oscillations are thus described as a driven harmonic oscillator, with restoring frequency $k\beta_o c = [(\Omega_o^2/\gamma_o^2) - (4\nu c^2/\gamma_o^3 r_o^2)]^{\frac{1}{2}}$ near the relativistic gyrofrequency. The solution to Equation (11) may be immediately given as

$$\delta r(z) = \frac{1}{k} \int_{-\infty}^{z} dz' \, S(z') \sin k(z - z') \tag{14}$$

so that

$$\delta\beta_r(z) = \beta_o \int_{-\infty}^{z} dz' \, S(z') \cos k (z \; z') \tag{15}$$

It follows that downstream of the gap,

$$\delta\beta_r(z > L) = \frac{k r_o}{2\gamma_o \beta_o} \left(1 - \frac{4\nu}{\gamma_o^3 \beta_o^2 k^2 r_o^2} \right) \int_{o}^{L} dz' \, \delta\gamma'(z') \sin k (z - z') \tag{16}$$

where $S(z')$ has been inserted and integrations by parts performed, under the assumption that $\delta\gamma'(z)$ vanishes for $z < 0$ or $z > L$. The growth in normalized edge emittance across the gap may be given as

$$\Delta\varepsilon_n = r_o \gamma_o \delta\beta_r \tag{17}$$

since $\delta\beta_r$ and $\delta\beta_\phi$ are $\pi/2$ out of phase for cyclotron oscillations which exceed the equilibrium precession velocity, and since $|\delta r| << r_o$ (except for poorly designed gaps such as those of Figure 1).

From Equations (8) and (16), it is possible to investigate the influence upon emittance growth of factors such as the gap shape and length, as well as the beam parameters γ_o, ν, and r_o. It is also possible to estimate how emittance growth will cumulate over many gaps. By returning to Equation (15), the specific effect of gap-to-gap spacing can be studied, and from the original Equation (4), the criterion for magnetic tuning may be obtained. Finally, the effect of fluctuations in current may be assessed. Each of these various facets of emittance control design will be discussed in turn.

2.3 Effect of Gap Shape and Length Upon Emittance Growth

Equation (16) suggests that smooth transitions in $\delta\gamma(z)$ across the gap are to be desired. Equation (8) indicates that there is a particular value of the Budker parameter $\nu = I_b/(\beta_o mc^3/e)$, namely

$$\nu_o = \Delta\gamma \Big/ \left(2\ell n \frac{b(z = 0+)}{b_o} \right) \tag{18}$$

for which $\delta\gamma(z)$ may be continuous for any continuous gap shape $b(z)$. Let the gap shape $b(z)$ be parameterized as

$$\frac{b(z)}{b_o} = \left[\frac{b(z=0+)}{b_o}\right]^{f(z)} \tag{19}$$

where $f(z)$ is any continuous function between $f(0) = 1$ and $f(L) = 0$, and b_o is the radius of the drift tube upstream and downstream of the gap. It then follows from Equation (8) that

$$\delta\gamma'(z) = \Delta\gamma\left[\left(1 - \frac{\nu}{\nu_o}\right)\delta(z) - \frac{\nu}{\nu_o} f'(z)\right], \quad 0 < z < L \tag{20}$$

and $\delta\gamma'(z) = 0$ outside of the gap.

One particular gap shape which we have examined is given by Equation (19) with the choice

$$f(z) = f_o(z) \equiv 1 - \frac{z}{L} + \frac{1}{2\pi}\sin\frac{2\pi z}{L} \tag{21}$$

where L is the length of the gap. From Equations (16) and (20), one finds that for any function $f(z)$ such that $f'(z)$ is symmetric about $z = L/2$,

$$\delta\beta_r = \frac{k r_o \Delta\gamma}{2\gamma_o \beta_o}\left(1 - \frac{4\nu}{\gamma_o^3 \beta_o^2 k^2 r_o^2}\right)\left[\left(1 - \frac{\nu}{\nu_o}\right)\sin k z + \frac{\nu}{\nu_o} h(kL)\sin k\left(z - \frac{L}{2}\right)\right] \tag{22}$$

where

$$h(kL) \equiv -\int_o^L dz\ f'(z)\cos k\,(z - L/2) \tag{23}$$

and therefore

$$\Delta\varepsilon = \frac{k r_o^2 \Delta\gamma}{2\beta_o}\left(1 - \frac{4\nu}{\gamma_o^3 \beta_o^2 k^2 r_o^2}\right)\left\{\left[1 - \frac{\nu}{\nu_o}\left(1 - h(kL)\cos\frac{kL}{2}\right)\right]^2 + \frac{\nu^2}{\nu_o^2} h^2(kL)\sin^2\frac{kL}{2}\right\}^{\frac{1}{2}} \tag{24}$$

is the magnitude of the growth in edge emittance excitations. Gaps for which $\nu = \nu_o$ will be said to be impedance matched, which is generally desirable, as it eliminates the δ-function kicks at the beginning of the gap. For impedance-matched gaps,

$$\Delta\varepsilon_n = \frac{k r_o^2 \Delta\gamma}{2\beta_o}\left(1 - \frac{4\nu}{\gamma_o^3 \beta_o^2 k^2 r_o^2}\right)\left|h(kL)\right| \tag{25}$$

and for the particular gap of Equation (21),

$$h_o(kL) = \frac{\sin\frac{kL}{2}}{\frac{kL}{2}\left(1 - \frac{k^2L^2}{4\pi^2}\right)} \tag{26}$$

In general, it may be shown that $|h(kL)| \leq 1$ and that $h(o) = 1$. The function $h(kL)$ has a central lobe near $kL = 0$, and smaller side lobes for kL large. Obviously, longer gaps yield lower emittance growth, but at the expense of a longer accelerator. Nevertheless, simply having a smooth gap allows a reduction in emittance growth below that seen in Figure 1. For example, Figure 2 shows the beam transport through an $f_o(z)$ gap for which $L = 10$ cm $= 0.77\,\lambda$ (where $\lambda = 2\pi/k$ is the wavelength of the envelope oscillations). The result is that the growth in normalized edge emittance is reduced by a factor of three below that of the square gap in Figure 1, to a level of $\Delta\varepsilon_n \approx 0.05$ rad-cm.

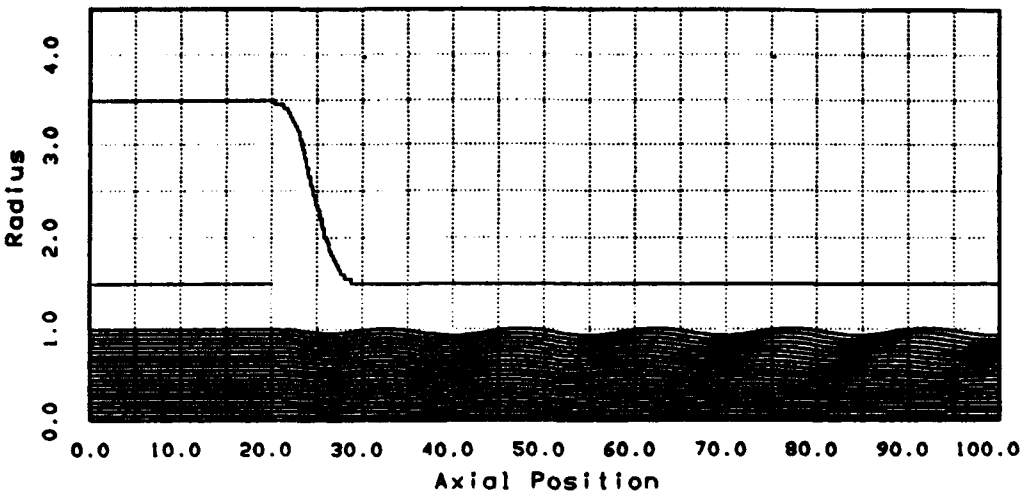

$V_{INJ} = 1.0$ MV $V_{GAP} = 0.25$ MV $I = 5.0$ kA $B_z = 2.5$ kG

$L_{GAP} = 10$ cm $\approx 0.77\lambda$ $\Delta\varepsilon_{n\ edge} \approx 0.050$ rad-cm

Figure 2. Transport of a high current beam past a smooth, narrow, impedance-matched gap.

For almost any smooth gap shape function $f(z)$, the gap excitation function $h(kL)$ will be found to have nulls at certain discrete values of kL. For the function $f_o(z)$, the nulls of $h_o(kL)$ occur at

$$\frac{kL}{2\pi} = \frac{L}{\lambda} = 2, 3, 4, \ldots \qquad (27)$$

The physics of such nulls is that for gaps of these lengths, the image charge perturbations applied to the beam during the first half of the gap are cancelled by countervailing perturbations applied during the second half of the gap. An example of beam acceleration through a gap of length chosen for cancellation of excitations is shown in Figure 3, for an $f_o(z)$ gap for which $L = 26$ cm $\approx 2\lambda$. The result is that a high degree of cancellation was indeed observed, with the growth in normalized edge emittance reduced an additional factor of nine below that of the gap in Figure 2, to a level of $\Delta\varepsilon_n \approx 0.0057$ rad-cm.

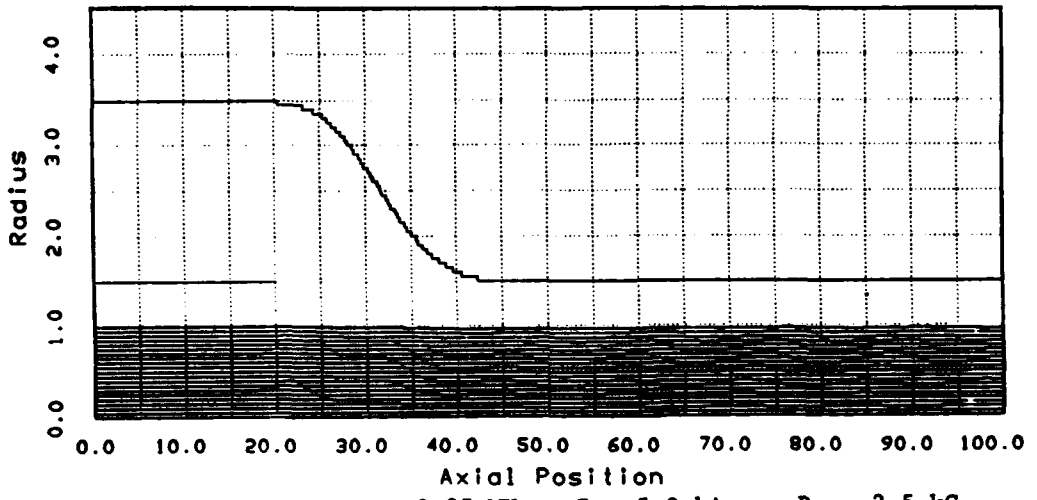

$V_{INJ} = 1.0$ MV $V_{GAP} = 0.25$ MV $I = 5.0$ kA $B_z = 2.5$ kG

$L_{GAP} = 26$ cm $\approx 2\lambda$ $\Delta\varepsilon_{n\ edge} \approx 0.0057$ rad-cm

Figure 3. Transport of a high current beam past a smooth, wide, impedance-matched gap.

Unfortunately, the strategy of selecting the gap lengths L to be a multiple of envelope wavelengths λ is expensive. Equation (12) reveals that for well-magnetized relativistic beams, λ is approximately proportional to $\gamma(z)/B_z(z)$, which normally increases significantly down the multi-gap accelerator. Therefore, successive gaps would have to be made successively longer in order to continue to exploit the intragap cancellations. It will be seen that alternate emittance control techniques are much less onerous than this, although intragap cancellation might be used in the first few gaps.

It may be observed from Equation (25) that as the beam passes down the accelerator to higher and higher energy, the amount of gap excitation should diminish. The current corrections to the wave number k [i.e., Equation (12)] and to the emittance growth [i.e., Equation (25)], which are proportional to $I_b/\gamma_o\beta_o B_z^2 r_o^2$, will become insignificant at high energy. Likewise, kL will diminish with energy (unless L is continually increased), so that $h(kL)$ approaches unity. Therefore, at high energy, the amount of emittance growth for impedance-matched gaps should approach

$$\Delta\varepsilon_n \approx \frac{\Omega_o r_o^2 \Delta\gamma}{2\gamma_o \beta_o^2 c} \tag{28}$$

which declines as γ^{-1} if $B_z r_o^2$ and $\Delta\gamma$ are uniform down the accelerator. Figure 4 illustrates the acceleration of a 22 MeV, 5 kA, 0.5 cm beam through a 0.25 MeV gap, in a 10 kG guide field--along the same 2.5 kG-cm^2 flux surface as that of the beams in Figures 2 and 3. The predicted growth in normalized edge emittance of 0.0080 rad-cm is in good agreement with the observed value of 0.0077 rad-cm, which is only about 15% of the emittance growth seen in Figure 2 at much lower energy.

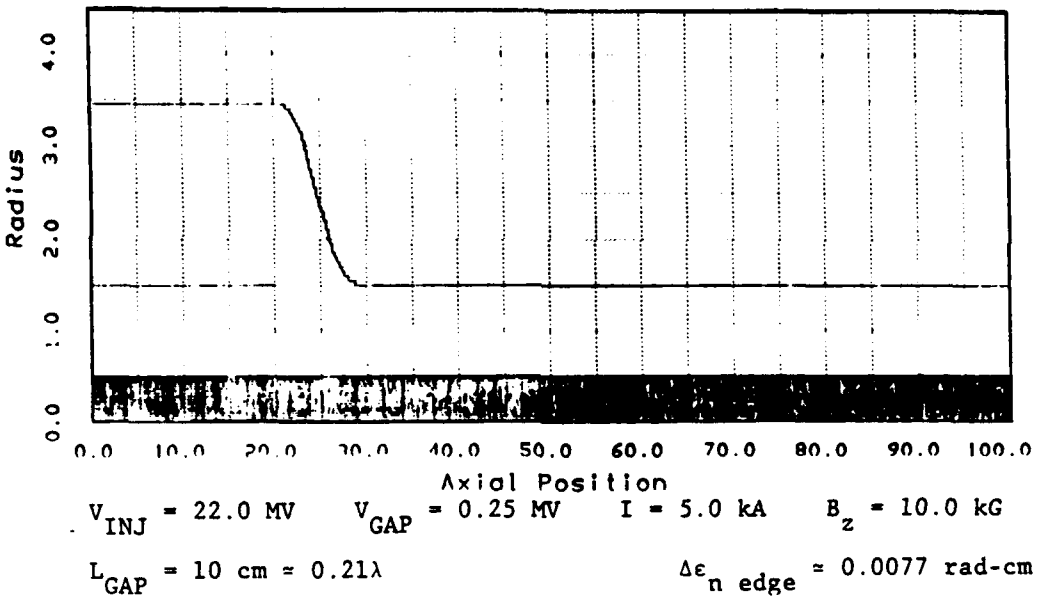

Figure 4. Transport of a high current, high energy beam past a smooth, narrow, impedance matched gap.

2.4 Cumulation of Emittance Growth Through Multiple Gaps

The emittance growth given by Equations (16) and (17), and by Equations (25) and (26) for an $f_o(z)$ gap shape, represents that caused by the excitation of "new" envelope oscillations during the acceleration through a single gap of a beam which is presumed to be in equilibrium upstream of the gap. The upstream equilibrium obeys the envelope Equation (4) with the primed quantities equal to zero:

$$\frac{\Omega_o^2}{4c^2} r_o - \frac{2I_b}{mc^3/e} \frac{1}{\gamma_o \beta_o r_o} - \frac{(P_\phi^2 + \varepsilon_n^2)}{r_o^3} = 0 \tag{29}$$

Therefore, the preexisting thermal emittance ε_n influences the equilibrium beam radius r_o only very weakly, since $\varepsilon_n^2 \ll P_\phi^2$ for beams from immersed cathodes. The solutions

given in Equations (14) and (15) to the linearized envelope equation reflect tacitly the assumed upstream initial conditions of equilibrium: $\delta r = \delta\beta_r = 0$ at $z = -\infty$.

It may be observed from these linearized solutions that the emittance growth $\Delta\varepsilon_n$ of new envelope oscillations is virtually independent of the preexisting thermal (i.e., phase-mixed) emittance ε_n, except via the weak influence of ε_n upon the beam radius r_o.

One must also assess the extent to which the preexisting thermal emittance may be amplified during the beam transit through the acceleration gap. Such amplification is known to be worse for the case of sudden (nonadiabatic) changes in the transverse force balance. We have previously shown[7] that during sudden acceleration from γ_o to γ_1 in a gap for which the solenoidal field strength B_z is unchanged, the amplification of thermal emittance is given by

$$\frac{\varepsilon_{n1} - \varepsilon_{no}}{\varepsilon_{no}} \approx \left(\frac{8\nu c^2}{\gamma_o r_o^2 \Omega_o^2}\right)^2 \frac{(\gamma_1 - \gamma_o)^2}{8\gamma_1^2} << \frac{(\Delta\gamma)^2}{8\gamma_1^2} \tag{30}$$

where the strong inequality is valid for a well-magnetized beam from an immersed cathode. When $\Delta\gamma = \gamma_1 - \gamma_o$ and $B_z r_o^2$ are constant down the accelerator, the amount of thermal amplification declines as $\gamma^{-4} B_z^{-2}$ and hence is of no consequence beyond the first few gaps. However, even in the first gap the amplification is likely to be negligible, being less than 10^{-3} for the example of the beam and gap parameters of Figures 1 through 3.

It is therefore concluded theoretically that amplification of thermal emittance should be negligible, and that the emittance growth $\Delta\varepsilon_n$ of new envelope oscillations should be insensitive to the amount of preexisting thermal emittance ε_n.

It is entirely possible that the gap-to-gap spacing D may be short enough that new envelope oscillations excited in one gap may not have phase mixed yet when the beam reaches the next succeeding gap. The higher the beam quality, the more likely this is, and as we shall see, the beam excitations may add constructively or destructively, depending upon the phasing which results from kD. Since the beam radius is not much perturbed for solenoidal transport of beams from immersed cathodes, the emittance excitations are proportional to the velocity (or momentum) perturbations, as indicated in Equation (17). if the gap-to-gap spacing is appropriately selected, the velocity (and hence emittance) excitations from one gap may be removed by destructive interference from those created at the next gap. An unfortunate choice of gap-to-gap spacing, as in Figure 1, may allow the successive excitations to add constructively. Finally, if the phasing of the velocity perturbations is uncorrelated, or random from gap to gap, then the emittance excitations will cumulate according to

$$\varepsilon_{n\,Tot} = \left[\sum_{i=1}^{N} \left(\Delta\varepsilon_{ni}\right)^2\right]^{\frac{1}{2}} \approx \left[\int_{\gamma_o}^{\gamma_f} \frac{d\gamma}{\Delta\gamma} \left(\Delta\varepsilon_n(\gamma)\right)^2\right]^{\frac{1}{2}} \tag{31}$$

where the sum over gaps may be approximated by an integral over energy for the case of many gaps which each add only a small increment $\Delta\gamma mc^2$ in energy. Equation (31) also applies for the cumulation of preexisting thermal emittance with newly excited emittance from envelope oscillations.

In Figure 5, a diagnostic is shown of the rms emittance excited by the gap of Figure 2. With a cold input beam, the rms emittance increases by $\Delta\varepsilon \approx 0.035$ rad-cm across the gap. By comparison, Figure 6 shows the acceleration through the same gap of a beam with initial rms thermal emittance of $\varepsilon_{n\,input} = 0.014$ rad-cm. In Figure 7, the rms emittance diagnostic shows emittance growth to a final rms output emittance of $\varepsilon_{n\,output} = 0.037$ rad-cm. It may be seen that the emittance has indeed cumulated in accordance with the rms law of Equation (31), and that the amount of emittance growth across the gap is $\Delta\varepsilon_n = 0.035$ rad-cm, just as for the case of the cold input beam. Therefore, as theoretically anticipated, the emittance growth is insensitive to the initial thermal emittance, and moreover, there is no additional amplification of the initial thermal emittance.

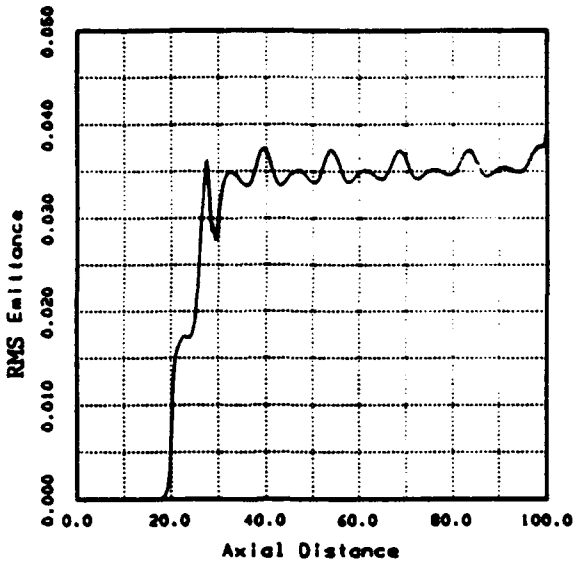

$\varepsilon_{rms\ input} = 0$ $\Delta\varepsilon_{n\ rms} = 0.035$ rad-cm

Figure 5. Emittance growth during acceleration of a high current, initially cold beam through a smooth, narrow, impedance matched gap.

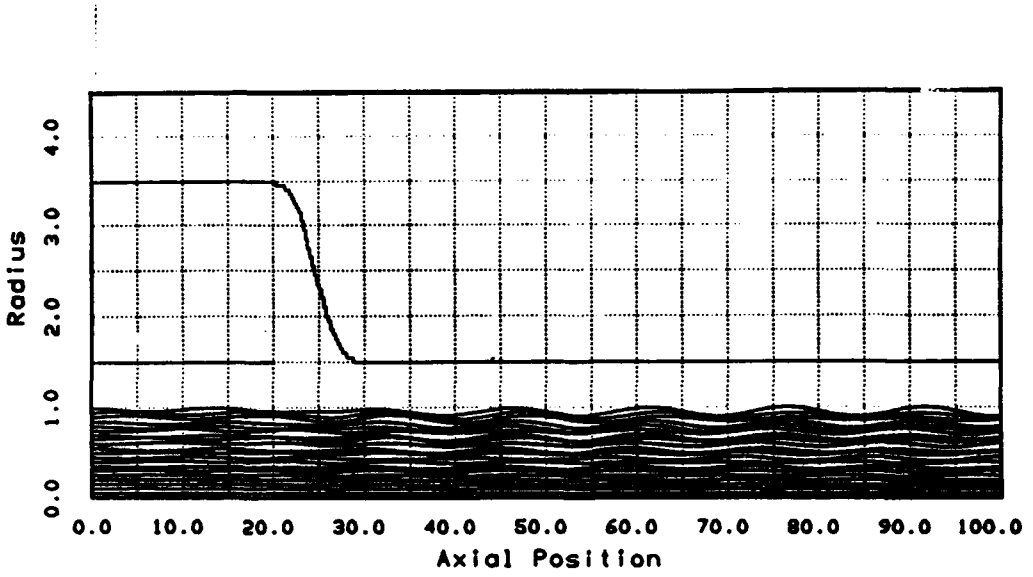

$V_{INJ} = 1.0$ MV $V_{GAP} = 0.25$ MV $I = 5.0$ kA $B_z = 2.5$ kG

$L_{GAP} = 10$ cm $= 0.77\ \lambda$ $\varepsilon_{RMS\ INPUT} = 0.014$ rad-cm $\Delta\varepsilon_{n\ RMS} = 0.035$ rad-cm

Figure 6. Transport of a high current, warm beam past a smooth, narrow impedance matched gap.

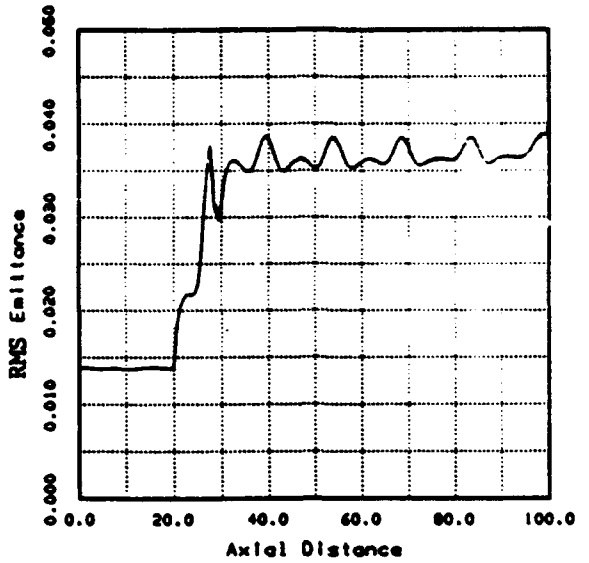

$$\varepsilon_{rms\ input} = 0.014 \text{ rad-cm} \qquad \Delta\varepsilon_{n\ rms} = 0.035 \text{ rad-cm}$$

$$\varepsilon_{rms\ output} = \left[(0.014)^2 + (0.035)^2\right]^{\frac{1}{2}} = 0.037 \text{ rad-cm}$$

Figure 7. Emittance growth during acceleration of a high current, initially warm beam through a smooth, narrow, impedance matched gap.

Finally, the previous result of Equation (25) may be inserted into Equation (31) to estimate the amount of cumulative emittance resulting from the acceleration of a high current beam through multiple uncorrelated, but impedance-matched gaps. If the small current corrections to the cyclotron frequency [c.f., Equation (12)] are neglected, one obtains

$$\varepsilon_{n\ ToT} \approx \left[\int_{\gamma_o}^{\gamma_f} d\gamma \ \frac{\Omega_o^2 r_o^4 \Delta\gamma}{4c^2\gamma^2\beta^4}\ h^2(kL)\right]^{\frac{1}{2}} \lesssim \frac{\Omega_o r_o^2}{2\beta_o^2 c^2}\left(\frac{\Delta\gamma}{\gamma_o}\right)^{\frac{1}{2}} \qquad (32)$$

where in performing the integral in Equation (32) we have assumed that $\Delta\gamma$ and $B_z r_o^2$ remain constant down the accelerator, and the bound $h^2(kL) \leq 1$ has been invoked. (As γ increases, kL tends to decrease and $h(kL) \to 1$ as the gap transitions appear more and more abrupt to the beam.)

Inasmuch as the integrand of Equation (32) declines as γ^{-2}, one reaches the familiar conclusion that emittance growth is most severe at the beginning of the accelerator. However, the cumulative emittance estimated in Equation (32) for multiple, abrupt, uncorrelated, impedance-matched gaps is not likely to be low enough for applications demanding a very high quality beam. For example, a beam injected at 1 MeV across 0.25 MeV gaps along a 2.5 kG-cm^2 flux surface is expected to have cumulative emittance excitation of $\varepsilon_{n\ Tot} \lesssim 0.35$ rad-cm. Therefore, emittance control techniques other than the use of smooth gap shaping and impedance-matching are likely to be needed to satisfy the stringent beam quality requirements for applications such as driving high performance free electron lasers.

2.5 Effect of Gap-to-Gap Spacing Upon Emittance Growth

Let D be the distance from the beginning of one gap to the beginning of the next gap, so that it encompasses the length L of gap acceleration plus a length $D-L$ of drift

space between gaps. As noted earlier, if D is short enough and the beam quality high enough, the envelope oscillations excited in one gap may not have phase mixed yet when the beam reaches the next succeeding gap. In this case there is the possibility of either constructive or destructive interference between the excitations produced at two successive gaps. Under the assumption that the acceleration per gap ($\Delta\gamma$) is small enough that linearized theory remains valid for at least two gaps, the solution of Equation (15) may be directly applied to beam transport through two successive gaps. Noting that the source function $S(z)$ is nonzero only within the gaps (i.e., $0 \le z \le L$ and $D \le z \le D + L$), one finds that for impedance-matched gaps, the velocity perturbation downstream of the second gap is given by

$$\delta\beta_r \ (D + L < z < 2D) = \left(\delta\beta_r\right)_{\text{Gap 1}} \left[\sin k\left(z - \frac{L}{2}\right) + \sin k\left(z - D - \frac{L}{2}\right)\right]$$

$$= \left(\delta\beta_r\right)_{\text{Gap 1}} 2\cos\frac{kD}{2} \sin k\left(z - \frac{D+L}{2}\right) \tag{33}$$

where

$$\left(\delta\beta_r\right)_{\text{Gap 1}} = \frac{k r_o \Delta\gamma}{2\gamma_o \beta_o}\left(1 - \frac{4\nu}{\gamma_o^3 \beta_o^2 k^2 r_o^2}\right) h(kL) \tag{34}$$

in agreement with Equation (22). The magnitude of normalized emittance growth after two impedance-matched gaps is therefore

$$\Delta\epsilon_n(2 \text{ Gaps}) = \Delta\epsilon_n(1 \text{ Gap}) \ 2\left|\cos\frac{kD}{2}\right| \tag{35}$$

where $\Delta\epsilon_n(1 \text{ gap})$ is given in Equation (25).

One observes that a constructive, reinforced response should occur for spacings

$$D_R = n\lambda = \frac{2\pi n}{k} \qquad (n = 1, 2, \ldots) \tag{36}$$

while a destructive interference, null response should occur for spacings

$$D_N = (n + \tfrac{1}{2})\lambda = \frac{\pi(2n+1)}{k} \qquad (n = 0, 1, 2, \ldots) \ . \tag{37}$$

Constructive reinforcement of beam excitations is illustrated in Figures 8 and 9, for a spacing $D \approx 29$ cm $\approx 2\lambda$, with the same beam and gap parameters which were used in Figure 2. The reinforced response is quantitatively apparent in Figure 9.

The case of destructive interference is illustrated in Figures 10 and 11, for a spacing $D \approx 21.5$ cm $\approx 3\lambda/2$, with the same beam and gap parameters as before. In this case, the second gap achieves about 75% cancellation of the excitation from the first gap, such that the pair of gaps produces only one-fourth of the single gap excitation.

Although the physics of the destructive interference of excitations from two successive gaps is the same as that of the intragap cancellation discussed earlier, the optimization of the gap-to-gap spacing D seems relatively more attractive as an emittance control technique than the optimization of the gap length L. This is partly because it is easier to change the length of drift space between gaps than it is to change the gap shape itself. Moreover, gap-to-gap nulling can be achieved with only one-half wavelength spacing, whereas intragap cancellation generally requires the gap length alone to be longer than this [e.g., $L_{min} = 2\lambda$ for the $f_o(z)$ gap]. Finally, optimized gap-to-gap spacing is most rewarding at the low energy end of a multi-gap accelerator, where the emittance growth hazard is greatest.

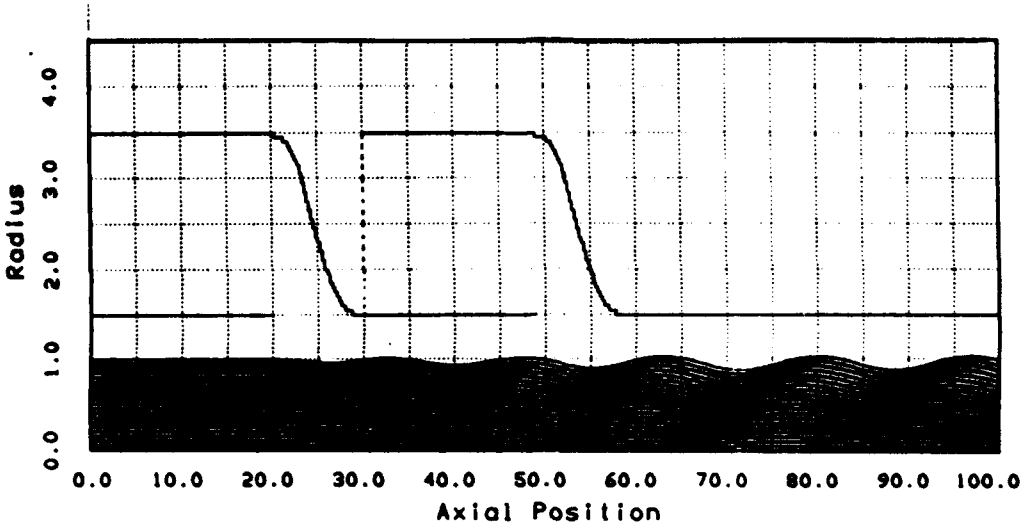

V_{INJ} = 1.0 MV V_{GAP} = 0.25 MV per gap I = 5.0 kA B_z = 2.5 kG

L_{GAP} = 10 cm $D_{GAP\text{-}TO\text{-}GAP}$ = 29 cm ≈ 2λ

Figure 8. Transport of a high current beam past two smooth, narrow, impedance matched gaps, spaced for constructive addition of individual gap excitations.

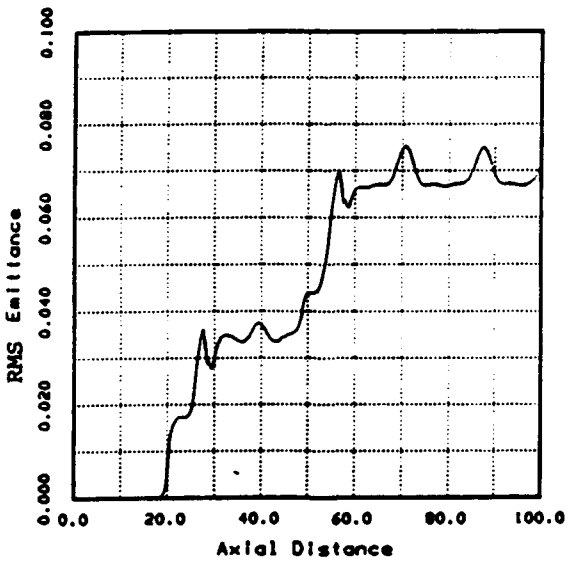

Figure 9. Constructive addition of individual excitations from two gaps spaced two wavelengths apart.

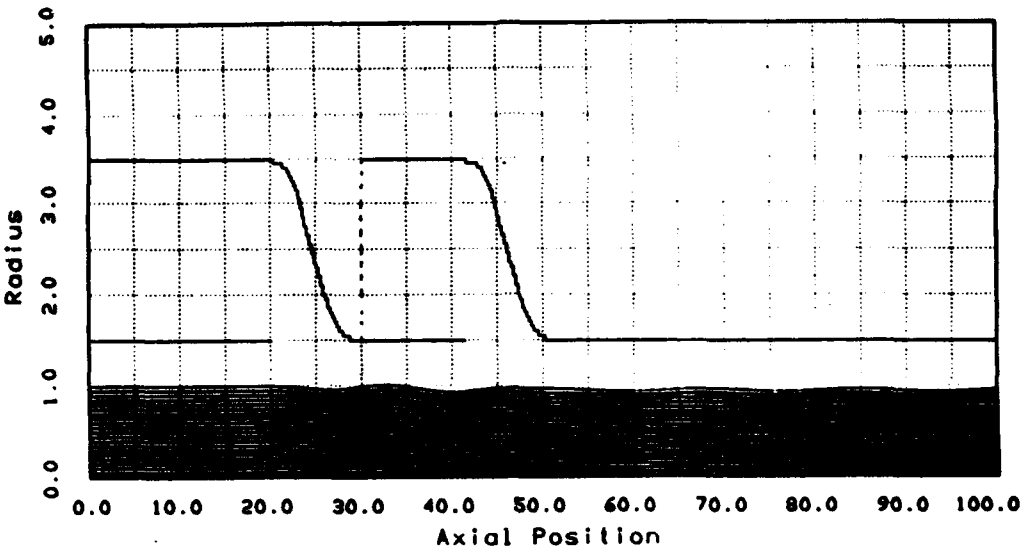

$V_{INJ} = 10$ cm $\quad V_{GAP} = 0.25$ MV per gap $\quad I = 5.0$ kA $\quad B_z = 2.5$ kG

$L_{GAP} = 10$ cm $\quad D_{GAP\text{-}TO\text{-}GAP} = 21.5$ cm $\approx \frac{3}{2}\lambda$

Figure 10. Transport of a high current beam past two smooth, narrow, impedance matched gaps, spaced for destructive interference of individual gap excitations.

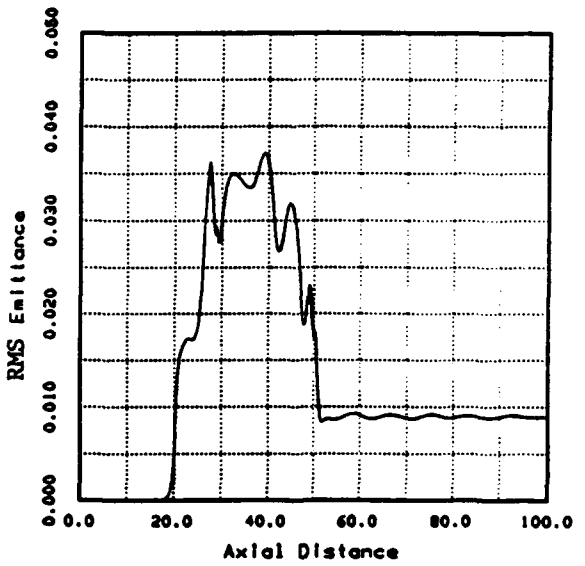

Figure 11. Destructive interference of individual excitations from two gaps spaced one and one-half wavelength apart.

2.6 Effect of Magnetic Tuning Upon Emittance Growth

A final, powerful technique of emittance control is to exploit the tuneability which solenoidal magnetic transport affords. With this technique, programmed magnetic perturbations are introduced within the acceleration gap in such a manner that the magnetic Lorentz force perturbations just exactly offset the gap force perturbations. As reported previously,[7] the prescription for the necessary magnetic tuning is obtained directly from the envelope Equation (4) by requiring that $r' = r'' = 0$ and that r remain constant. One obtains

$$\frac{B_z^2(z)}{B_z^2(-\infty)} = 1 + \frac{4c^2}{\Omega_o^2(-\infty)\, r_o^2}\left[-\frac{\gamma\gamma'' r_o^2}{2} + \frac{2I_b}{mc^3/e}\left(\frac{1}{\gamma\beta} - \frac{1}{\gamma_o\beta_o}\right)\right] \qquad (38)$$

The γ'' term in Equation (38) represents the magnetic tuning necessary to compensate for the perturbed radial electric fields due to image charges in the acceleration gap, while the I_b term represents the magnetic tuning necessary to compensate for the alteration in the degree of cancellation between the E_r and $\beta_z B_\phi$ forces which arise from the self space charge of the beam.

The theoretical prescription for magnetic tuning which is given by Equation (38) is implemented into a practical design by using a least-squares fit routine to select an array of realizable magnetic coils near the gap region to best achieve the desired magnetic profile. An example of the magnetic tuning required for the beam and gap parameters of Figure 2 is shown in Figure 12. The magnetic field strength needs to be varied by a few percent over a distance of a few centimeters, which seems feasible.

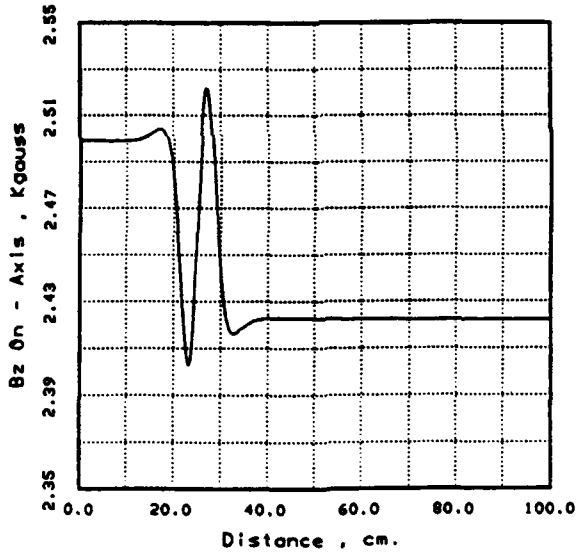

Figure 12. Magnetic tuning required to compensate image charge perturbations in a smooth, narrow, impedance matched gap.

The effect of this magnetic tuning, implemented with realistic coil currents, upon the beam emittance growth is shown in Figure 13. The normalized edge emittance growth is reduced about a factor of six, from 0.050 rad-cm to 0.008 rad-cm.

As might be expected, the best results for emittance control are realized through the simultaneous application of techniques such as smooth gap shaping, impedance matching,

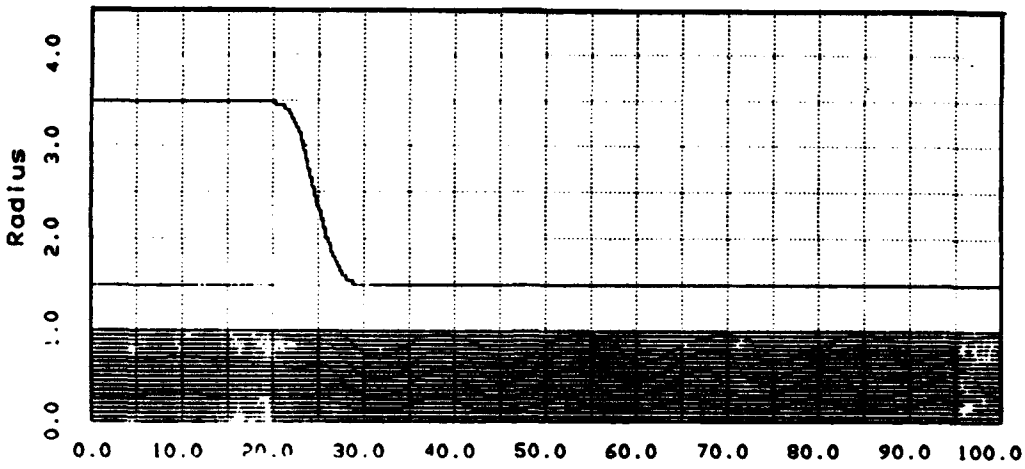

V_{INJ} = 1.0 MV V_{GAP} = 0.25 MV I = 5.0 kA B_z = 2.5 kG ± δB_z

L_{GAP} = 10 cm $\Delta\varepsilon_{n\ edge}$ = 0.008 rad-cm

Figure 13. Transport of a high current beam past a smooth, narrow, impedance matched, magnetically tuned gap.

optimum gap-to-gap spacing, and magnetic tuning. Figures 14 and 15 display the emittance growth of a 1 MeV beam accelerated through two successive 0.25 MeV gaps. In comparison with the case shown in Figure 1, for which the growth in edge emittance is $\Delta\varepsilon_n$ = 0.30 rad-cm, the combined use of these techniques has resulted in a reduction in emittance growth by a factor of about 72, to $\Delta\varepsilon_n$ = 0.0042 rad-cm (or $\Delta\varepsilon_{n\ rms}$ = 0.003 rad-cm). Of this total improvement, a factor of three may be attributed to the smooth shaping and impedance matching, a factor of three may be attributed to the magnetic tuning, and a factor of eight results from the use of gap-to-gap spacing selected for destructive interference rather than reinforcement of excitations.

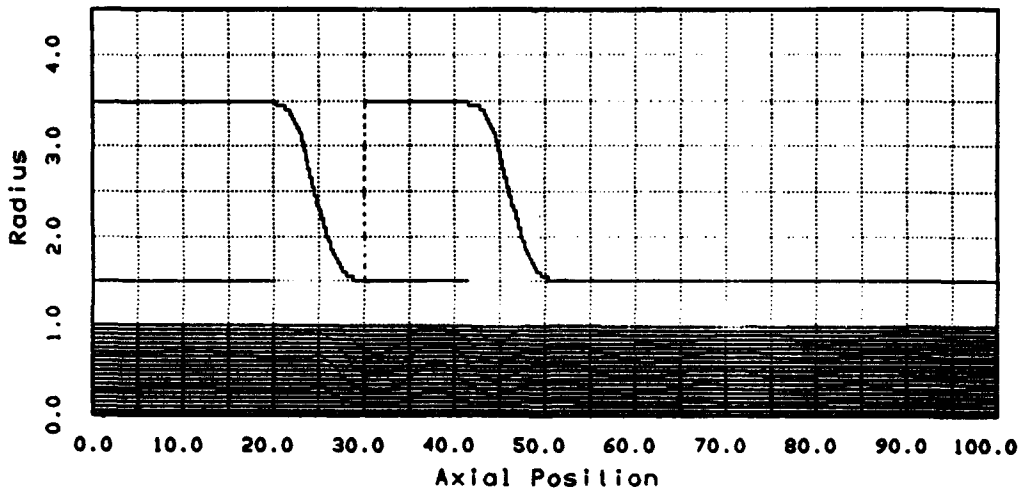

V_{INJ} = 1.0 MV V_{GAP} = 0.25 MV per gap I = 5.0 kA B_z = 2.5 kG ± δB_z

L_{GAP} = 10cm $D_{GAP\text{-}TO\text{-}GAP}$ = 21.5 cm ≈ $\frac{3}{2}\lambda$ $\Delta\varepsilon_{n\ edge}$ = 0.0042 rad-cm

Figure 14. Transport of a high current beam past two smooth, narrow, impedance matched, magnetically tuned gaps, spaced for destructive interference of individual gap excitations.

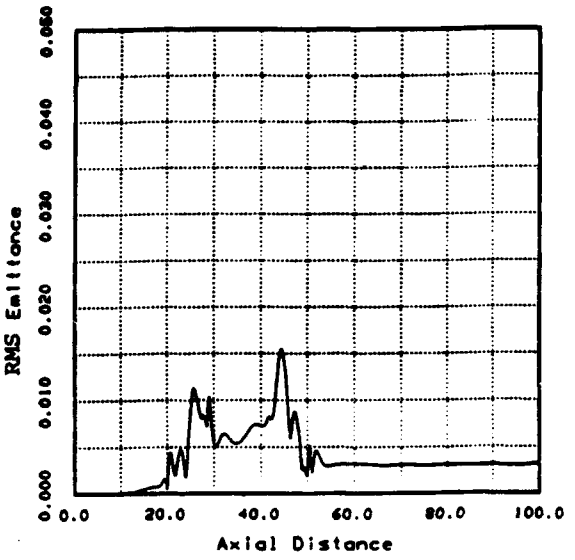

Figure 15. Combined emittance control techniques of smooth, impedance matched gaps, with magnetic tuning, and spacing for destructive interference of individual gap excitations effectively suppresses emittance growth.

2.7 Effect of Current Fluctuations Upon Emittance Growth

The gap design will be impedance-matched only if the beam current is such that $\nu = \nu_o$, given in Equation (18). Likewise the magnetic tuning will be designed for a particular beam current. Consequently, it is important to investigate the sensitivity of these emittance control techniques to fluctuations in the beam current. Some small current fluctuations may generally be expected, and it is desirable that good quality beams be achievable for a range of beam current about the design current.

When the acceleration gap is not magnetically tuned, the influence of the beam current upon the gap excitation and the consequent emittance growth is seen in Equations (22) and (24). In addition to the explicit ν-dependence, it must also be remembered that the envelope wave number k is also dependent upon I_b (or ν) according to Equation (12). Although this ν-dependence is not algebraically simple, investigation reveals that it is reasonably smooth. As ν/ν_o is varied from zero to two, the normalized emittance growth $\Delta\varepsilon_n$ tends to fluctuate at most a factor of about two, with a broad minimum for ν/ν_o somewhat less than one. For abrupt gaps (i.e., $kL < 1$), the sensitivity of the gap excitation to ν/ν_o becomes very slight. In the case of well-magnetized, low ν/γ_o beams, for which k becomes insensitive to ν, the gap excitation is quadratically dependent on ν according to Equation (24), and the validity of the above conclusions regarding the ν-dependence may be verified.

When the acceleration gap is magnetically tuned, magnetic fluctuations are programmed in accordance with Equation (38). This magnetic tuning may be accomplished in principle for any anticipated beam current--provided that the ν-dependent energy fluctuations of Equations (8) and (20) can be matched by the required magnetic fluctuations of Equation (38). However in practice, the rapid energy fluctuations at the entrance to the gap represented by the δ-function in Equation (2), which occur when the gap is not impedance-matched, will be difficult to match magnetically. Therefore, magnetic tuning is likely to be practical only for impedance-matched gaps, and if the beam current deviates from the impedance-matched value, some beam excitation will then occur. The amount of this beam excitation is easily seen to be

$$\delta\beta_r = \frac{k r_o \Delta\gamma}{2\gamma_o\beta_o}\left(1 - \frac{4\nu}{\gamma_o^3\beta_o^2 k^2 r_o^2}\right)\left(1 - \frac{\nu}{\nu_o}\right)\left[\sin k z - h(kL)\sin k\left(z - \frac{L}{2}\right)\right] \qquad (39)$$

and therefore the growth in normalized edge emittance excitations is

$$\Delta\varepsilon_n = \frac{k\, r_o^2\, \Delta\gamma}{2\beta_o}\left(1 - \frac{4\nu}{\gamma_o^3 \beta_o^2 k^2 r_o^2}\right)\left(1 - \frac{\nu}{\nu_o}\right)\left[1 + h^2(kL) - 2h(kL)\cos\frac{kL}{2}\right]^{\frac{1}{2}} \qquad (40)$$

for a magnetically tuned gap. When the gap is abrupt, $h(kL) \approx 1$ and the magnitude of magnetically tuned emittance growth approaches

$$\Delta\varepsilon_n(kL < 1) \approx \frac{k\, r_o^2\, \Delta\gamma}{2\beta_o}\left(1 - \frac{4\nu}{\gamma_o^3 \beta_o^2 k^2 r_o^2}\right)\left(1 - \frac{\nu}{\nu_o}\right)\frac{kL}{2} \quad . \qquad (41)$$

Equations (40) and (41) for magnetically tuned emittance growth may be compared with Equations (24) or (25) for emittance growth in gaps without magnetic tuning. For the case of abrupt gaps, magnetic tuning is predicted to reduce the emittance growth by a factor of $\frac{1}{2}kL\,(1 - \nu/\nu_o) << 1$. It is clear that magnetic tuning should still remain effective even in the presence of modest current fluctuations, so long as these are not excessive.

To test these theoretical predictions of the impact of current fluctuations upon emittance growth, simulations were performed of both magnetically tuned and untuned gaps, for which the beam current was varied by ±10% about 5 kA. The observed growth in rms emittance is listed in Table 1.

TABLE 1

OBSERVED RMS EMITTANCE (rad-cm)

	I_b = 4.5 kA	I_b = 5.0 kA	I_b = 5.5 kA
Untuned	0.031	0.035	0.037
Tuned	0.008	0.006	0.008

It is seen that current fluctuations of ~10% produced emittance fluctuations of ~10% in untuned gaps, but that magnetic tuning remains effective at reducing the amount of emittance growth which occurs.

2.8 Emittance Control During Injection into an FEL Wiggler

It is well known that emittance growth may occur if care is not taken during beam handoff between different focusing fields, such as during beam injection into an FEL wiggler. Wiggler focusing will be present in at least one plane and possibly in both planes containing the beam axis. Therefore an axial transition must be designed which is specific to the wiggler, whereby the beam is "matched" into the wiggler smoothly, by having the strength of the solenoidal magnetic field diminished slowly in conjunction with a slow increase in the strength of the wiggler focusing fields. Because this matching into the wiggler occurs at high beam energy, the prospect for emittance growth is lessened, in the same way that the expected gap excitations are lower at high beam energy.

In the case of beams which have been extracted initially from magnetic field-immersed diodes, it is not feasible to remove the beam from the solenoidal field prior to beam injection into the FEL wiggler. Rather, the solenoidal field must persist in the wiggler, albeit at a strength diminished from that in the accelerator. However, the solenoidal field need not play a significant role in the wiggler dynamics or the FEL operation. Previous studies[11,12] have shown that so long as the resonance condition in the electron wiggler trajectory is not approached

$$\frac{eB_z}{\gamma mc^2} << k_w \beta_z \qquad (42)$$

then the wiggler orbits are essentially the same type as for $B_z = 0$, and it has been reported that "stable trajectories with nearly constant axial velocities and relatively large wiggler amplitudes are possible." (Here $2\pi/k_w$ is the wiggler wavelength.)

It is true that the emittance control techniques of using smoothly shaped, impedance-matched gaps, optimized gap-to-gap spacing, and magnetic tuning could be equally well applied to the solenoidal transport of beams extracted from magnetically-shielded cathodes. Therefore, in addressing the decision as to whether the beam cathode should be magnetically shielded or field-immersed, the tradeoff is that field-immersed cathodes permit the demonstrated, brute-force achievement of high source brightness, and have simpler focusing field handoffs at both the front and end of the accelerator beam line, at the expense of having the solenoidal field persist in the FEL wiggler. It would seem that for FELs to be operated at wavelengths in the infrared and shorter, the electron beam energy will be high enough that condition (42) is well obeyed, and there should be no significant drawback to a solenoidal field-immersed wiggler. Therefore it appears desirable to harvest the advantages of field-immersed diodes.

3. CONCLUSIONS

It has been demonstrated herein that the very high quality electron beams required for applications such as driving short wavelength, high performance free electron lasers may be achieved through the use of certain emittance control techniques during the solenoidal magnetic transport and multi-gap acceleration of high current beams extracted from magnetic field-immersed diodes. Such compact, magnetic field-immersed diodes have the demonstrated capability to provide high current (~ 5 kA) beams at high brightness ($10^6 - 10^7 A/cm^2 - rad^2$). The commonly encountered problem of emittance growth at the low energy end of a multi-gap accelerator due to image charges bunched near the acceleration gaps may be controlled through a combination of techniques:

(1) Use of smoothly shaped, impedance-matched gaps;

(2) Use of optimized gap-to-gap spacing; and

(3) Use of tuned fluctuations in the solenoidal magnetic field within the gaps to compensate gap image charge perturbations.

Consequently it appears feasible to deliver from the multi-gap accelerator, high current beams whose high diode brightness is essentially preserved during transport and acceleration. If disruptive, high current beam kinking instabilities are also controlled, such high-brightness beams are uniquely capable of driving high performance FEL operation at wavelengths in the infrared and below.

4. ACKNOWLEDGEMENTS

This research was conducted under ONR Contract *N00014-88-C-0542*.

5. REFERENCES

1. T. J. Orzechowski, et al., IEEE J. Quantum Electron., Vol. QE-21, 831 (1985).

2. John L. Miller, "High Power Induction Free Electron Laser," Proc. SPIE Symposium on Lasers and Optics '89, Vol. 1040, paper 22 (1989).

3. P. T. Kirstein, G. S. Kino, and W. E. Waters, Space Charge Flow (McGraw-Hill, New York, 1967), Chap. 3.

4. A. Septier, Applied Charged Particle Optics (Academic Press, New York, 1983).

5. E. P. Lee and R. K. Cooper, Part. Accel. 7, 83 (1976).

6. G. J. Caporaso, A. G. Cole, and J. K. Boyd, IEEE Trans. Nucl. Sci. NS-32, 2605 (1985).

7. J. R. Thompson, M. L. Sloan, B. N. Moore, and J. R. Uglum, "Beam Handling and Emittance Control," Proc. SPIE Symposium on Innovative Science and Technology '88, Vol. 873, Microwave and Particle Beam Sources and Propagation, 198 (1988).

8. M. L. Sloan and H. A. Davis, Phys. Fluids 25, 2337 (1982).

9. M. L. Sloan and J. R. Thompson, "A Brief Note on Beam Quality in High Current, Field Immersed Diodes," Austin Research Associates Report No. 489 (1983).

10. C. W. Roberson, "Bright Electron Beams for Free Electron Lasers," Proc. SPIE Symposium on Free-Electron Generators of Coherent Radiation, 453, 320 (1983).

11. H. P. Freund and A. T. Drobot, Phys. Fluids 25(4), 736 (1982).

12. J. A. Pasour, F. Mako, and C. W. Roberson, J. Appl. Phys. 53(11), 7174 (1982).

APPENDIX E

BEAM BREAKUP IN LOW EMITTANCE ACCELERATOR CAVITIES

M. L. Sloan and James R. Thompson, Proc. SPIE, Intense Microwave and Particle Beams, Vol. 1226, 447 (1990).

Beam breakup in low emittance accelerator cavities

M. L. Sloan and James R. Thompson

Austin Research Associates
1901 Rutland Drive, Austin, Texas 78758

ABSTRACT

Proper inclusion of self-field effects and careful design has led to development of induction accelerator gap geometries which afford a factor of 5000 or higher improvement in beam brightness over conventional gap designs for multi-kiloampere, multi-MeV electron accelerators. Because of the resulting TEM-like power feed to the accelerator gap region in these designs, the usual low frequency beam breakup instability associated with the induction cavity is suppressed. However, this geometry exhibits a significant, high frequency beam breakup problem associated with cavity resonances in the gap region itself. Analysis of this mode and the current status of simulation studies and methods of suppression of this instability are presented.

1. INTRODUCTION

Recent advances in high current, solenoidal magnetic field guided, relativistic electron beam induction accelerator gap design provide typical increases in beam brightness of 10^3 to 10^4 over conventional designs.[1] Characteristic of such axisymmetric gap designs is geometric contouring of the gap itself to provide good impedance matching to the beam, resulting in a gap geometry typified by Fig. 1 (excerpted from Ref. 1).

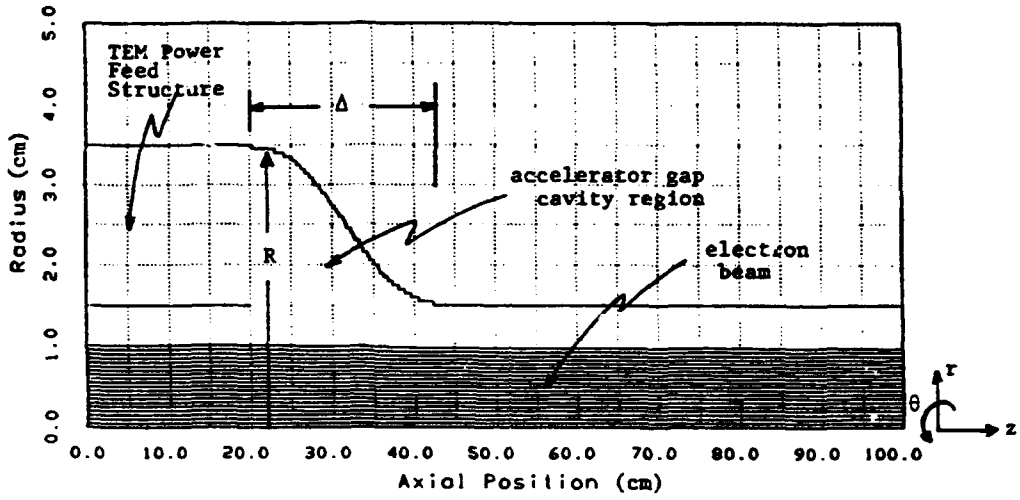

Figure 1. Low emittance acceleration gap geometry.

Specific features of this gap to be noted are the TEM-like power feed structure and the large gap width compared to the beam line radius. This large width provides an essentially adiabatic acceleration of the beam across the gap and only very small levels of the radial defocusing forces which lead to growth in beam emittance.

As has been pointed out by Miller,[2] such geometries carry the additional advantage that the low frequency cutoff character of the small radius TEM power feed structure effectively isolates the gap region from the usual induction cavity drive structure and thereby precludes the usual beam breakup (BBU) instability associated with coupling to the non-axisymmetric TM modes of such structures. Unfortunately, coupling can still occur between the beam and resonances associated with the gap region geometry itself. Although of much higher frequency than the more common BBU instability, this coupling may lead to a significant BBU instability for these low emittance accelerator gap geometries.

This high frequency instability exhibits certain additional features which distinguish it from the more classical BBU instability and which must be taken into account in any analysis or simulation of the instability process. First, due to the long gap width, the usual impulse, or short gap, approximation for calculating the perturbed electron motion in traversing the gap is inapplicable. Secondly, the complex geometry of the axisymmetric cavity prevents the decomposition of the cavity resonance eigenmodes into purely TE or TM type waves; rather, for purposes of determining quantitative values of amplification or growth rates, the eigenmodes and eigenfrequencies of the cavity must be accurately determined and the resulting eigenmode field values utilized in carrying out the requisite calculations. Finally, it can in general be shown that for axisymmetric systems, the dangerous $m = 1$ BBU modes that couple well to the beam exhibit a specific helicity and, in fact, only couple to one branch of the cyclotron wave associated with solenoidal magnetic field guided electron beams. This branch is, of course, the negative energy branch (which is the reason for instability in the first place); however, such helicity decoupling results in a somewhat different form of the governing equations and dispersion relation than is obtained from more conventional, strong focusing analyses (e.g., Refs. 3 and 4).

2. ANALYSIS OF THE BBU INSTABILITY

Consider an axisymmetric accelerator gap geometry and electron beam as typified by Fig. 1, where $R \sim 1\text{-}3$ cm characterizes the beam line dimension and $\ell \gg R$, the effective gap width. For such azimuthally symmetric systems, the fields and attendant beam displacements can be Fourier decomposed in the azimuthal coordinate θ, i.e.,

$$\vec{A}(\vec{x}) = \vec{A}(r,z) \exp(i m \theta) \tag{1}$$

where r, θ, z are the usual cylindrical coordinates.

As will be seen, the BBU instability consists of coupling of transverse beam displacements to the $m \neq 0$ vacuum modes of the cavity region.

2.1 Vacuum modes of the cavity

Under the gauge $\phi = 0$, $\vec{\nabla} \cdot \vec{A} = 0$, the vacuum modes are found from the eigenvalue equation

$$\nabla^2 \vec{A} + \omega_o^2 \vec{A} = 0 \tag{2}$$

where $\vec{A}(\vec{x})$ is the eigenmode vector potential and ω_c, a resonant eigenvalue of the cavity. [Here the speed of light c has been set to unity.] Typical values of ω_c for such cavities would be $\omega_c \geq \pi/R$ so that one may expect multi-gigahertz resonances for R in the 1-3 cm range.

Furthermore, for azimuthal dependences given by Equation (1), one may show that

$$A_r \pm i A_\theta \propto r^{m \pm 1} \quad \text{as} \quad r \to 0 \tag{3}$$

and

$$A_z \propto r^m (1 + \theta r^2 + \ldots) \quad \text{as} \quad r \to 0 \tag{4}$$

so that the most dangerous BBU modes are the $m = 1$ modes since these exhibit electromagnetic field components (specifically field components associated with $A_r - i A_\theta$) which do <u>not</u> vanish at $r = 0$ and can therefore couple strongly to the electron beam, which is localized to small radii near the center of the beam line.

We have henceforth restricted our attention to $m = 1$ perturbations.

2.2 Relativistic electron beam response

The equations for the perturbed transverse motion of a relativistic beam confined by a solenoidal magnetic field may be written (with $e = m = c = 1$)

$$\begin{aligned} (\partial_t + \partial_z)\, \tilde{p}_r &= \Omega \tilde{p}_\theta + (\tilde{E}_r - \tilde{B}_\theta) \\ (\partial_t + \partial_z)\, \tilde{p}_\theta &= -\Omega \tilde{p}_r + (\tilde{E}_\theta + \tilde{B}_r) \end{aligned} \tag{5}$$

where p_r, p_θ are the $m = 1$ perturbed transverse momentum components of the beam motion and Ω is the relativistic gyrofrequency associated with the solenoidal transport field.

Introducing the variables

$$p^{\pm} = \tilde{p}_r \pm i \tilde{p}_\theta \tag{6}$$

Equation (5) may be compactly written

$$(\partial_t + \partial_z \pm i\Omega)\, p^{\pm} = E_r \pm i E_\theta - (B_\theta \mp i B_r) \tag{7}$$

Expressed in terms of A_r, A_θ using Maxwell's equations we have

$$E_r \pm i E_\theta = -\partial_t (A_r \pm i A_\theta) \tag{8}$$

$$B_r \mp i B_\theta = \partial_z (A_r \pm i A_\theta) - (\partial_r A_z \mp A_z/r) \tag{9}$$

However, from Equations (3) and (4) we see that in the region of the beam $(r \to 0)$,

$$A_r = -iA_\theta \tag{10}$$

and

$$A_z/r = \partial_r A_z \tag{11}$$

so that the p^+ perturbation couples only to fields that vanish as r^2 for $r \to 0$, whereas the p^- perturbation couples to fields that are finite as $r \to 0$. It is this strong coupling to the p^- motion that constitutes the BBU instability, with p^+ remaining near zero. Therefore

$$p^- >> p^+ \longrightarrow p_\theta \cong i\tilde{p}_r \tag{12}$$

so that $p^- \cong 2\tilde{p}_r \cong -2i\tilde{p}_\theta$, allowing Equation (7) to be written

$$(\partial_t + \partial_z - i\Omega)\,\tilde{p}_r = F \equiv \partial_r A_z - (\partial_t + \partial_z)\,A_r \tag{13}$$

and

$$\tilde{p}_\theta = i\tilde{p}_r \tag{14}$$

valid for $r^2 \to 0$.

Finally, introducing the perturbed beam displacement ξ

$$(\partial_t + \partial_z)\,\xi \equiv \tilde{p}_r/\gamma \tag{15}$$

where γ is the usual relativistic gamma factor, we may show in the usual manner that the perturbed beam currents are given by

$$\begin{aligned} J_r &= (\partial_t + \partial_z)\,(n_o \xi) \\ J_\theta &= i J_r \\ J_z &= -\partial_r (n_o \xi) \end{aligned} \tag{16}$$

where $n_o = n_o(r, t-z)$ is the beam charge density.

2.3 Coupling of the beam motion to the vacuum cavity eigenmodes

Equations (13) and (15) determine the coupling of the vacuum cavity BBU fields to the electron beam displacement ξ. From Equation (16) we see that this displacement gives rise to perturbed currents, which, in turn, couple back through Maxwell's equations to the cavity eigenmodes to close the instability feedback loop.

The effects of the perturbed beam currents on the cavity eigenmode may be calculated in the usual manner: For oscillation frequencies ω near ω_o, the vector potential $\vec{A}$ may be expressed in terms of the cavity eigenmode

$$\vec{A}(\vec{x},t) = A(t)\,\vec{A}(\vec{x})\,\exp(-i\omega_o t) \tag{17}$$

where we assume the eigenmode $\vec{A}(\vec{x})$ is normalized

$$\int d^3x \left|\vec{A}(\vec{x})\right|^2 = 1 \tag{18}$$

The amplitude factor $A(t)$ is assumed slowly varying with respect to the $\exp(-i\omega_c t)$ factor.

If the governing Maxwell equation for $\vec{A}(\vec{x},t)$

$$\nabla^2 \vec{A} - \partial_t^2 \vec{A} = -4\pi \vec{J} \tag{19}$$

is multiplied by $\vec{A}^*(\vec{x}) \exp(+i\omega_c t)$ and integrated over all space, we obtain an equation for the slow-time evolution of $A(t)$

$$2i\omega_c \partial_t A = -4\pi \int \vec{J} \cdot \vec{A}^*(\vec{x})\, d^3x \tag{20}$$

Expressing $\vec{J}$ in terms of ξ using Equation (16) and noting that the integrations of $\vec{J} \cdot \vec{A}$ are confined to the region of the electron beam and hence to regions where r^2 is small so that Equations (10) and (11) hold, an integration by parts allows Equation (20) to be expressed

$$2i\omega_c \partial_t A = -2 \int d^3x \; \omega_{p_o}^2 F^* \xi \tag{21}$$

while Equation (7) may be written

$$\left[\partial_z - i(\omega_o + \Omega)\right]\left[\gamma(\partial_z - i\omega_o)\,\xi\right] = AF \tag{22}$$

The force F is expressible in terms of the eigenfunction components

$$F = \partial_r A_z - (\partial_z - i\omega_o) A_r \Big|_{r=0} \tag{23}$$

Here $\omega_{p_o}^2 = 4\pi n_o$ is the nonrelativistic plasma frequency of the beam.

The above expressions assume infinite Q of the cavity or time scales less than $Q/(2\omega_o)$. Inclusion of finite Q is effected by replacing

$$\partial_t \rightarrow \partial_t + \omega_c/(2Q) \tag{24}$$

in Equation (21).

Equations (21) through (24) provide a general description of the BBU instability for relativistic electron beams guided by solenoidal magnetic fields.

2.4 Further development

In order to proceed further, we assume that γ, Ω do not change significantly across the gap and that regenerative feedback within the gap can be neglected. This allows Equation (22) to be formally integrated across the gap to calculate the

change (i.e., amplification) in ξ and $\partial_z \xi$ due to the BBU fields in the gap region. The results are best expressed in terms of new variables

$$p \equiv \left[(\partial_z \xi - i\omega_c \xi)/i\Omega\right] \exp - i(\omega_c + \Omega/2)\, z$$

$$q \equiv \left[(i\omega_o \xi + i\Omega\xi - \partial_z \xi)/i\Omega\right] \exp - i(\omega_o + \Omega/2)\, z \tag{25}$$

Specifically we obtain

$$p = \left(p_o + \frac{A}{i\gamma\Omega} R\right) \exp(i\Omega z/2)$$

$$q = \left(q_o - \frac{A}{i\gamma\Omega} S\right) \exp(- i\Omega z/2) \tag{26}$$

where p_o, q_o are values of p, q before crossing the gap and p, q are the values at a distance z past the gap. In terms of p_o and q_o, Equation (21) may be expressed

$$2i\omega_o \frac{\partial A}{\partial t} = - 2\pi \omega_{po}^2 a^2 \,(p_o R^* + q_o S^*) \tag{27}$$

where the integration over rdr has been explicitly carried out for a beam of radius a.

The functions R and S in Equations (26) and (27) are the usual overlap functions defined

$$R \equiv \int_o^\Delta dz\, F(z) \exp - i(\omega_o + \Omega)\, z$$

$$S \equiv \int_o^\Delta dz\, F(z) \exp(- i\omega_o z) \tag{28}$$

with $F(z)$ given by Equation (23).

An examination of the propagation characteristics of p,q shows that p is that component of the beam displacement associated with the negative energy cyclotron mode, while q corresponds to an $m = 1$ ballistic positive energy mode of the beam. Similarly, R is the overlap function of the negative energy cyclotron mode with the cavity fields and S, the overlap function of the positive energy ballistic mode.

2.5 Cumulative spatial amplification factor

Because the eigenmode frequency is extremely high, finite Q effects should provide saturation of the temporal growth of A well before the electron pulse has traversed the gap. Therefore we examine Equations (27) and (28) with ∂_t replaced by $\omega_o/2Q$ in Equation (27), as prescribed by Equation (24).

The stability of a periodic series of gaps may then be determined by examining the cavity-to-cavity amplification factor λ, where

$$\begin{pmatrix} p \\ q \end{pmatrix} = \lambda \begin{pmatrix} p_o \\ q_o \end{pmatrix} \tag{29}$$

Values of $|\lambda| > 1$ are unstable.

From Equations (26) through (28), the eigenvalue equation for λ may be readily obtained

$$1 = \frac{\varepsilon}{\Omega} \left[\frac{|R|^2 \exp(i\Omega L/2)}{\lambda - \exp(i\Omega L/2)} - \frac{|S|^2 \exp(-i\Omega L/2)}{\lambda - \exp(-i\Omega L/2)} \right] \tag{30}$$

where $\varepsilon \equiv 2\pi \omega_{po}^2 a^2 Q/(\gamma \omega_o^2)$ and where L is the periodic gap-to-gap spacing. Excluding for the moment the (highly unlikely) case of exact gap-to-gap resonance $\exp(i\Omega L) = 1$, the unstable eigenvalue of Equation (30) may be expressed as

$$|\lambda| = 1 + \varepsilon |R|^2/\Omega \tag{31}$$

(assuming $\varepsilon|R|^2/\Omega < 1$). This eigenvalue corresponds to p finite, $q \approx 0$ and therefore is associated with the negative energy cyclotron mode coupling unstably to the positive energy eigenmodes of the gap acceleration structure, as might be expected.

Using Equations (23) and (28) and expressing $\omega_{po}^2 a^2$ in terms of the electron beam current, the amplification factor per gap may be written

$$|\lambda| = 1 + \frac{8\pi}{17} \frac{QI}{\Omega_o \omega_o^2} \frac{\left| \int_0^\Delta dz (\partial_r A_z - i\Omega A_r) \exp - i(\omega_o + \Omega) z \right|^2}{\int d^3x \, |\vec{A}|^2} \tag{32}$$

where I is the beam current in kiloamperes and Ω_o is the nonrelativistic gyrofrequency of the solenoidal guide magnetic field.

Several features of this amplification factor should be noted:

1. This is the amplification factor for a single gap. The values of Q, γ, Ω_o, and the eigenfunctions $\vec{A}$ are those of the gap in question. To determine the total amplification down the accelerator, the effects of each gap have simply to be multiplicatively cumulated.

2. The amplification scales linearly with the beam current and Q of the gap, and inversely with the magnetic field strength.

3. The amplification factor is always greater than unity. Therefore, each gap contributes further amplification and the best that can be done is to minimize the contribution from each gap individually.

4. There is no significant gap-to-gap tunings than may be employed to significantly decrease the BBU amplification, except for the $\exp(i\,\Omega\,L) \cong 1$ resonance tuning mentioned earlier. This resonance, if practical and achievable, couples the positive energy ballistic mode into the BBU process. Preliminary analysis indicates that such coupling may result in significant reduction, and possibly even damping of the BBU instability. However, analysis along these lines would require examination of the full transport matrix, Equations (26) through (28), and awaits further consideration.

5. The $i\Omega A_r$ term in the numerator is generally much smaller than the $\partial_r A_z$ term and in most cases can be neglected. The amount of A_z component is, of course, intimately linked with the TM content of the eigenmode and illustrates the significant growth to be expected if the eigenmode is strongly TM in character.

6. Finally, because $\omega_o \Delta > 1$, one may obtain some phase cancellation from the $\exp i(\omega_o + \Omega)\, z$ term in the numerator. Such cancellation is lacking in the more classical short gap, low frequency BBU situations.

3. STATUS OF SIMULATION AND BBU MINIMIZATION STUDIES

In order to accurately determine the amplification as given by Equation (32), detailed and accurate knowledge of the eigenmode structure and the cavity Q must be obtained. Accordingly, an axisymmetric eigensolver RESONANT, using relaxation and scrubbing procedures detailed in Ref. 5, was implemented.

Using RESONANT, specific acceleration gap geometries may be investigated and the eigenmode structure and eigenfrequencies determined. Specific attention is paid to the on-axis A_z eigenmode component, since it is this TM-like component that dominates coupling to the beam.

Once a likely gap design has been identified, a second BBU simulation code BREAKUP may be run to provide BBU amplification factors over the range of relevant frequencies and also to ascertain the effects of resistive loading (Q spoiling) on BBU coupling.

These two simulation codes, which have just currently been brought on line, will provide a rapid assessment capability for examination of low emittance accelerator gap geometry BBU problems in future studies.

A definitive assessment of these cavity structures must await completion of these studies. However, even a cursory examination shows that the BBU instability problem may be severe for such cavities.

For example, for a geometry characterized by an outer beam line $R = 3.5$ cm, inner beam line of 1.5 cm and a gap spacing $\Delta = 10$ cm (a geometry very similar to that of Fig. 1, except for the shorter gap spacing), the RESONANT code has

identified six resonant frequencies in the 1.9 to 5.1 GHz which may prove troublesome from a BBU point of view. A subsequent run with the BREAKUP code covering this frequency band shows significant amplification at these resonances, with the peak amplification occurring at $\omega\Delta x/c = 0.37$ (here $\Delta x = 0.5$ cm). Examination of the eigenmode structure shows this mode contains a significant TM component. A plot of BBU amplification versus frequency is presented in Fig. 2.

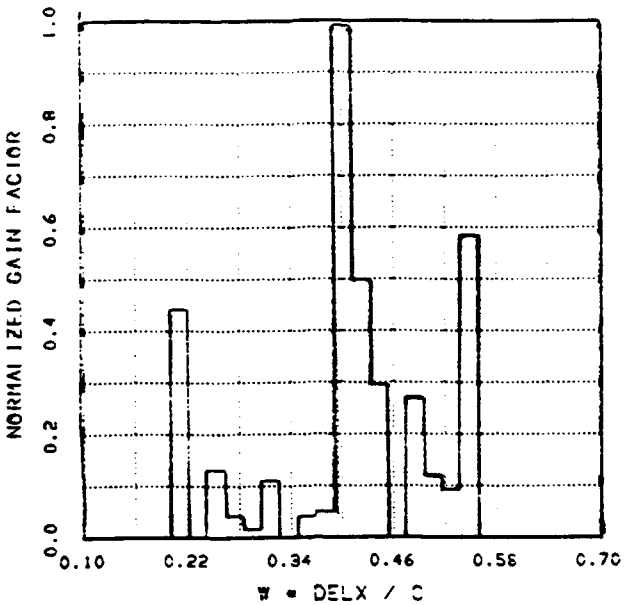

Figure 2. Normalized BBU gain curve.

Loading of the cavity with resistive material judiciously positioned so as not to interfere with the acceleration process, but at the same time to resistively load the offending cavity eigenmode does spoil this particular eigenmode. However, subsequent BREAKUP runs show the peak growth simply shifting to a higher $\omega\Delta x/c = 0.44$ resonance that is not as affected by the resistive loading, as can be noted in Fig. 3.

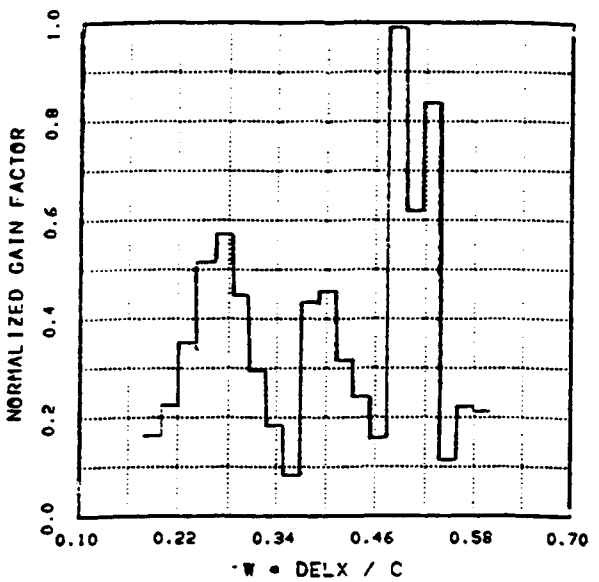

Figure 3. Normalized BBU gain curve showing shift to higher resonance.

Continued Q spoiling of the cavity tends to "wash out" the resonances, with the BBU instability converted to a broad-band resistive wall type instability characterized by the amplification profile seen in Fig. 4.

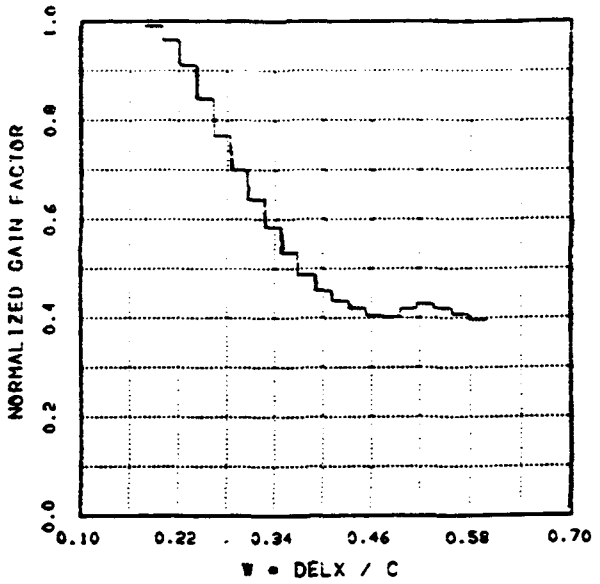

Figure 4. Normalized gain curve for highly-damped cavity.

A preliminary calculation of the BBU gain in this cavity structure for a 5 Kamp electron beam guided by a 5 KG solenoidal magnetic field yields a gain on the order of several precent per gap. Such a gain would result in a non-negligible BBU amplification for a 100-200 gap accelerator and points out the need for further study and optimization of these low emittance accelerator gaps.

6. ACKNOWLEDGEMENTS

This research was conducted under ONR Contract N00014-88-C-0542.

7. REFERENCES

1. J. R. Thompson, et al., "Beam Handling and Emittance Control," Proc. SPIE, Microwave and Particle Beam Source and Directed Energy Concepts, Vol. 1061, 454 (1989).

2. R. B. Miller, et al., J. Appl. Phys. 63 (4), 997 (1988).

3. W. K. H. Panofsky and M. Bander, Rev. Sci. Instruments 39, 206 (1968).

4. Y. Y. Lau, Phys. Rev. Lett. 63, No. 11, 141 (1989).

5. W. E. Drummond, et al., "A Summary and Final Report for the Proof of Principle Auto-Resonant Accelerator Experimental Program," Appendix B, Austin Research Associates Report No. I-ARA-82-U-30 (1982).

APPENDIX F

LOW EMITTANCE ACCELERATOR CAVITY DESIGN TO MINIMIZE AMPLIFICATION OF BEAM BREAKUP MODES

M. L. Sloan, J. R. Thompson, and C. S. Kueny, Proc. 9th International Conference on High-Power Particle Beams, Vol. I, 305, Washington, DC (May 1992).

LOW EMITTANCE ACCELERATOR CAVITY DESIGN TO MINIMIZE AMPLIFICATION OF BEAM BREAKUP MODES

M. L. Sloan, J. R. Thompson, C. S. Kueny
Austin Research Associates, Austin, Texas 78746

Abstract

Theoretical analysis and computer simulation have been applied to obtain cavity designs that dramatically reduce cumulative beam breakup amplification for solenoidally focused, high current, relativistic electron beam multiple gap induction accelerators. Specific use is made of low emittance, long gap designs which provide phase cancellation and attendant reduced beam-eigenmode coupling; an effect the usual short gap,or impulse, approximation cannot address. Specific comparison with a standard short gap cavity design for a 50 MeV, 10 kA induction accelerator illustrates the significant improvement in beam breakup suppression that obtains with the low emittance long gap accelerator cavity designs.

I. Introduction

Beam breakup instability processes have been found to pose significant problems for high current, multi-MeV induction electron accelerators [1,2], particularly the cumulative type B instability [3]. Some improvement in performance has been gained by utilization of gas focusing or similar increase in focusing strength [4]; however, persistent beam breakup problems have often precluded operation of such accelerators at full design goals.

Over the past several years a new class of impedance matched induction accelerator gap geometries have been developed which provide significant improvement in maintenance of beam brightness at high beam currents [5]. These new geometries are characterized by long, adiabatic accelerating gaps and TEM power feed structures, as illustrated in Figure 1. Although initial conjectures that such structures might be immune to beam breakup [2] were shown under subsequent analysis to be incorrect [6], intensive investigation during the past 12 months has demonstrated that such structures can be configured to significantly reduce beam breakup well below levels achievable with conventional accelerating cavity geometries.

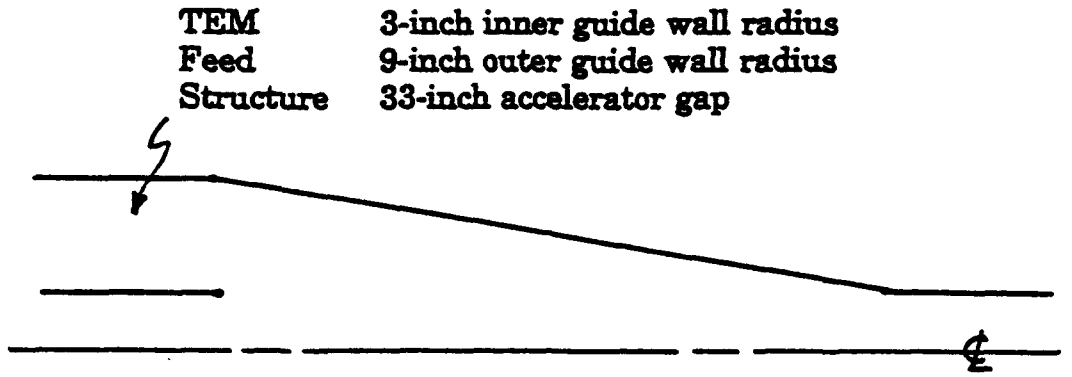

Figure 1. High brightness accelerating cavity.

II. Procedures for Investigation of Beam Breakup

Using the single mode approximation, the cumulative beam breakup gain per gap for a solenoidal magnetic field guided relativistic electron beam may be expressed [6]:

$$G = 2.5\,\frac{QI}{\omega^2 B}\,\frac{\left|\int_0^L dz\,\left[\partial_r E_z - (\partial_z - i\omega)\,E_r\right]_{r=0}\,\exp\left[-i\,(\omega+\Omega)\,z/c\right]\right|^2}{\int d^3x\;|E|^2} \qquad (1)$$

where I is the beam current in kiloamperes; B, the magnetic guide field in kilogauss; ω, the frequency of the cavity resonance; Ω, the relativistic cyclotron frequency; Q, the resonant cavity quality factor; L, the accelerator gap length; and E(r,z), the electric field of the cavity resonance.

For a conventional small gap accelerating cavity (i.e., $L \rightarrow 0$) of volume $\pi R^2 L$ dominated by a TM E_z field, Equation (1) yields the conventional beam breakup gain scaling:

$$G \sim \frac{QIL}{BR^2} \qquad (2)$$

Given that cavity geometry, beam current and focusing strength are often fixed by other considerations, the usual procedure employed to mitigate beam breakup is to

devise dissipative loading of accelerating cavity structures to reduce Q. This procedure is effective up to a point; in practice the overall minimum attainable Q is usually of the order of 2 - 10.

However, in addition to Q spoiling of the accelerating cavity, Equation (1) indicates a further approach offered by the high brightness, wide gap cavity designs; namely, phase cancellation between the propagating negative energy beam eigenmode and the cavity fields, as indicated by the overlap integral in the numerator of Equation (2). Specifically, if the cavity eigenmode is sufficiently extended in z [e.g., of the form exp (-z/ℓ)] and the focusing wavelength sufficiently short [$\Omega\ell/c = B\ell/1.7\gamma > 1$], significant phase cancellation may occur resulting in a reduced gain of the form:

$$G \sim \frac{QI\ell}{BR^2} \frac{1}{(1+0.35B^2\ell^2/\gamma^2)} \qquad (3)$$

In order to determine whether such improvements can be realized with the high brightness gap designs, a relativistic electron beam, cumulative beam breakup simulation code, BREAKUP, has been developed and benchmarked against known analytic solutions. This simulation code determines the beam breakup amplification factor over a specified frequency band for acceleration gap structures of arbitrary axisymmetric design and arbitrary resistive loading. Using BREAKUP, conventional high current, multi-MeV electron accelerator cavity structures as well as the high brightness structures have been examined and the resulting total amplification factors compared. One specific comparison is noted below.

III. Comparison of Conventional and High Brightness Cavity Structures

Typical of conventional accelerator cavity design is the structure shown in Figure 2, which is modeled after an ATA design [7]. By appropriate loading, the Qs of this cavity can be brought in line with quoted values [7] and the resulting beam breakup amplification calculated by BREAKUP. As noted, the third TM resonance appears to dominate beam breakup [7]. This is borne out by the

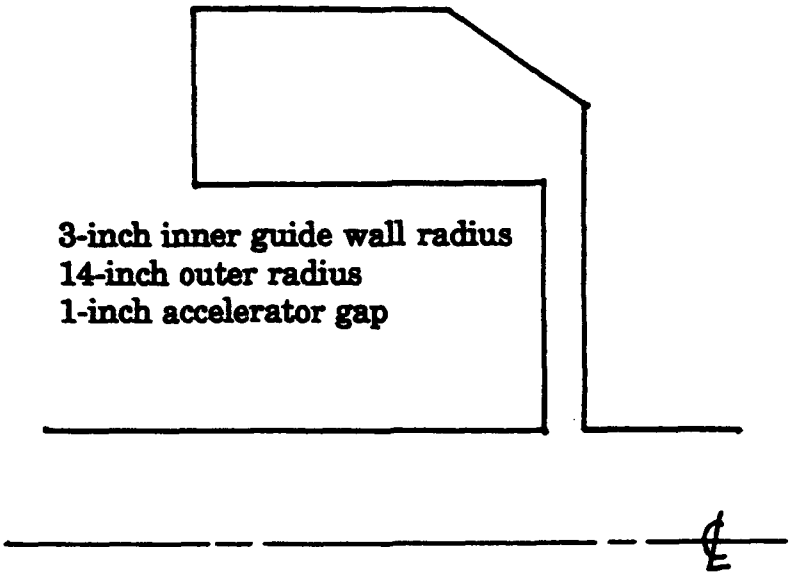

Figure 2. Conventional accelerator cavity.

BREAKUP simulation data shown in Figure 3 which spans the frequency space of the second and third cavity resonances. The peak gain value for this cavity is calculated by BREAKUP to be

$$G = \frac{I}{18B} \qquad (4)$$

Similarly, the beam breakup characteristics of the high brightness accelerating cavity of Figure 1 have been examined. An exhaustive search was conducted to determine the best achievable Q spoiling of the cavity. This will not be detailed here; suffice it to say that cavity loading dominated by a relatively simple 50 Ohms per

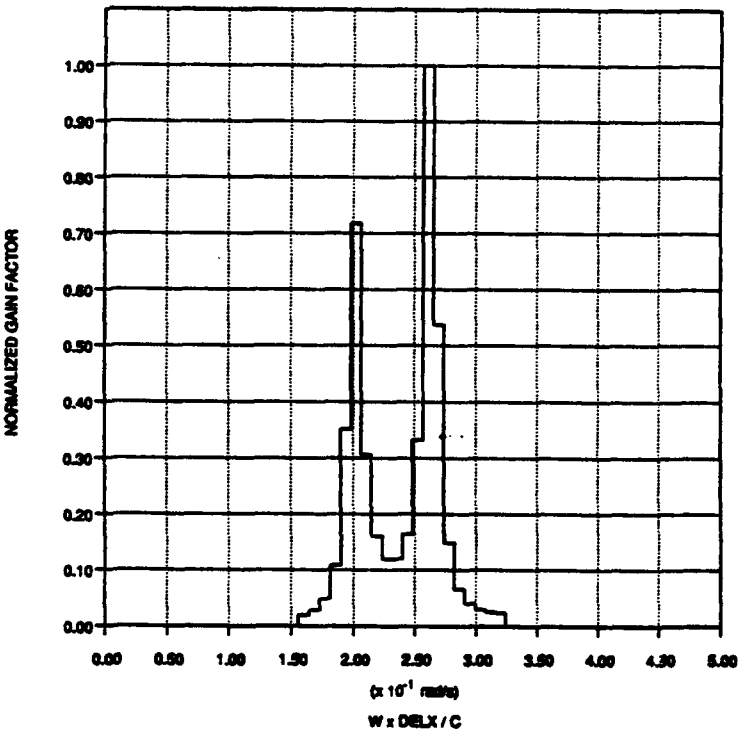

Figure 3. Conventional cavity gain curve.

square resistive sleeve insert in the TEM power feed line proved optimum. The BREAKUP-computed gain curve for this cavity is shown in Figure 4, with a peak gain given by

$$G = \frac{I}{34B} \qquad (5)$$

We note, however, that the above BREAKUP simulations were carried out for very small magnetic field values, in the range of 10^{-2} γ kilogauss. If we raise the value of the magnetic guide field a factor of 10, the narrow gap amplification formula remains unchanged; however, the high brightness cavity gain as computed by BREAKUP simulation code shows a lower numerical value G = I/(59 B), indicating the onset of phase cancellation reduction. With another factor of 10 increase in magnetic field, the gain curve shown in Figure 5 is obtained, exhibiting little of the original resonance structuring of Figure 4, with a marked decrease in gain to G = I/(5000 B). These lower values are consistent with the phase cancellation reduction factor of Equation (3). Indeed, a good fit to the Equation (3) scaling obtains for an ℓ = 25 cm, allowing the high brightness cavity gain to be expressed.

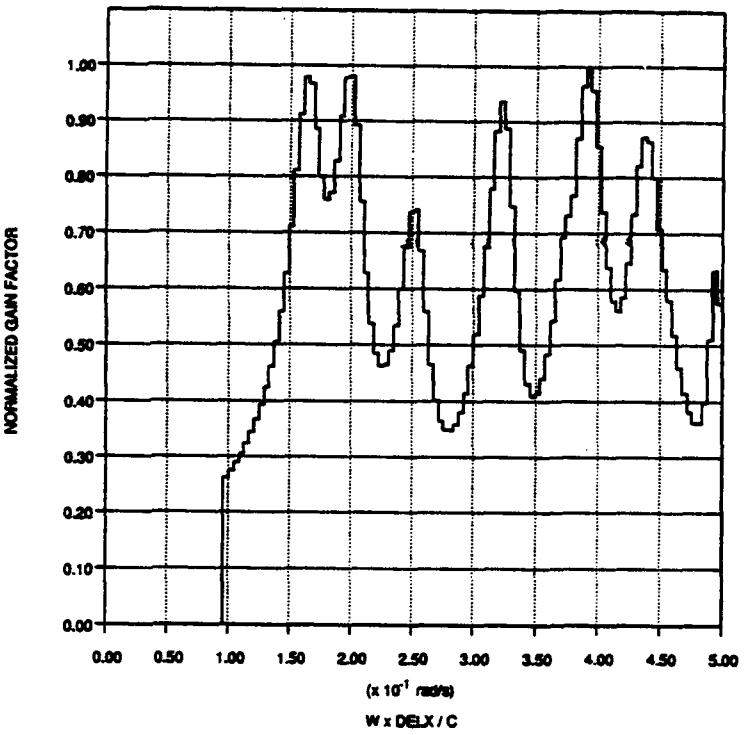

Figure 4. High brightness cavity gain curve.

$$G = \frac{I}{34B} \frac{1}{(1 + 230B^2/\gamma^2)} \qquad (6)$$

The gain formula for the standard narrow gap cavity of course shows no such reduction.

In order to calculate the total gain through an accelerator, the gains given by Equations (4) and (6) may be cumulatively summed over the number of accelerating cavities, starting with $\gamma = 1$ up to the final desired γ. For acceleration of a 10 kA electron beam to 50 MeV energy, utilizing 200 250 kV/gap accelerating cavities, the overall gain for the standard cavity design is given by

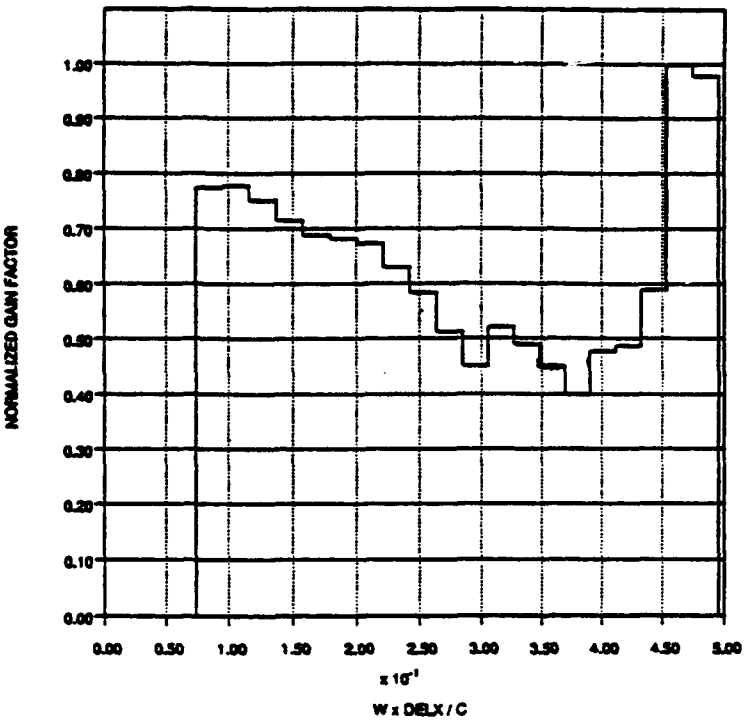

Figure 5. High brightness cavity gain curve showing phase cancellation reduction.

$$G = \exp\left(\frac{111.}{B}\right) \tag{7}$$

while the cumulative gain for the high brightness cavity may be expressed (allowing the replacement of the sum with an appropriate integral)

$$G = \exp\left[\frac{58.8}{B}\left(1 - 0.15B \arctan\left(\frac{1}{0.15B}\right)\right)\right] \tag{8}$$

The comparison of the number of e-folds of beam breakup for the two different cavities is shown in Table 1 for magnetic fields ranging from 1.0 to 10.0 kilogauss.

TABLE I

NUMBER OF E-FOLDS

B[kG]	STANDARD DESIGN	HIGH BRIGHTNESS DESIGN
1.0	110.	46.
2.0	56.	18.
3.0	37.	9.5
4.0	28.	5.6
5.0	22.	3.6
6.0	19.	2.4
7.0	16.	1.7
8.0	14.	1.2
9.0	12.	0.91
10.0	11.	0.69

The ATA literature [8] clearly indicates the desirability of limiting beam breakup amplification to less than 10 total e-folds down the accelerator. With the conventional cavity, this would require a rather large 10 kilogauss magnetic guide field, while the high brightness cavity would allow such reduced e-folds to be achieved with about 1/3 that value. Or stated another way, with a nominal 6.0 kilogauss guide field, the conventional cavity accelerator would exhibit some 19 e-folds, or an overall gain of some 2×10^8, while a high brightness cavity accelerator would suffer a total overall beam breakup gain of only 11.

IV. Summary

The large accelerating gap inherent to the high beam brightness cavity structures provides a means of significant reduction of cumulative beam breakup gain through phase cancellation between the negative energy beam eigenmode and the attendant cavity eigenmodes. Follow-on experimental investigation of such

designs to confirm their inherent beam breakup suppression, as well as high brightness advantages, should be carried out.

V. References

1. G. J. Caporaso, A. G. Cole, and K. W. Struve, "Beam Breakup Instability Experiments on ETA and Predictions for ATA," IEEE Trans. Nuc. Sci., Vol. NS-30, 1983, p. 2507.

2. R. B. Miller, B. M. Marder, P. D. Coleman, and R. E. Clark, J. Appl Phys. 63 (4), 997 (1988).

3. Y. Y. Lau, Phys. Rev. Lett. 63, 1141 (1989).

4. G. J. Caporaso, F. Rainer, W. E. Martin, D. S. Prono, and A. G. Cole, "Laser Guiding of Electron Beams in the Advanced Test Accelerator," Phys. Rev. Lett., Vol. 57, 1986, p. 1591.

5. J. R. Thompson, M. L. Sloan, J. R. Uglum, and B. N. Moore, "Beam Handling and Emittance Control," Proc. SPIE, Microwave and Particle Beam Sources and Directed Energy Concepts, Vol. 1061, 454 (1989).

6. M. L. Sloan and James R. Thompson, "Beam Breakup in Low Emittance Accelerator Cavities," Proc. SPIE, Intense Microwave and Particle Beams, Vol. 1226, 447 (1990).

7. R. J. Briggs, et al., IEEE Trans NS-28, 3360 (1981).

8. D. S. Prono, "Recent Progress of the Advanced Test Accelerator," IEEE Trans. Nuc. Sci., Vol. NS-32, 1985, p. 3144.

VI. Acknowledgement

This research was carried out under ONR Contract N00014-88-C-0542.

APPENDIX G

RETROFIT OF THE ATA DRIVE STRUCTURE FOR BEAM BREAKUP SUPPRESSION

M. L. Sloan and J. R. Thompson, "Retrofit of the ATA Drive Structure for Beam Breakup Suppression," I-ARA-92-U-20.

RETROFIT OF THE ATA DRIVE STRUCTURE

FOR BEAM BREAKUP SUPPRESSION

M. L. Sloan and J. R. Thompson
Austin Research Associates

I. Introduction

Recently discovered adiabatic accelerating gap structures that allow significant improvements in beam brightness for high current relativistic electron beam accelerators [Ref. 1] have also been shown to provide substantial improvement in beam breakup control. In particular, a comparison was recently made between conventional narrow gap accelerating structures and the new high brightness adiabatic gap structures for a 50 MeV 10 kA solenoidal B field guided electron beam accelerator, such as typified by the LLNL Advanced Test Accelerator (ATA). Data from this study [Ref. 2] indicates that the ATA could have operated at the nominal 3 kG guide field level using these advanced gap designs and achieved full operation at 10 kA and 50 MeV without beam breakup disruption. Using the nominal narrow gap design, a guide magnetic field of over 10 kG would have been required.

Although the effectiveness of such designs was not disputed, criticism was immediately raised by LLNL personnel that such gap designs were incompatible with engineering constraints dictated by limitations on the size, shape, and placement of the drive ferrites and the desirability to maintain as short an accelerator as possible.

In order to address these concerns head-on and demonstrate that such accelerating structures can be configured consistent with practical engineering considerations, we have conceptually retrofitted an ATA narrow gap drive structure with a high brightness design. This retrofit involves only the interior of the 6-inch diameter vacuum drift space and does not alter in any way the guide magnetic field coil geometry, ferrite core structure, power coupling, loading of the ferrite cavity, or any other aspects of the ATA drive structure exterior to the 6-inch beam line.

The resulting modified ATA accelerating structure provides a 4-inch drift tube and a 21 cm accelerating gap. Although by no means optimized, this structure again demonstrates the improvement in beam breakup control attendant to such gap designs, particularly the significant reduction in beam breakup growth in the early stages of acceleration where significant phase cancellation can occur across the wide gap. In this brief note, these improvements are quantified.

II. ATA Accelerating Gap Structure Characteristics

The ATA accelerating module structure is shown in Figure 1, excerpted from Reference 3. The attendant electromagnetic resonant cavity structure relevant to beam breakup is depicted in Figure 2. With appropriate loading, the Qs of the resonances of this cavity can be brought in line with values noted for ATA. Using the ARA BREAKUP simulation code, the beam breakup amplification factor as a function of frequency can then be determined, as shown in Figure 3. The observed unstable cavity resonances are consistent with the ATA literature.

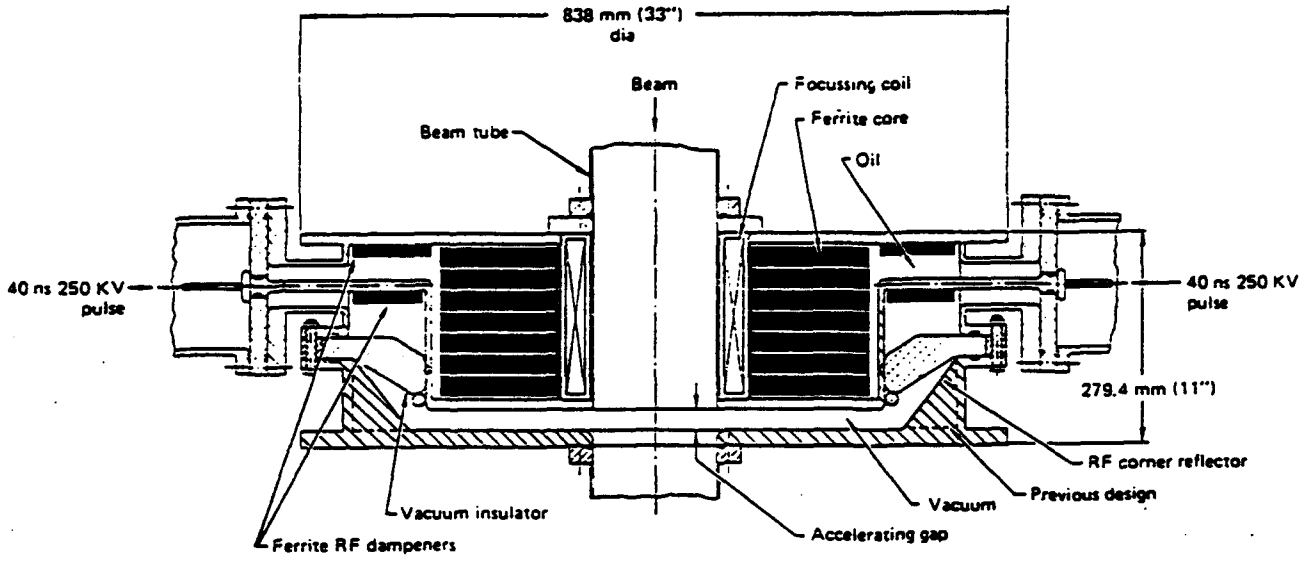

Figure 1. ETA/ATA acceleration module.

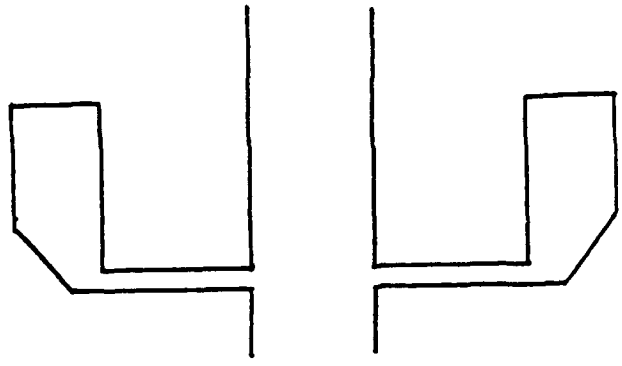

Figure 2. ATA cavity structure relevant to beam breakup.

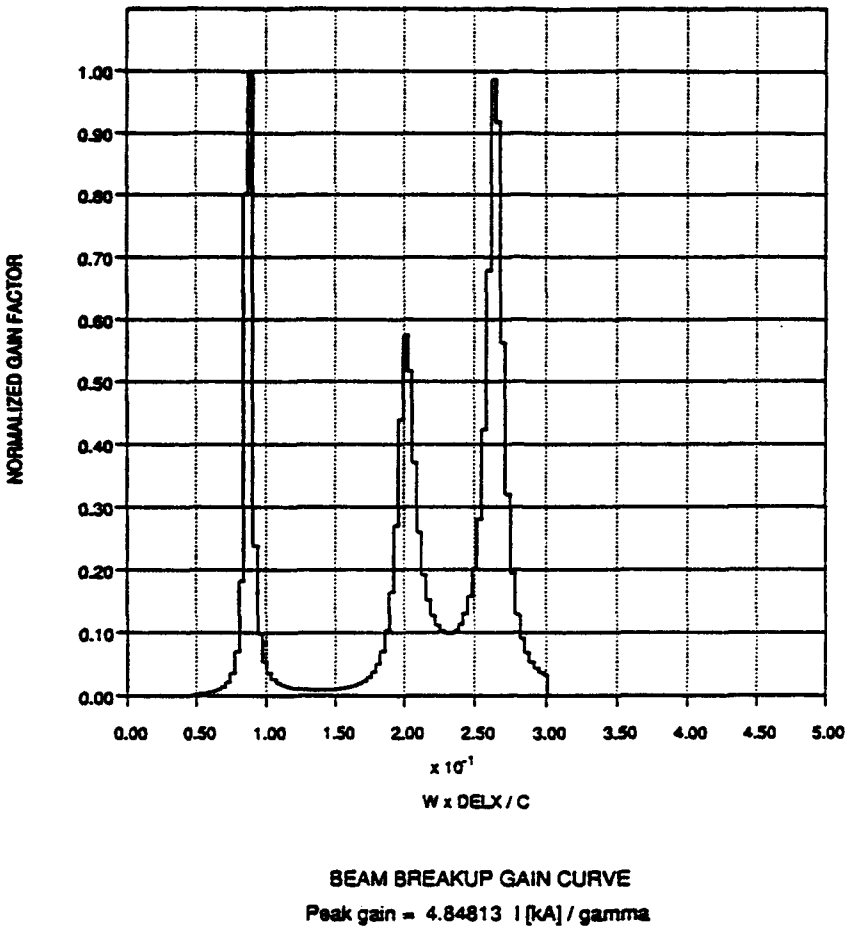

Figure 3. Beam breakup amplification for ATA Structure (DELX = 1.25 cm)

III. Retrofit of the ATA Acceleration Module

Figure 4 depicts the retrofit of the ATA cavity to accommodate an adiabatic high brightness acceleration structure. As can be seen, the original ATA radial gap has been swung 90 degrees into a TEM feed structure, an integral component of the high brightness design. This TEM structure, impedance matched to the beam current and gap voltage, subsequently opens into a 21 cm accelerating gap that provides adiabatic acceleration of the beam with minimum degradation of beam brightness. Because this more complicated geometry introduces additional modes localized to the gap region which are not well damped by the ferrite loading of the outer cavity (the short TEM structure providing some isolation between the gap region and the outer cavity), a resistive sleeve of 30 ohms per square is introduced along the inner wall of the TEM feed structure to spoil the Q of the new modes.

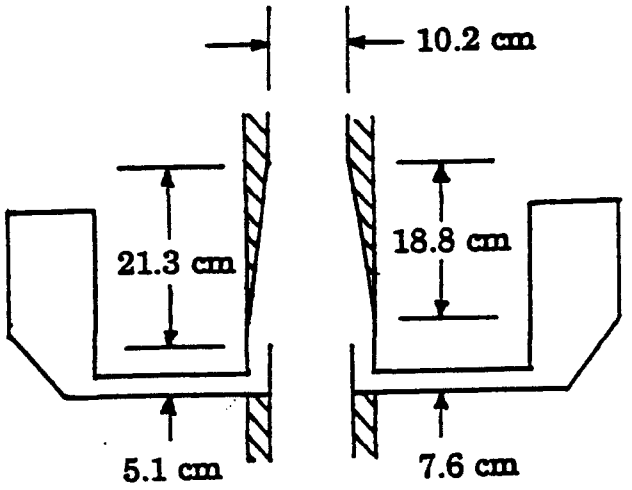

Figure 4. Retrofit of ATA with adiabatic gap structure consisting of 5.1 cm TEM power feed and 21.3 cm gap.

The resulting beam breakup gain curve is shown in Figure 5.[1] It will be noted that the lowest three unstable modes correspond to the unstable modes of the unmodified ATA cavity structure, Figure 3, with the first mode at a somewhat reduced growth rate, indicating some isolation provided by the short TEM feed structure. In addition to these first three modes, there are now at least two distinct additional modes at f = 1.2 GHz ($\omega\Delta/c = 0.32$) and f = 1.4 GHz ($\omega\Delta/c = 0.36$) which have no counterpart in the narrow gap design, being instead modes associated with the relatively smaller 4-inch diameter, wide gap accelerating structure. These modes are seen to exhibit growth rates somewhat smaller, but comparable to the lower frequency modes.

---

6 [1]In Figures 3 and 5, the upper range of frequency is the respective TE waveguide cutoff frequency for each structure, since BREAKUP is configured to investigate only the spatially amplifying, beam coupled beam breakup instability and does not extend to the higher frequency electromagnetically coupled breakup regime. This high frequency regime generally exhibits much weaker growth due to significant phase cancellation for both narrow gap as well as high brightness gap designs. As amply attested by the ATA experience, it is the virulent beam coupled resonant cavity modes that are of primary concern for high current electron induction linacs.

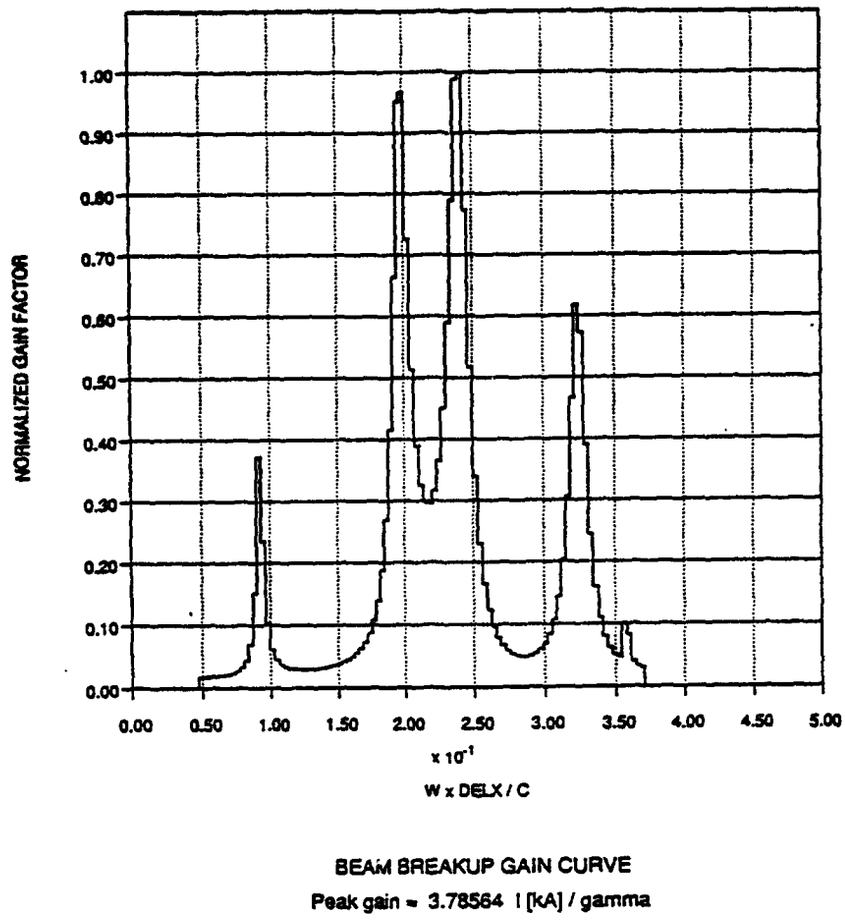

Figure 5. Beam Breakup Amplification for Adiabatic Gap Structure (DELX = 1.25 cm)

Were these somewhat reduced growth rates the only benefits of the wide gap design, further consideration of such gaps would not be called for. However, as shown in Reference 2, a considerable additional benefit obtains for operation at sufficiently high magnetic guide field (or sufficiently low γ) that the breakup eigenmode spans several cyclotron wavelengths (c/Ω) in the wide gap region. In such cases, the scaling of the breakup amplification A changes from the narrow gap formula:

$$A \sim \frac{c}{\Omega} \qquad (1)$$

to a significantly reduced rate for $\Omega\ell/c > 1$:

$$A \sim \frac{c}{\Omega} \frac{1}{1 + \Omega^2 \ell^2 / c^2} \qquad (2)$$

where ℓ characterizes the longitudinal extent of the beam breakup mode in the gap region.

This change in scaling of the beam breakup amplification factor reflects phase cancellation between the beam motion and the electromagnetic fields in the gap region.

We point out that the growth rates depicted in Figures 3 and 5 for the standard, narrow gap and the adiabatic wide gap geometries, respectively, were both calculated in the limit of very small guide fields, specifically $\Omega/c = 0.012 \text{ cm}^{-1}$ so that $\Omega\ell/c < 1$ and, as would then be expected for comparable Q loading, the growth rates in the two cases are comparable.

If we now increase Ω/c by a factor of 100 so that we move to the other extreme of large values of $\Omega\ell/c$, we note the following: Were the adiabatic cavity design to follow the conventional narrow gap scaling, Eq. 1, we would expect to see only a factor of 100 reduction in beam breakup amplification. However, BREAKUP simulation of the retrofitted ATA cavity in this $\Omega/c = 1.2 \text{ cm}^{-1}$ high field regime, Figure 6, shows reduction of the peak gain from

$$A = 3 - 4 \; I/\gamma \qquad (3)$$

to

$$A \leq 3 \times 10^{-5} \; I/\gamma \qquad (4)$$

resulting in an overall reduction of about 10^5, well above the 10^2 narrow gap design reduction factor. This again demonstrates the very significant reduction in beam breakup amplification afforded by phase cancellation in adiabatic gap designs.

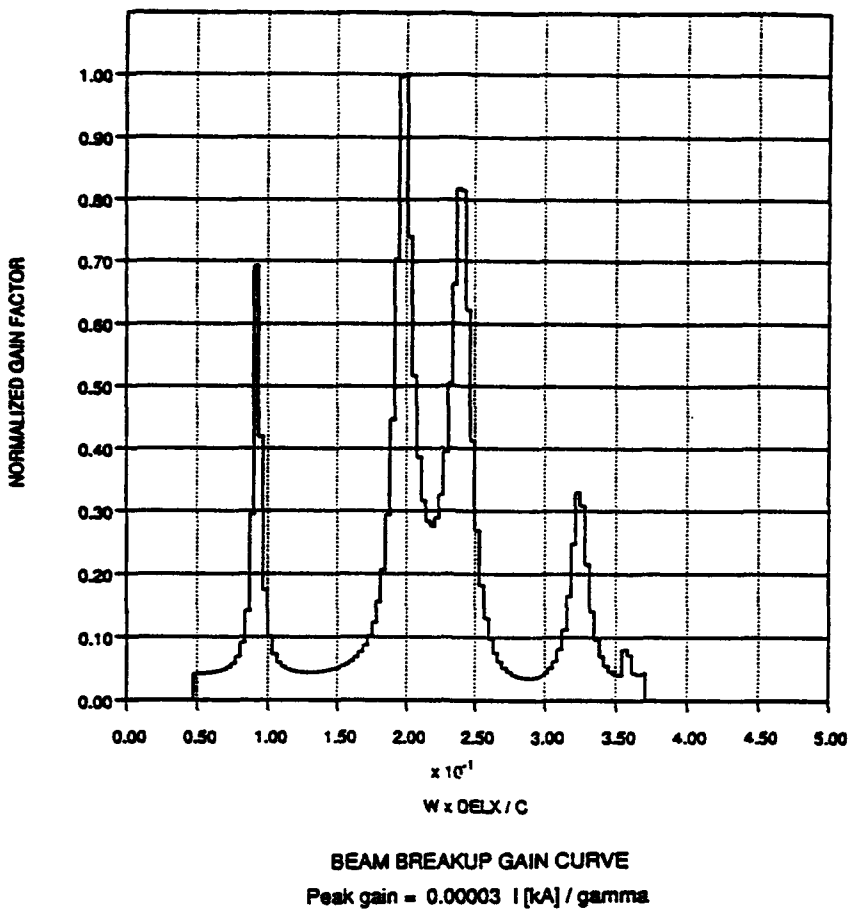

Figure 6. Phase cancellation reduction of beam breakup amplification for adiabatic gap structure.

III. Summary

To address concerns raised about the practicality of high brightness adiabatic gap geometries for high current inductive electron beam accelerators, a conceptual retrofit to the ATA standard narrow gap drive structure was carried out to:

1. Provide a high brightness, reduced beam breakup adiabatic accelerating gap geometry in the region of the beam, while

2. Maintaining undisturbed the magnetic guide field coil placement, ferrite core structure, ferrite cavity design, power feed structures, and all other aspects of the original ATA engineering design exterior to the 6-inch vacuum drift tube.

Even under the constraints of this retrofit, which in no way constitutes an optimum design, the superior beam breakup suppression characteristics of the high brightness adiabatic accelerating gap structures are demonstrably maintained.

IV. References

1. J. R. Thompson, et. al., "Beam Handling and Emittance Control," Proc. SPIE, Microwave and Particle Beam Sources and Directed Energy Concepts, Vol. 1061, 454 (1989).

2. M. L. Sloan, et. al., "Low Emittance Accelerator Cavity Design to Minimize Amplification of Beam Breakup Modes," to be published in Proceedings of 9th International Conference on High-Power Particle Beams (1992).

3. R. J. Briggs, et. al., IEEE Trans. NS-28, 3360 (1981).

V. Acknowledgement

This research was carried out under ONR Contract N00014-88-C-0542.

APPENDIX H

OPTIMIZED CAVITY DESIGN FOR BBU SUPPRESSION

APPENDIX H

OPTIMIZED CAVITY DESIGN FOR BBU SUPPRESSION

The long adiabatic acceleration gap geometries that have demonstrated such remarkable beam brightness characteristics also offer significant advantages over more standard narrow gap designs in suppression of beam breakup. These advantages have been noted before [Refs. 1,2]; however, they are again here reiterated for sake of completeness.

A typical adiabatic accelerator gap geometry is shown in Figure 1. The features that are noteworthy for BBU control are:

1. The TEM co-axial power feed structure, as opposed to the radial power feed structures typical of narrow gap designs, and

2. The long accelerator gap cavity, again in contrast to the very narrow accelerating gap of more conventional design.

The advantages for BBU control that derive from these features are discussed below.

A. Advantages deriving from the TEM feed

The TEM coax power feed structure is helpful in two distinct ways:

1. Such a structure is cut off to m = 1 (BBU displacement) modes for all frequencies below

$$\omega < 1/b \qquad (1)$$

(in fact, the actual cutoff lies between 1/a and 1/b). For values of b ~ 5-10 cm, this cutoff frequency would be of the order of $\omega \sim 4 \times 10^9$ (f = 700 MHz). Therefore, the TEM power feed provides isolation between low frequency modes associated with the larger ferrite drive structure geometries (typically many tens of centimeters in dimension) and the few centimeter radius accelerator gap cavity proper, as noted by Miller [Ref. 3]. This isolation thus reduces the BBU problem to BBU instability of the modes of the coax feed structure and/or adiabatic gap geometry proper, with typical frequencies of 1 GHz or higher.

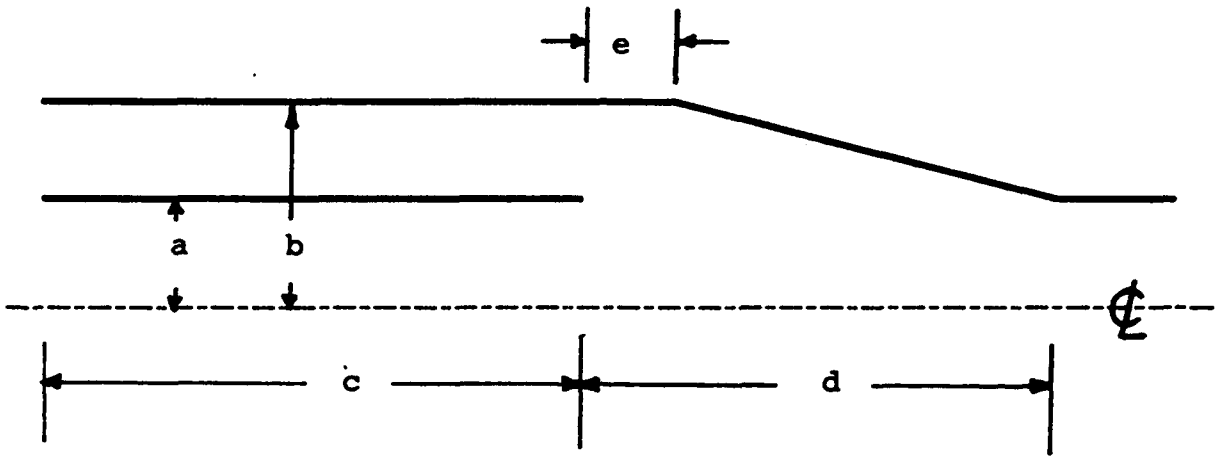

Figure 1. **Adiabatic gap design (baseline values of parameters a - e given in Table 1).**

2. The coax feed structure furthermore provides a very natural method of resistive loading of the BBU m = 1 modes without any adverse effect on the m = 0 driving fields. As contrasted to the TM011 and similar BBU modes for narrow gap radial feed structures whose m = 1 electric field patterns are qualitatively the same as the driving m = 0 fields (namely, large Ez fields, zero Eθ and Er fields), the m = 0 drive fields feeding through the coax structure are entirely Er, while the m = 1 BBU modes in the coax structure exhibit significant components of both Eθ and Ez. Therefore, the coax structure can be loaded with resistive structures of finite conductivity in the θ and/or z direction to provide effective Q spoiling of the m = 1 BBU modes without any effect on the m = 0 drive fields. Such loading moreover provides further isolation of the induction ferrite drive apparatus from the gap region even for frequencies above the m = 1 coax cutoff through resistive damping of the modes as they traverse the coax feed.

Theory indicates that optimum loading of the coax feed is achieved by placement of a resistive sleeve or liner midway between the inner and outer radii of the coax structure, with a liner resistance R_l given by

$$R_l = 377\,((b-a)/(b+a))^2 \qquad [\text{ohms/sq}] \tag{2}$$

and a resulting effective damping length L_l given by

$$L_l = (b+a)^2/(b-a) \tag{3}$$

B. <u>Advantages deriving from the long adiabatic gap</u>

A second advantage provided by the long adiabatic accelerating structures for suppression of BBU growth is phase cancellation. As noted previously [Ref. 1, Appendix E of this report], the raw BBU gain for a solenoidally guided high current electron beam traversing a gap of arbitrary geometry can be expressed

$$G = \frac{1}{17} \frac{QI}{\Omega_0 \omega^2} \frac{|R|^2}{u} \tag{4}$$

where I is the beam current measured in kiloamperes, Q is the usual cavity quality factor,

$$U = \int |A|^2 / 8\pi \; d^3x \tag{5}$$

and $\Omega_0 \equiv \gamma \Omega$ is the nonrelativistic gyrofrequency associated with the guide solenoidal B field. The quantity U is a measure of the total energy in the BBU eigenmodes and

$$R = \int_0^d (\partial_r A_z - i\Omega A_r) \exp -i(\omega + \Omega)z \; dz \tag{6}$$

is the overlap integral of the electron beam m = 1 negative energy displacement mode

$$\xi = \xi_0 \exp[i(\omega + \Omega)z - i\omega t] \tag{7}$$

and the electric fields of the unstable cavity resonance.

For narrow gap geometries where A and $\exp i(\omega + \Omega)z$ do not vary significantly across the gap, both U and R scale as the gap dimension d, so that the BBU gain factor of Equation (4) is seen to scale linearly with d. Hence the generally-accepted lore that accelerator gaps should be made as narrow as possible, and operated at the highest electric field stress practical, to minimize BBU.

However, for adiabatic gaps where $(\omega + \Omega)d > 1$, significant phase cancellation can occur in the overlap integral of Equation (6), so that in the limit of large d the gain factor asymptotes from a linear in d scaling to one inversely proportional to d:

$$G \propto d \rightarrow \frac{1}{(\omega + \Omega)^2 d} \tag{8}$$

Such behavior offers significant reduction in BBU gain, particularly at the low energy (low γ) end of the accelerator where $\Omega d = \Omega_0 d/\gamma > 1$.

C. Optimized adiabatic gap design

These attributes have been utilized in the design and optimization of a specific adiabatic gap geometry for BBU suppression. In particular, investigation and optimization has been carried out in the adiabatic cavity design of Figure 1 with the following specific baseline geometry:

TABLE 1

a	= 5 cm
b	= 7 cm (6-in. diameter)
c	= 55 cm
d	= 25 cm
e	= 3 cm

The b/a ratio is consistent with impedance-matched acceleration of a 10 kA, 250 kv gain per gap beam (24 Ohm impedance), not untypical of high current induction accelerator operation.

The EIGENMODE code was used to determine the resonant frequencies of this particular structure, using a $\Delta = 1.25$ cm (1/2-in) numerical gridding. The $m = 1$ resonant frequencies below the drift tube TE cutoff frequency $\omega\Delta \sim 0.4$ were found to be[1]

[1]For assessing beam-coupled BBU amplification, only frequencies below the drift tube cutoff frequency can be considered. Frequencies above that will result in electromagnetic radiation co-propagating with the beam from cavity to cavity. Investigation of BBU instability from such modes lies outside the scope of this effort; however, in general it has been noted that such modes do not give rise to significant BBU because of the phase cancellation between the beam and the co-propagating mode. Rather, as clearly demonstrated by the LLNL ATA experience [Ref. 4,5], it is the individual cavity resonances below drift tube cutoff that are generally most dangerous.

TABLE 2

$\omega\Delta = 0.20$ (f = 760 MHz)
$\omega\Delta = 0.22$ (f = 840 MHz)
$\omega\Delta = 0.26$ (f = 990 MHz)
$\omega\Delta = 0.32$ (f = 1.2 GHz)
$\omega\Delta = 0.38$ (f = 1.5 GHz)

Using this and the related eigenmode field pattern as guides, variation of the cavity geometry as well as the resistive loading of this particular structure were then carried out to determine an optimized configuration for suppression of BBU. The results of this survey are summarized below.

1. θ-Z Resistive Liner Inserts Studies

The BREAKUP code was used to study BBU behavior over the span of frequencies indicated by the EIGENMODE data for the baseline geometry cavity of Figure 1 operated in the low B field (or conversely, high γ) regime where phase cancellation effects are not operative. Specifically, a value of $\Omega\Delta = 0.01$ was chosen and a cylindrical sleeve of resistive material of varying lengths and resistivities was inserted midway between the inner and outer walls of the TEM coax power feed structure, as indicated in Figure 2. As noted earlier, such a sleeve will not affect the $m = 0$ acceleration fields of the cavity, but does provide damping of the $m = 1$ BBU modes through Ohmic dissipation of currents induced in the z and θ directions by the BBU fields.

Equation (2) indicates an optimum liner resistance of about 10 Ohms/sq for the baseline $b = 7$ cm and $a = 5$ cm values. Subsequent BREAKUP simulations confirm this optimum value. In Figures 3 through 6, the BBU gain curve is plotted

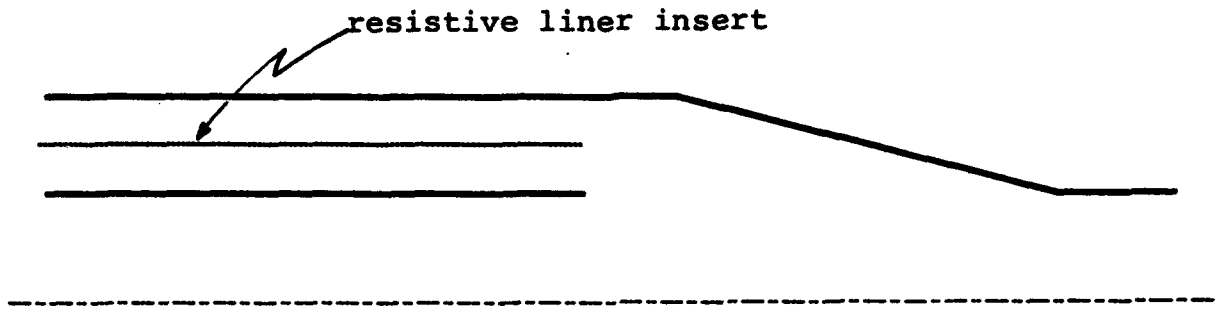

Figure 2. Baseline accelerator gap geometry showing resistive liner insert.

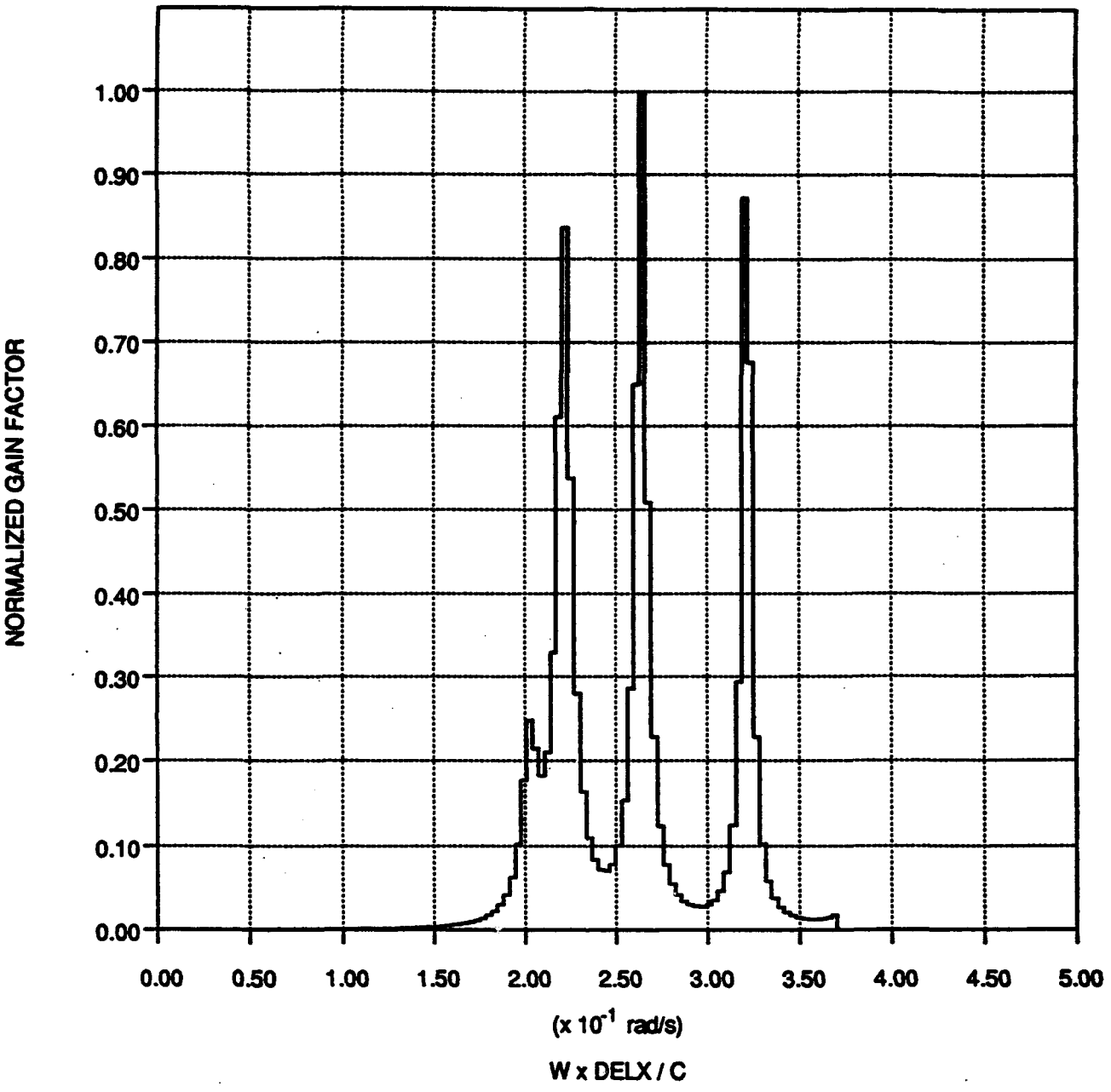

Figure 3. BBU gain curve for 30 Ω/sq insert.

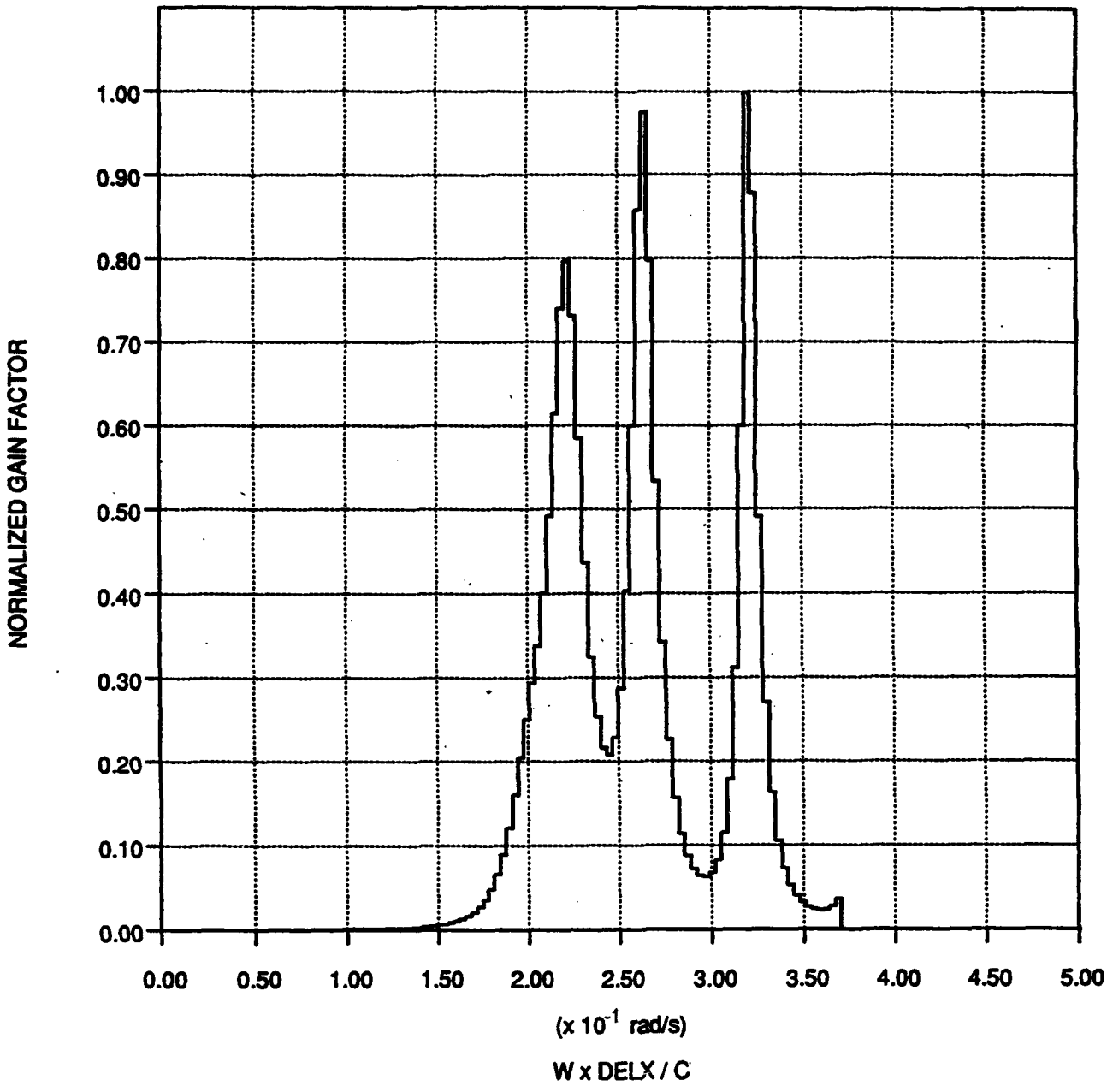

Figure 4. **BBU gain curve for 15 Ω/sq insert.**

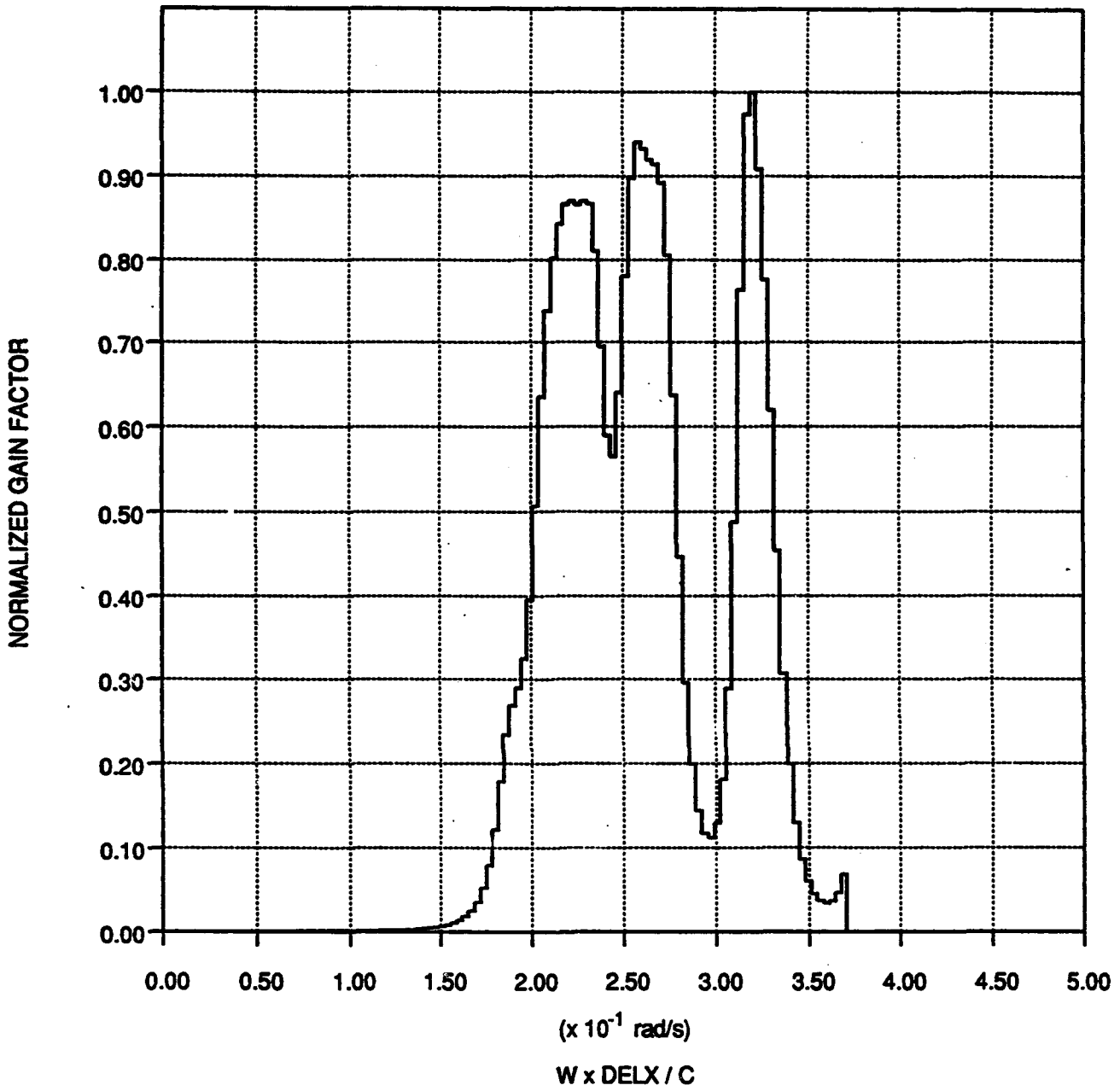

Figure 5. BBU gain curve for 8 Ω/sq insert.

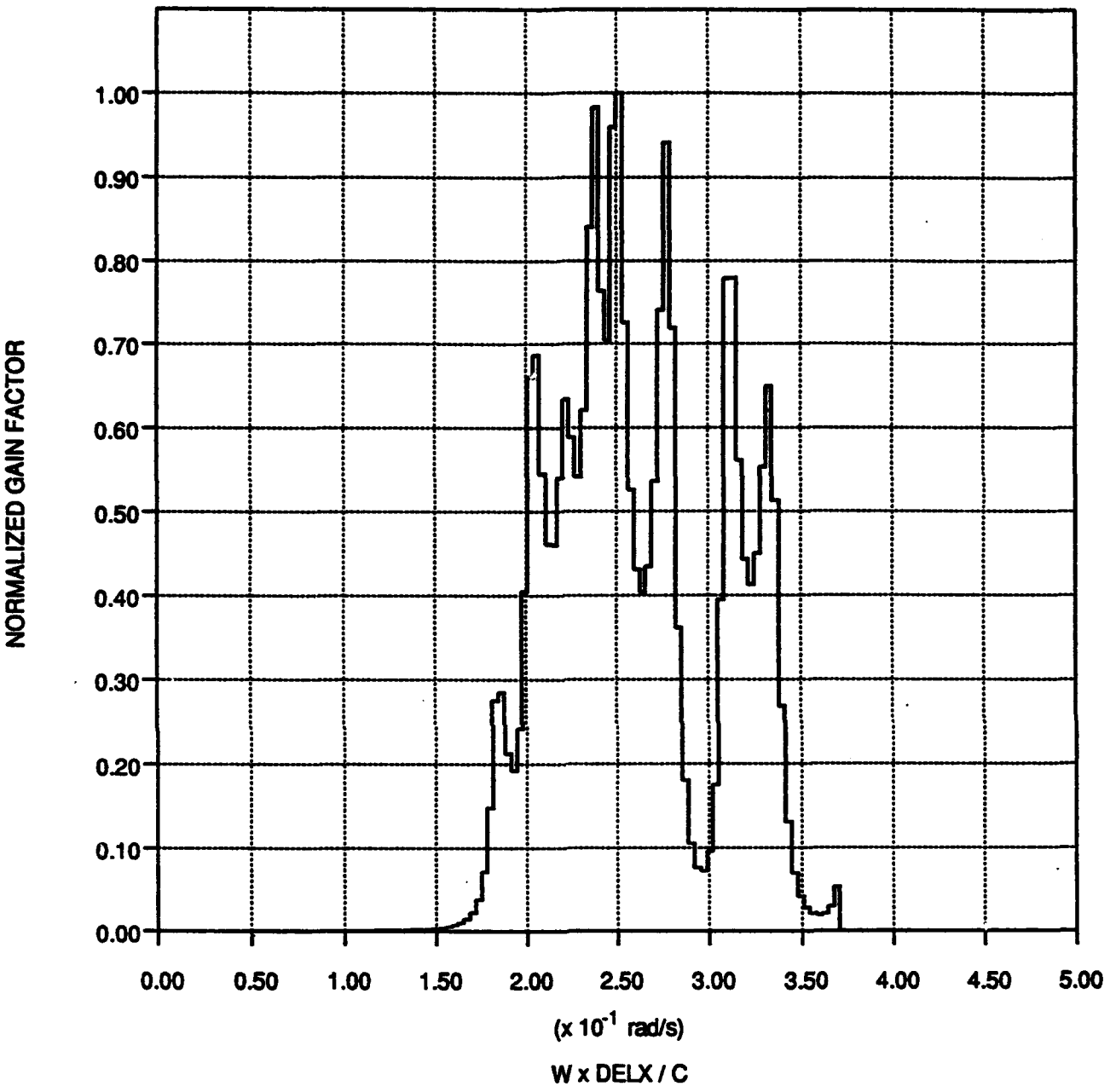

Figure 6. BBU gain curve for 4 Ω/sq insert.

for liner resistances of 30, 15, 8 and 4 Ohms/sq, respectively. In all four cases, the liner was chosen equal in length to the $c = 55$ cm coax feed structure. As can be noted, the 8 Ohms/sq provided optimum suppression of BBU.

2. Extended θ-Z Resistive Liner Insert

From Equation (3), the damping length for the baseline liner parameters is found to be 72 cm, so that when sized to the full $c = 55$ coax feed length, such a liner provides somewhat less than a full e-fold of damping and isolation. Accordingly, further suppression might obtain with a longer resistive liner structure. Such is indeed the case. Figure 7 depicts a liner/cavity geometry where the liner which extends past the end of the coax feed across the accelerator gap proper (some 60 cm. in length). The BBU gain curve for this configuration is given in Figure 8. Two features should be noted. First, the overall gain of the unstable modes is reduced. But secondly, because the resistive material now extends into the accelerator gap proper where it can couple directly to the self fields of the electron beam (as opposed to coupling through the cavity fields), a low frequency resistive wall contribution to overall beam instability is evident, peaking at $\omega \sim 0.03$ (115 Mhz). However, this instability contribution is significantly lower than the gain due to BBU growth of the cavity resonances and would not be of concern for operation of the accelerator gap in this configuration.

What would, however, be of concern is the fact that the portion of the resistive liner extending across the accelerating gap would now affect the $m = 0$ accelerating fields. Therefore, such an extended liner configuration would not prove practical.

3. Resistive Liner Insert with Infinite Z Conductivity

Theoretical considerations suggested that improvement might be provided under the scalar resistivity sleeve insert discussed above by configuring a liner with finite θ resistivity, but zero z resistivity. Such a liner would be relatively simple to fabricate; however, BREAKUP simulation studies of such a configuration show somewhat poorer performance than the simple resistive liner insert. Specifically, in Figures 9 through 12, the BBU gain curves for such a liner are depicted. These are to be compared to the previous gain curves of Figures 3 through 6. The accelerator

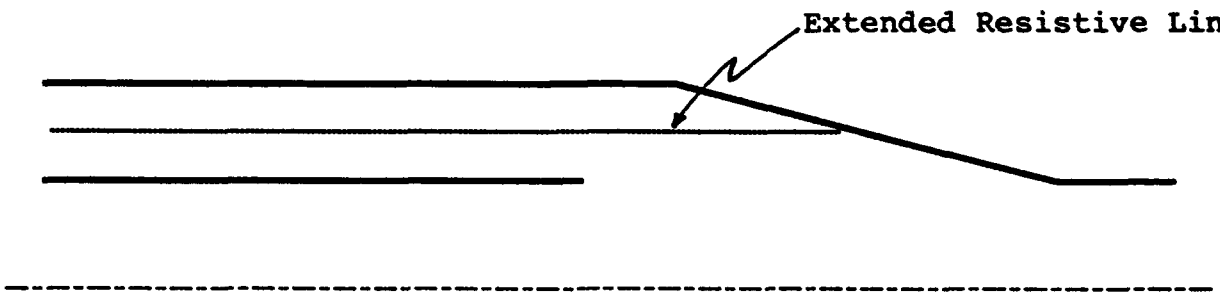

Figure 7. **Baseline accelerator gap geometry showing extended resistive liner insert.**

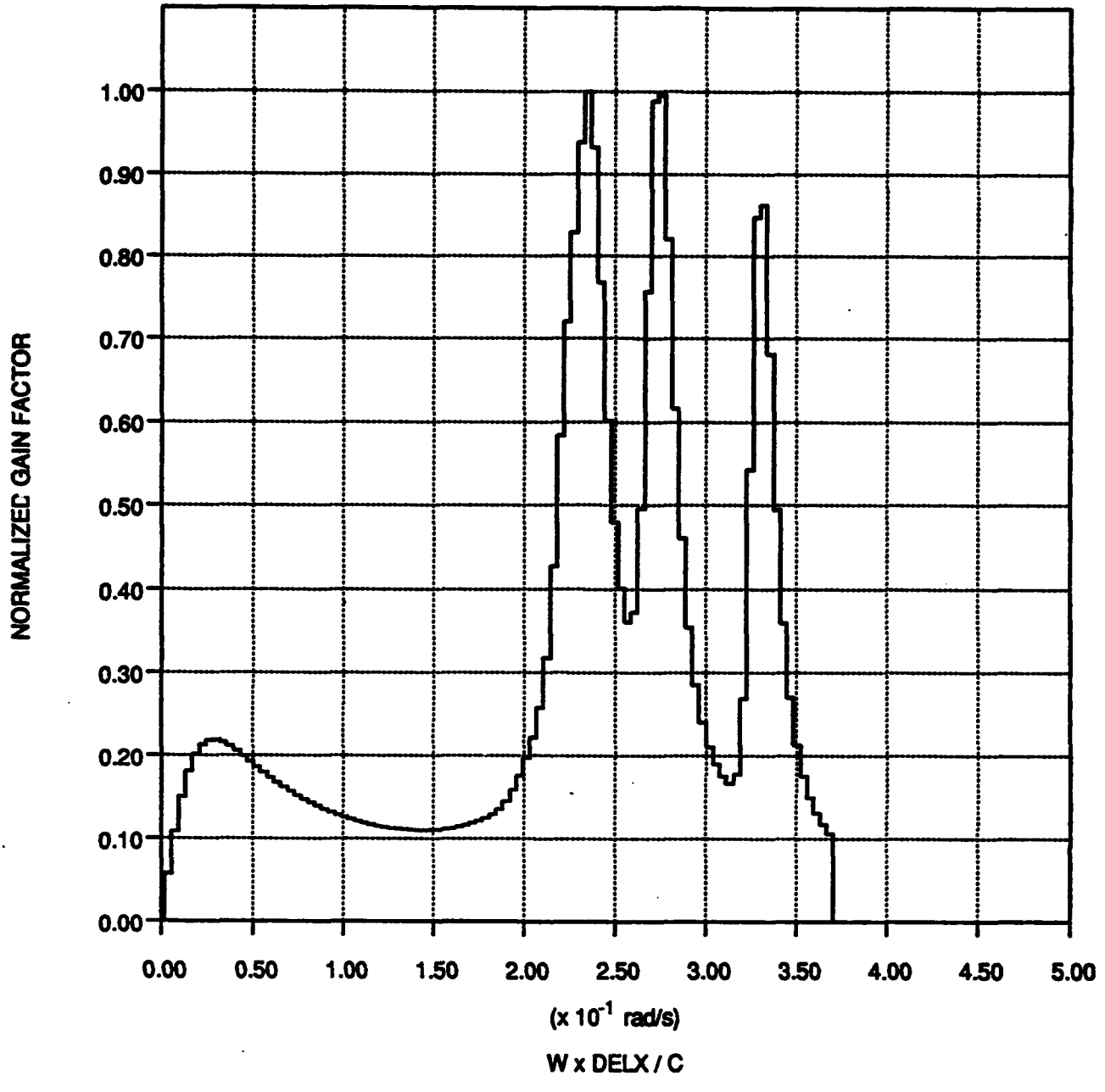

Figure 8. BBU gain curve for extended 8 Ω/sq insert.

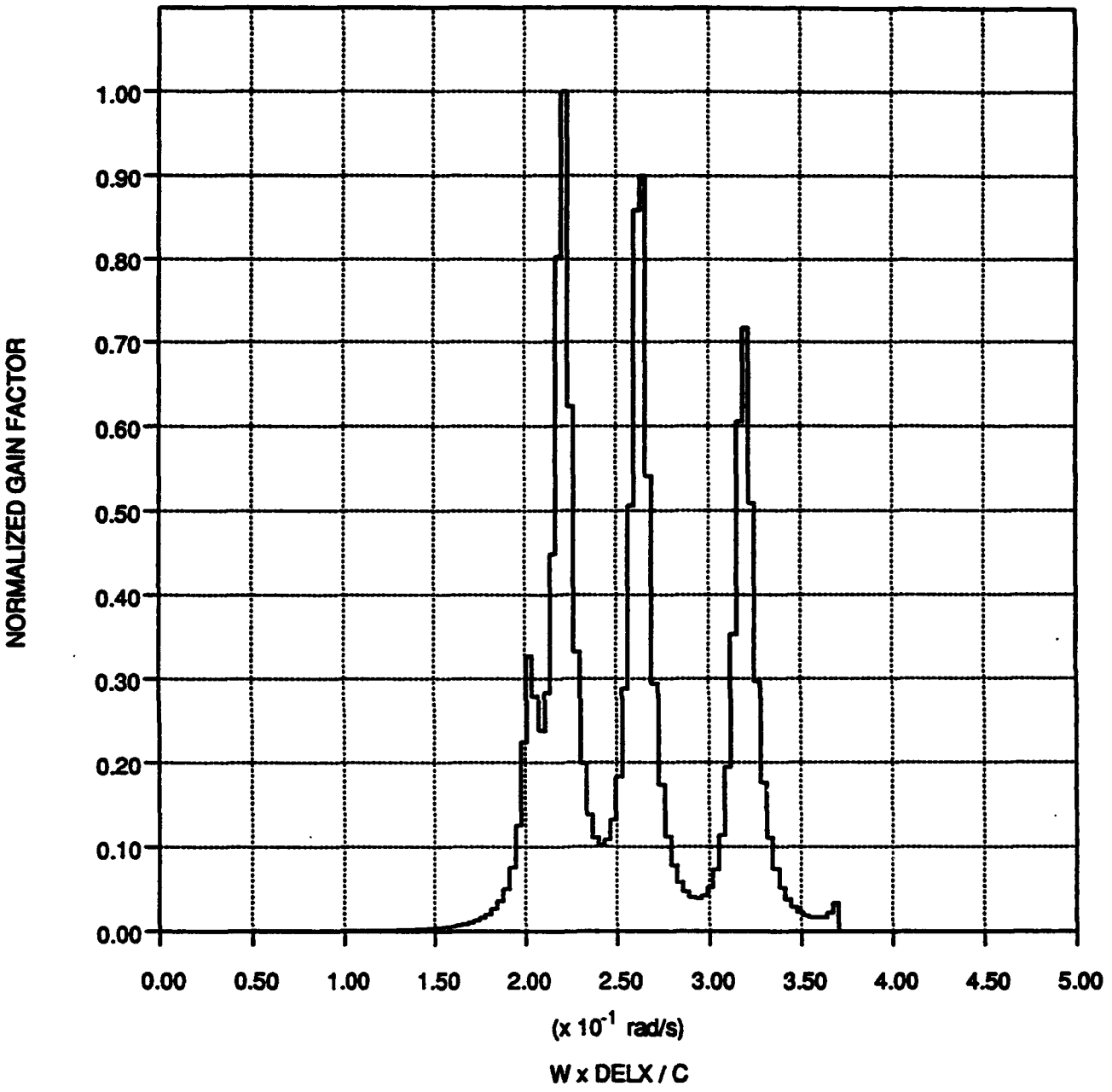

Figure 9. BBU gain curve for Z-shorted 32 Ω/sq insert.

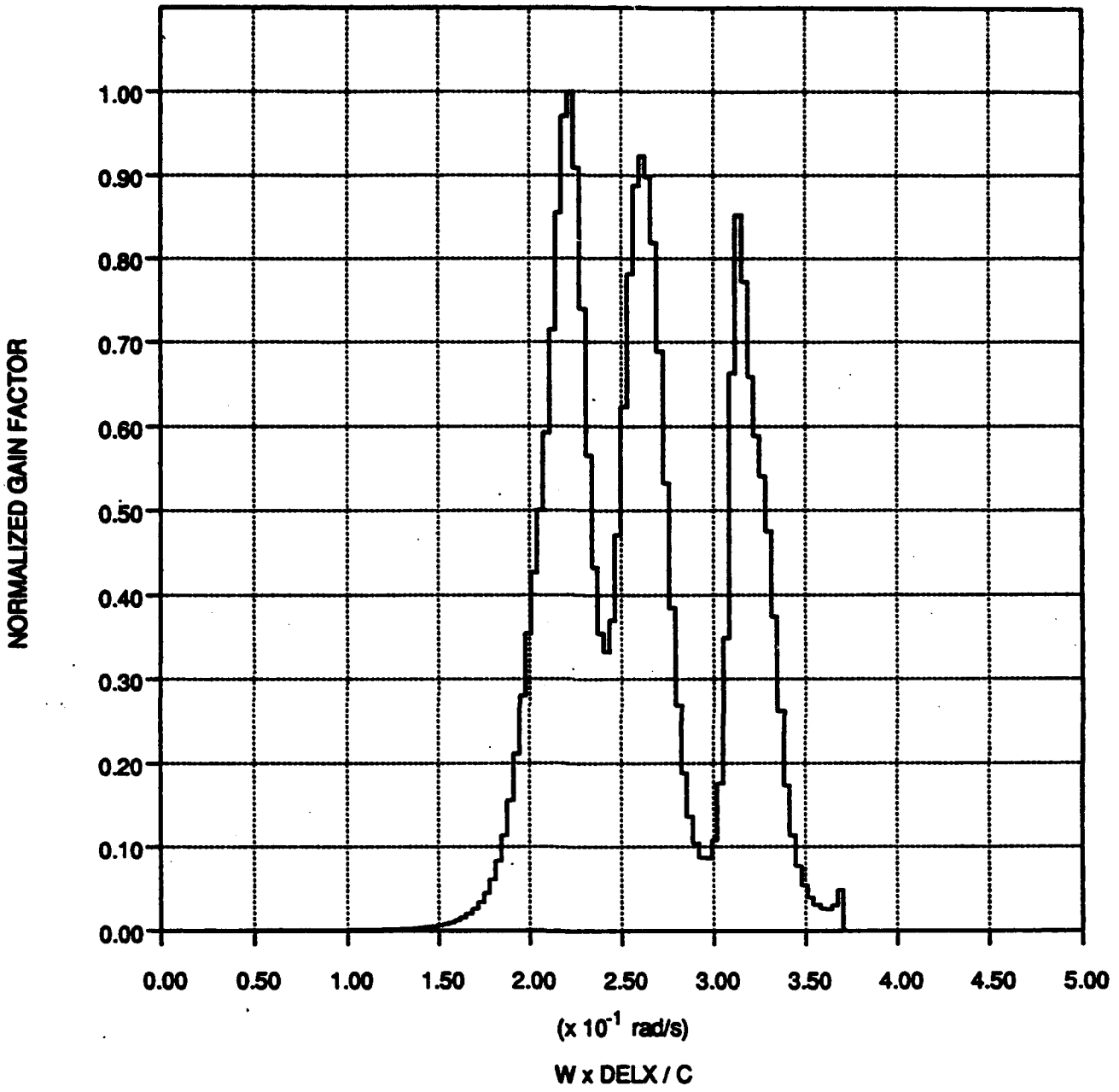

Figure 10. BBU gain curve for z-shorted 16 Ω/sq insert.

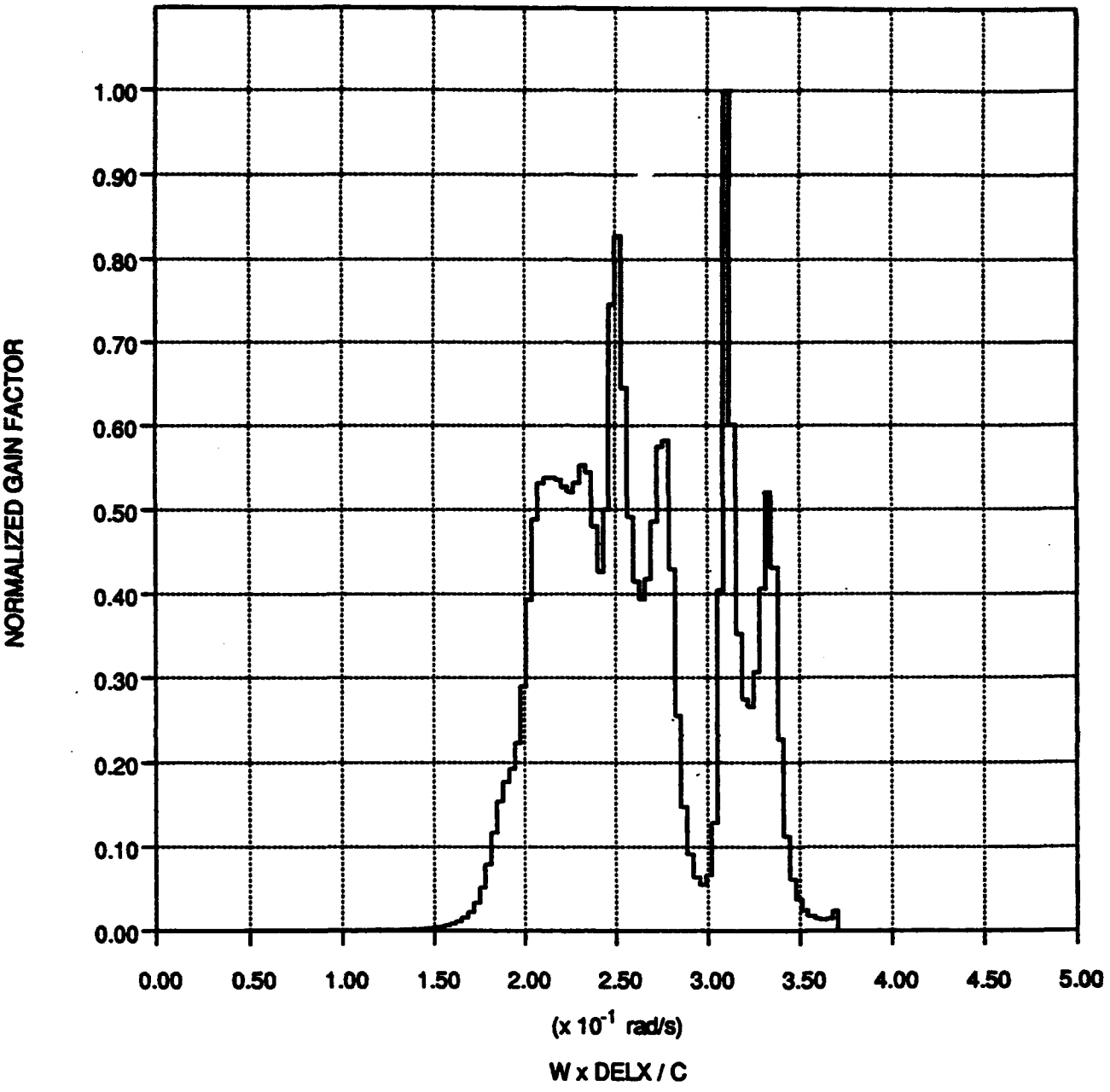

Figure 11. BBU gain curve for z-shorted 8 Ω/sq insert.

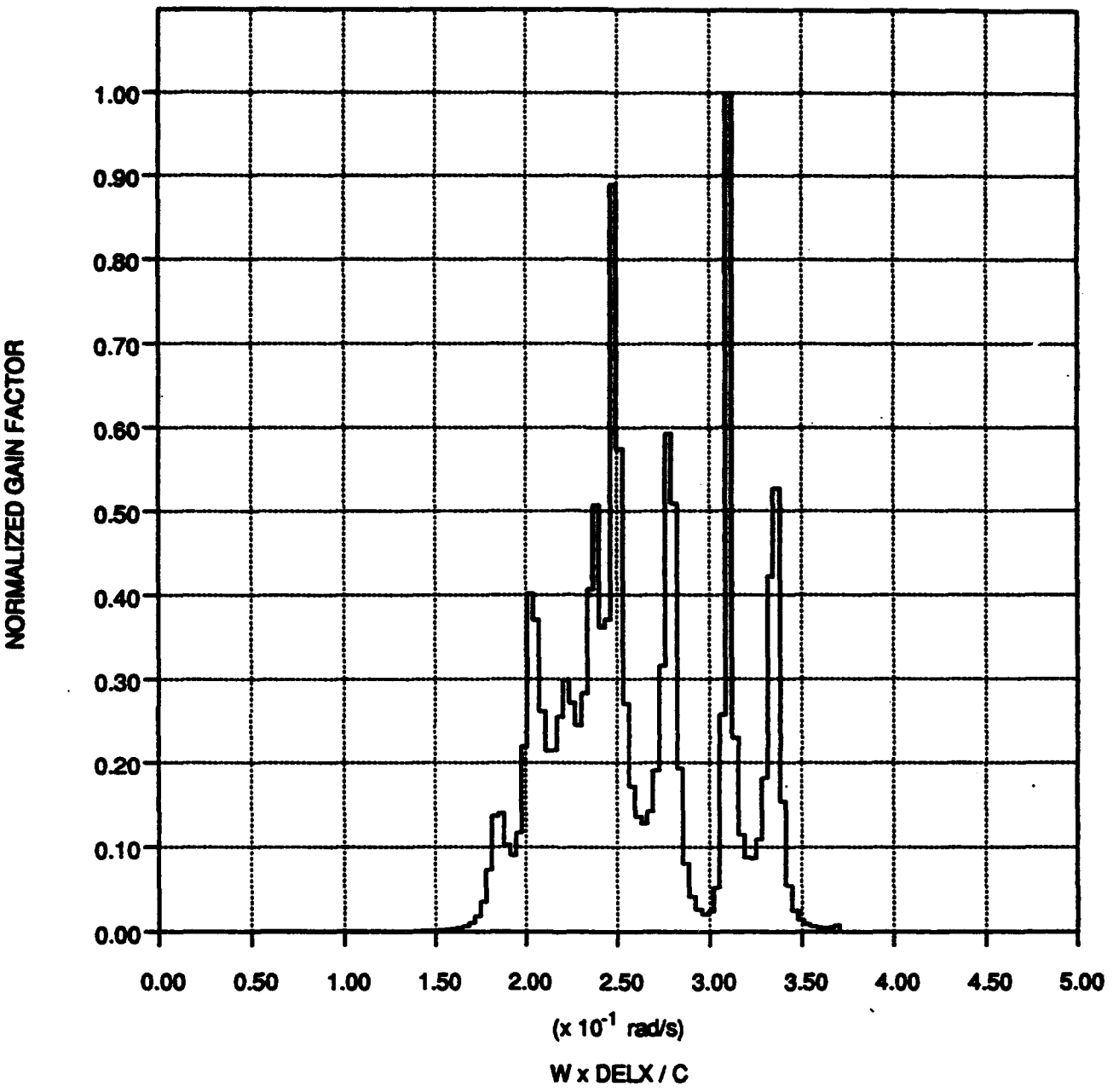

Figure 12. BBU gain curve for z-shorted 4 Ω/sq insert.

gap geometry as well as resistive liner length (55 cm) were essentially identical in the two cases; the only significant difference is that the liner of Figures 9 through A12 has zero z resistance.

4. Baseline Parameter Variations

Additional BREAKUP simulations were undertaken utilizing the 8 Ohm/sq resistive liner structure which had proved optimum (Figure 5), but where specific changes were made to the baseline accelerator gap geometry. In Figure 13, the gain curve is depicted for an accelerator gap where the gap width parameters d and e were both increased form their respective baseline values of 25 cm and 3 cm to

$$d = 53 \text{ cm}$$

$$e = 33 \text{ cm}$$

A second variant on this cavity where the accelerator gap region was increased slightly in radius to 7 cm to 9 cm (resulting in a 2 cm bulge in the accelerator structure depicted in Figure 2) was also examined. The gain curve for this geometry is given in Figure 14.

Although more adiabatic, both structures proved poorer in performance than the shorter baseline cavity and were not further studied.

5. Phase Cancellation Reduction of BBU for the Optimum Cavity Design

The result of these studies showed that the 8 Ohm/sq scalar resistive liner loaded baseline cavity geometry proved to afford optimum suppression of BBU gain in the high γ (or conversely low B) regime where phase cancellation within the accelerator gap is at a minimum. The observed peak gain noted from Figure 5 is

$$G = 3.5\, I[ka]/\gamma \quad \text{for} \quad \Omega\Delta = 0.01\,. \tag{9}$$

This formula may be written in invariant form

$$G = 0.14 \quad \frac{I[kA]}{\Omega_0\, a} \tag{10}$$

which is valid for all cavity structures of similar shape (i.e., those which will scale to the baseline parameters of Table 1) operating in the small d, minimum phase

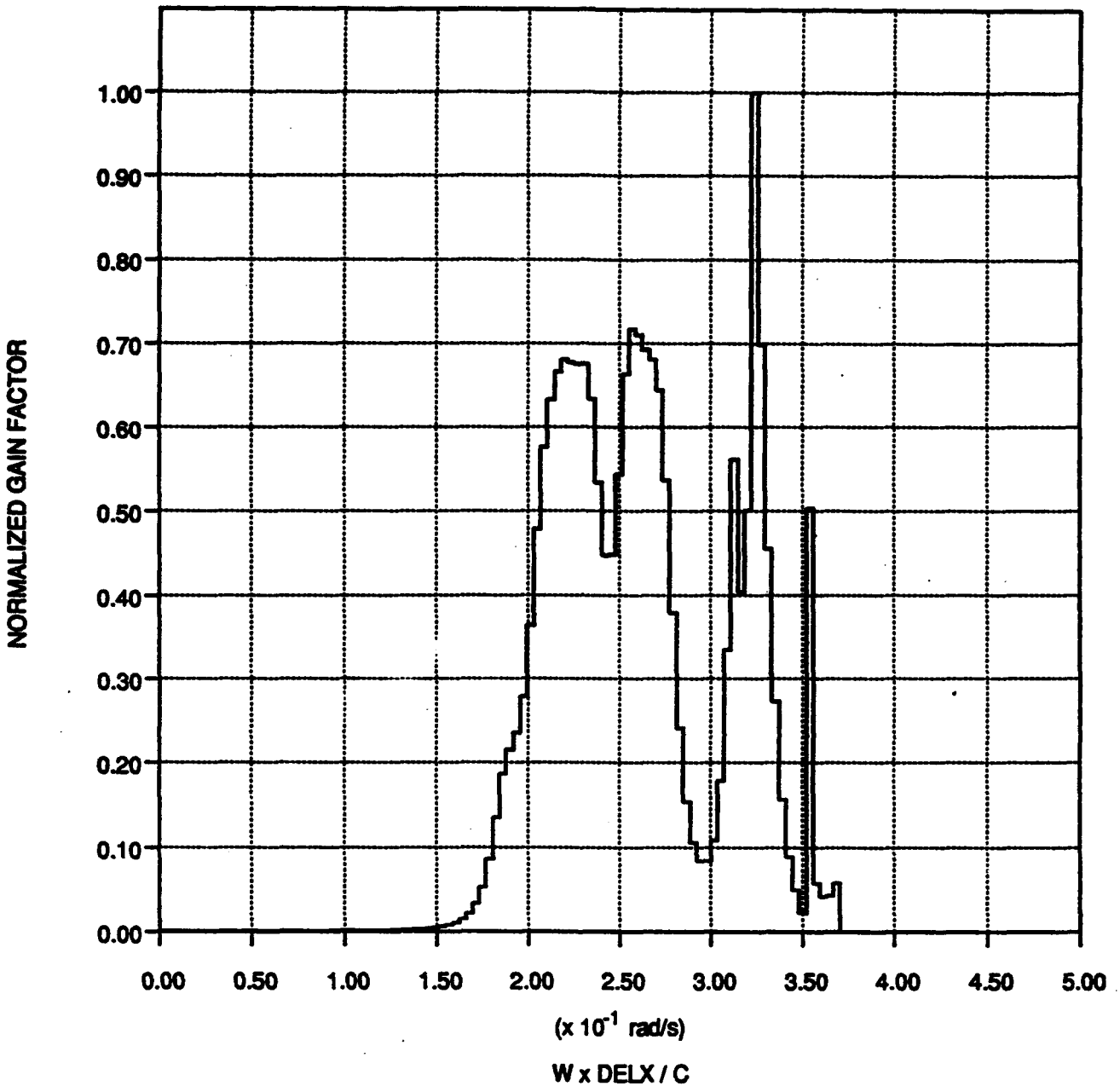

Figure 13. BBU gain curve for d = 53 cm, e = 33 cm geometry.

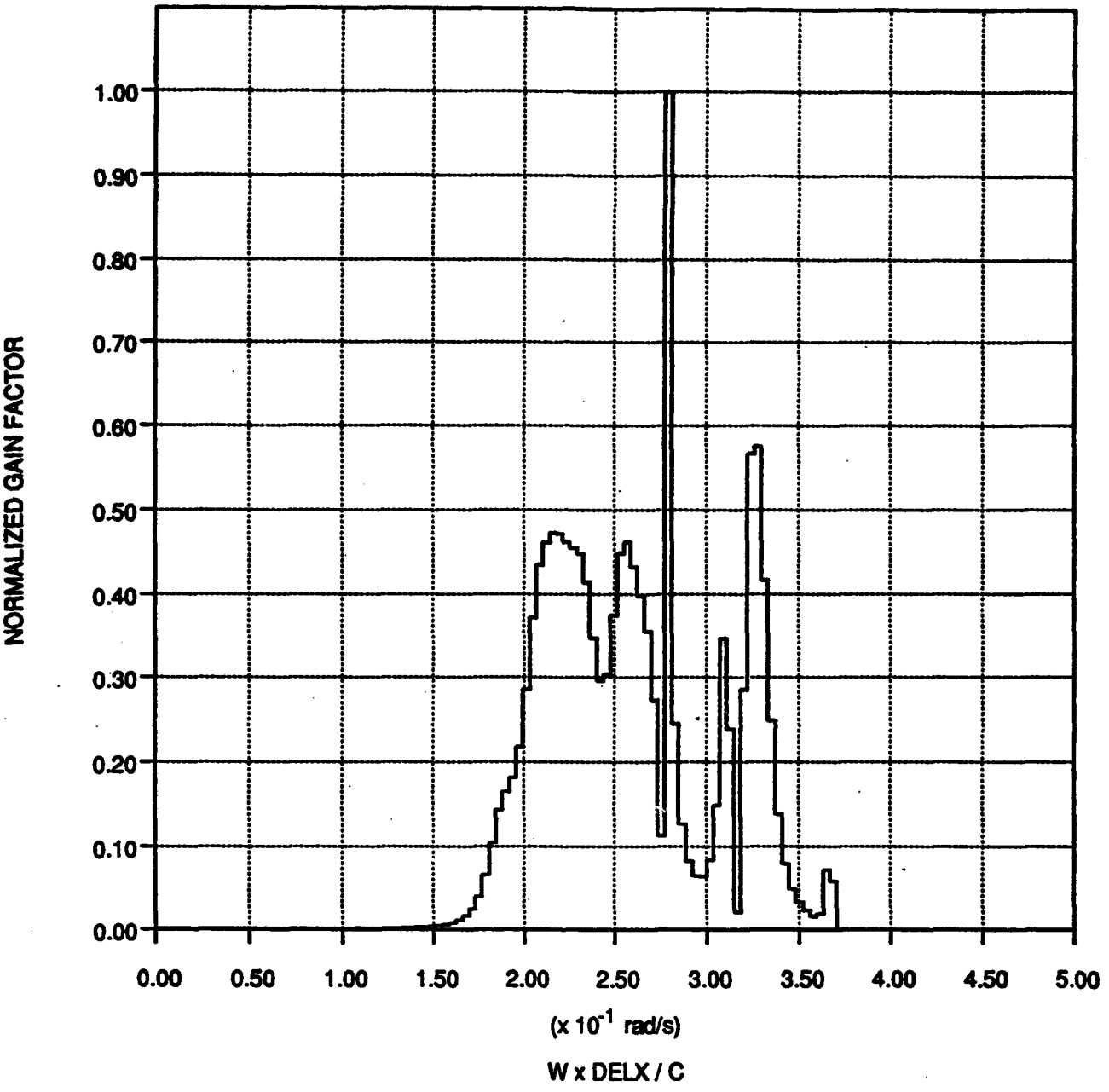

Figure 14. BBU gain curve for gap geometry with bulge.

cancellation regime, provided that the Ohms/sq resistance of the insert liner is maintained.[2]

This geometry has been subsequently examined for larger values of $\Omega\Delta$; specifically

$$\begin{aligned} \Omega\Delta &= 0.01 \quad \text{(original case, Figure 5)} \\ \Omega\Delta &= 0.10 \\ \Omega\Delta &= 1.00 \end{aligned} \tag{11}$$

Data from these last two BREAKUP simulations is shown in Figures 15 and 16, respectively. Written in invariant form, the peak BBU gain for each case may be expressed

$$G = 0.07 \quad \frac{I[kA]}{\Omega_0 a} \tag{12}$$

and

$$G = 2.4 \times 10^{-4} \quad \frac{I[kA]}{\Omega_0 a} \tag{13}$$

Therefore, operating at sufficiently high values of $\Omega\Delta$ results in dramatic reduction of BBU gain over and above the $1/\Omega_0$ scaling. These additional reductions are the result of phase cancellation effects.

By comparing the numerical coefficients of Equations (10), (12) and (13), it can be seen that phase cancellation effects (which are buried in the numerical coefficient) are coming into play at about $\Omega\Delta = 0.1$, where the numerical coefficient is down by a factor of 2 from the $\Omega\Delta \rightarrow 0$ limit, Equation (10). Since we know from theoretical considerations that such effects arise when $\Omega d_{eff} \sim 1$, we can conclude that d_{eff} (that region of the gap d occupied by the BBU resonance) is in the range of 10-20 cm for

---

[2]This means, for example, that cavity structures twice as large, but operated at one-half the magnetic guide field strength, exhibit identical BBU gain. And conversely. One may also note that the gain formula is independent of the beam energy γ, another feature that makes BBU especially troublesome for multi-gap accelerators, since there is no reduction in gain at the higher energies even though the beam is significantly "stiffer" at high γ.

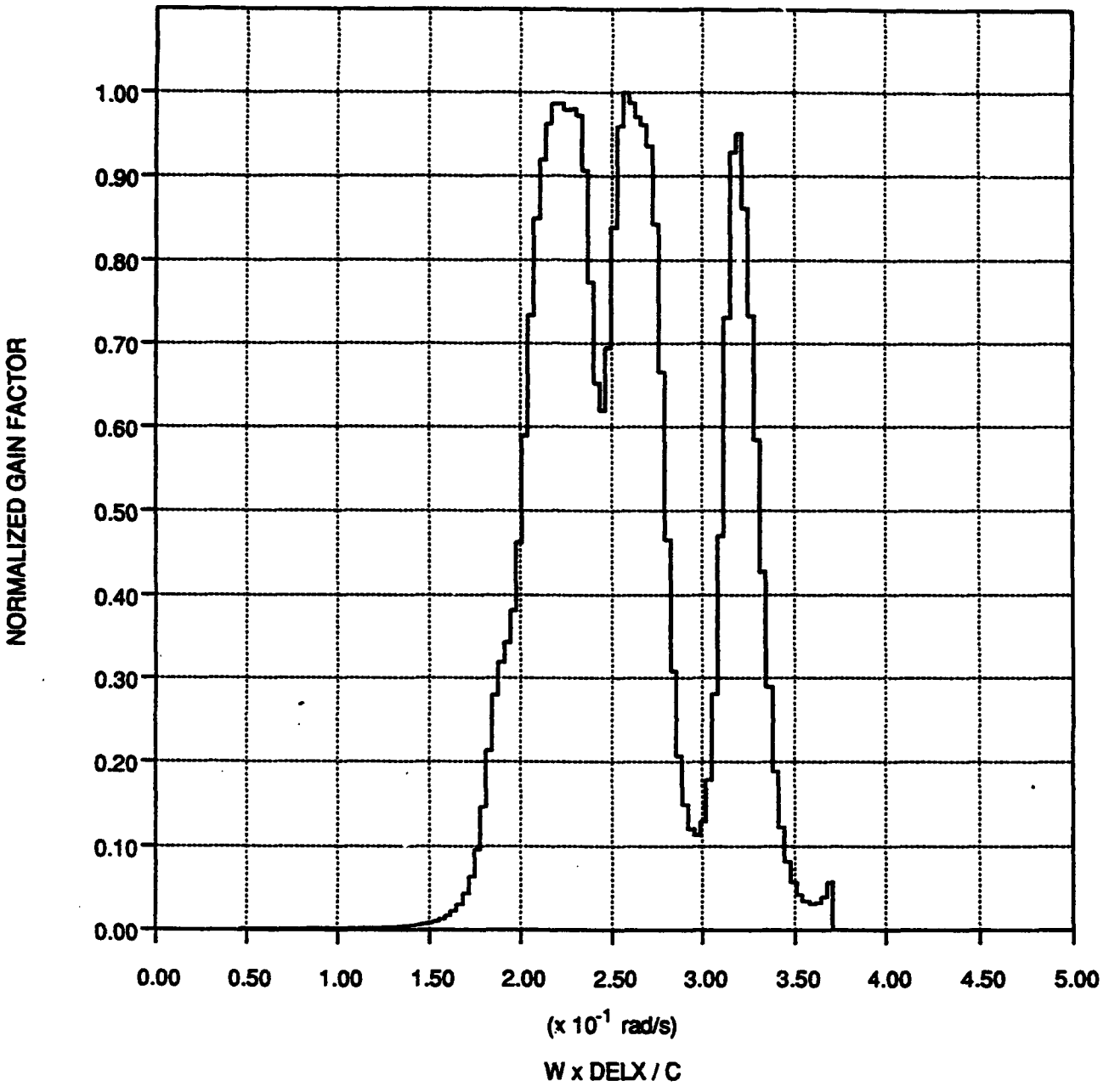

Figure 15. BBU gain curve for 8 Ω/sq insert, but $\Omega\Delta = 0.10$.

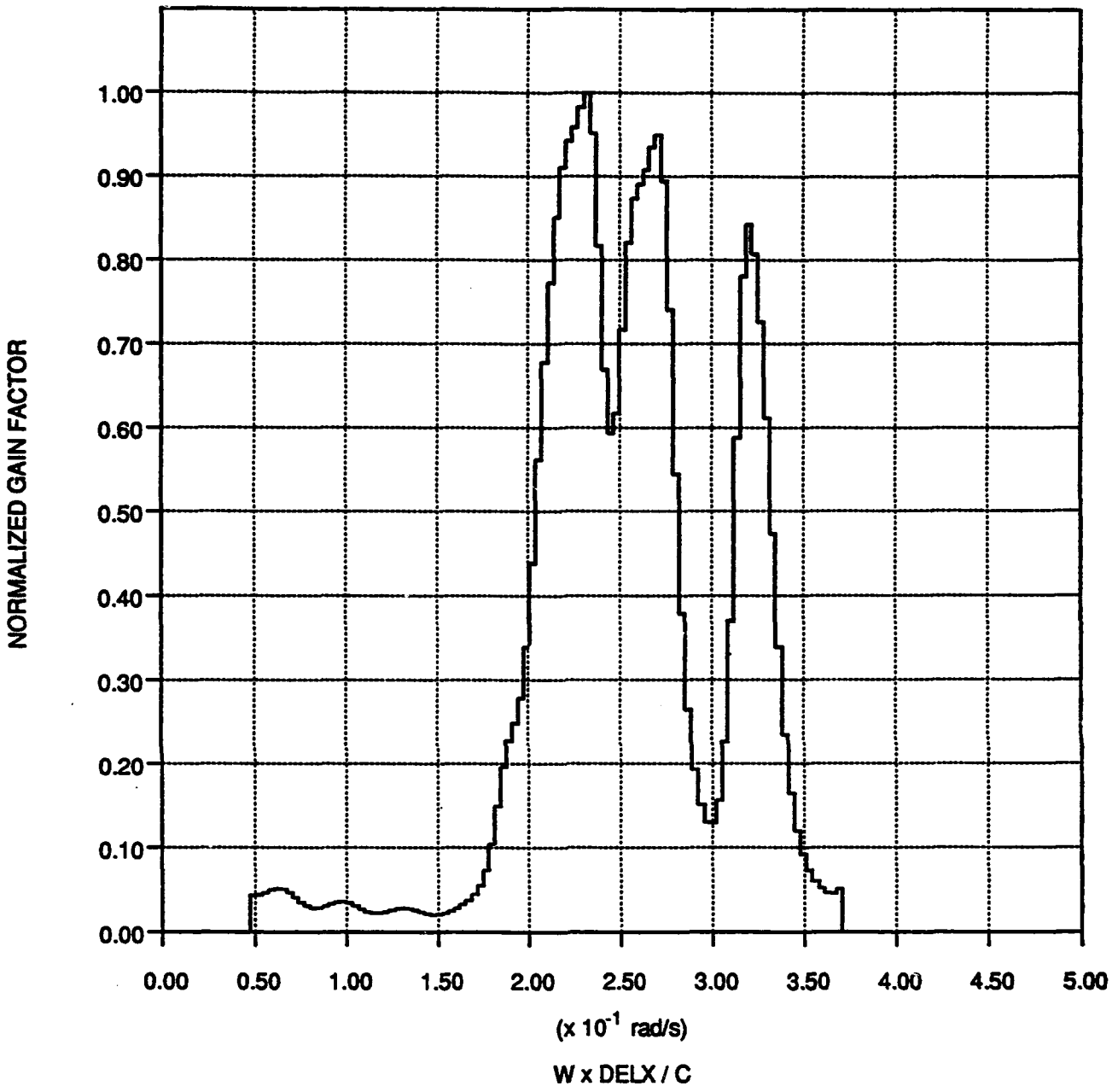

Figure 16. BBU gain curve for 8 Ω/sq insert, but $\Omega\Delta = 1.0$.

the baseline design, a value consistent with the physical dimensions of the cavity and in accord with the discussion above.

As evidenced in the data of Figures 15 and 16, and as noted previously [Ref. 2, included as Appendix F of this report], phase cancellation operation offers a very attractive means for dramatic reduction of the BBU gain in the lower energy end of the accelerator. Indeed, such reduction can have a significant impact on the overall cumulative BBU gain through the entire accelerator.

D. References

1. M. L. Sloan and James R. Thompson, "Beam Breakup in Low Emittance Accelerator Cavities," Proc. SPIE, Intense Microwave and Particle Beams, Vol. 1226, 447 (1990).

2. M. L. Sloan, J. R. Thompson, and C. S. Kueny, "Low Emittance Accelerator Cavity Design to Minimize Amplification of Beam Breakup Modes," Proc. 9th International Converence on High-Power Particle Beams, Vol. I, 305 (1992).

3. R. B. Miller, B. M. Marder, P. D. Coleman, and R. E. Clark, J. Appl. Phys. 63 (4), 997 (1988).

4. R. J. Briggs, et al., IEEE Trans. NS-28, 3360 (1981).

5. D. S. Prono, "Recent Progress of the Advanced Test Accelerator," IEEE Trans. Nuc. Sci., Vol. NS-32, 3144 (1985).

APPENDIX I

BBU SUPPRESSION BY RESONANT GAP-TO-GAP SPACING WITH SUPPLEMENTAL FOCUSING

APPENDIX I

BBU SUPPRESSION BY RESONANT GAP-TO-GAP SPACING WITH SUPPLEMENT FOCUSING

INTRODUCTION

RESONANT GAP-TO-GAP SPACING

From the results of Appendix E, it is seen that the evolution of solenoidally guided $m = 1$ perturbed beam displacement ξ due to propagation through a single accelerating gap of width Δ may be described by the transformation

$$\begin{bmatrix} p \\ q \end{bmatrix} = G \begin{bmatrix} p_o \\ q_o \end{bmatrix} \tag{1}$$

where

$$\begin{aligned} p &= \frac{1}{i\Omega} \frac{d\xi}{dt} e^{-i(\omega_o + \Omega/2)z} , \\ q &= \left(\xi - \frac{1}{i\Omega} \frac{d\xi}{dt} \right) e^{-i(\omega_o + \Omega/2)z} \end{aligned} \tag{2}$$

The matrix G is given by

$$G = \begin{bmatrix} 1 + \frac{\varepsilon}{\Omega}|R|^2 & \frac{\varepsilon}{\Omega} RS^* \\ -\frac{\varepsilon}{\Omega} R^* S & 1 - \frac{\varepsilon}{\Omega}|S|^2 \end{bmatrix} \tag{3}$$

where

$$\varepsilon = \frac{8\pi}{17} \frac{QI}{\gamma \omega_o^2} \tag{4}$$

and where ω_o is the resonant frequency of the accelerating gap, Q is the quality factor, I is the beam current in kiloamps, and γ is the relativistic gamma of the

beam. The quantity $\Omega = (eB)/(\gamma mc)$ is the relativistic gyrofrequency associated with the guide field and R and S are the overlap integrals defined as

$$R = \int_0^{\Delta} dz\, F_r(z)\, e^{-i(\omega_0 + \Omega)z}$$
$$S = \int_0^{\Delta} dz\, F_r(z)\, e^{-i\omega_0 z} \tag{5}$$

where

$$F_r(z) = \left(\frac{\partial A_z}{\partial r} - \frac{dA_r}{dt} \right)_{r=0} \tag{6}$$

is the radial force on the beam arising from the $m = 1$ resonant cavity electromagnetic fields. The quantities R and S reflect, respectively, the coupling of the negative energy BBU destabilizing component of beam displacement $[\exp - i\ (\omega_0 + \Omega)z)]$ and the positive energy BBU stabilizing component $[\exp (-i\ \omega_0 z)$ with the cavity fields.

In these coordinates, transport through a solenoidally focused drift space of length L is given by the matrix

$$S = \begin{bmatrix} e^{i\Omega L/2} & 0 \\ 0 & e^{-i\Omega L/2} \end{bmatrix} . \tag{7}$$

The total transformation for the gap followed by the drift space is then given by the matrix product SG. The resulting matrix has eigenvalues λ given by [c.f., Appendix E, Equation (30)]

$$1 = \frac{\varepsilon}{\Omega} \left[\frac{|R|^2 e^{i\Omega L/2}}{\lambda - e^{i\Omega L/2}} - \frac{|S|^2 e^{-i\Omega L/2}}{\lambda - e^{-i\Omega L/2}} \right] \tag{8}$$

where the eigenvalues λ provide the cavity-to-cavity amplification factor:

$$\begin{bmatrix} p \\ q \end{bmatrix} = \lambda \begin{bmatrix} p_o \\ q_o \end{bmatrix} \quad . \tag{9}$$

Away from the resonant gap-to-gap spacings $\Omega L = 2\pi n$, the unstable eigenvalue is given approximately by $|\lambda| = 1 + g$ where $g \equiv \varepsilon|R|^2/\Omega$ is the raw BBU gain of the accelerating gap structure. However, near the resonances this amplification factor is reduced, and if the resonance condition is exactly satisfied and $|R| \leq |S|$, then $|\lambda| = 1$ (i.e., no amplification).

The unstable eigenvalue is plotted in Figure 1 for three values of $|R|^2/|S|^2$, with $g = 0.1$. The notch of reduced growth is evident for $\Omega L \approx 2\pi$. Elsewhere $|\lambda|$ asymptotes to the expected value $|\lambda| = 1 + g = 1.1$.

The expression (9) is strictly accurate for an infinite periodic system. To see how well this models the actual behavior of a finite number of accelerating gaps and drift tube elements, the transformation given by the matrix SG was applied to randomly chosen initial conditions (p_o, q_o) a large but finite number of times. Figure 2 shows the growth in BBU amplitude $(|p|^2 + |q|^2)^{1/2}$ as a function of the number of cavities traversed, for the case $|R| = |S|$.[1] [In this case the matrix G reduces to

$$G = \begin{bmatrix} 1 + g & g \\ -g & 1 - g \end{bmatrix} \tag{10}$$

where $g \equiv \varepsilon|R|^2/\Omega = \varepsilon|S|^2/\Omega$.]

Results are shown for the cases $\Omega L = 2\pi$, $\Omega L = 2.02\pi$ and $\Omega L = 2.2\pi$, with $g = 0.1$. For $\Omega L = 2.2\pi$ (far from the notch), the growth is initially secular, but transitions to the expected exponential growth (with growth rate $1 + g$) once the unstable eigenmode has had time to establish itself. On the other hand, for $\Omega L = 2\pi$ (exactly in the notch), the growth remains secular. This slow secular BBU growth poses no threat to accelerator operation.

---

[1] It is generally true that $|R| \approx |S|$, except in those cases where phase cancellation effects are important, when generally $|R| < |S|$. These effects are discussed in Appendices E, F and H of this report.

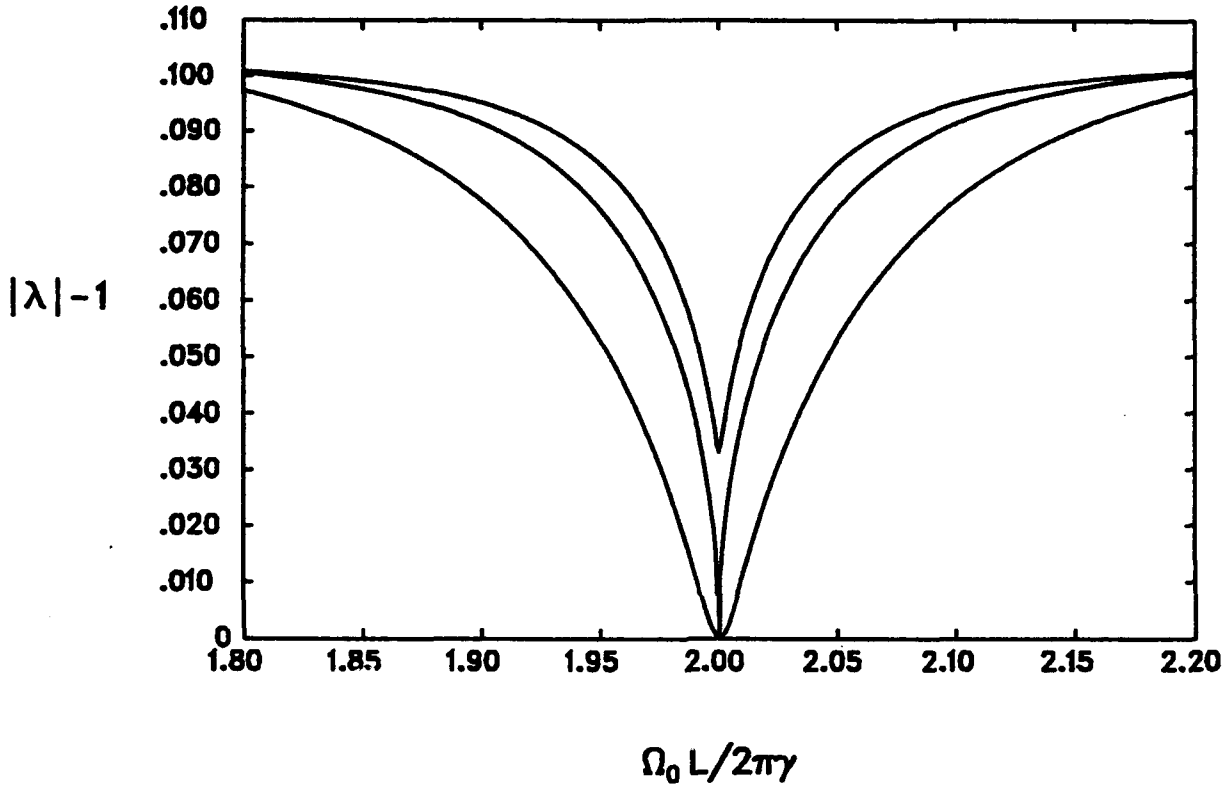

Figure 1. Unstable eigenvalue for raw BBU gain $g = 0.1$, with (a) $|R|^2 / |S| = 0.333$, (b) $|R|^2 / |S| = 1.0$, (c) $|R|^2 / |S| = 3.0$.

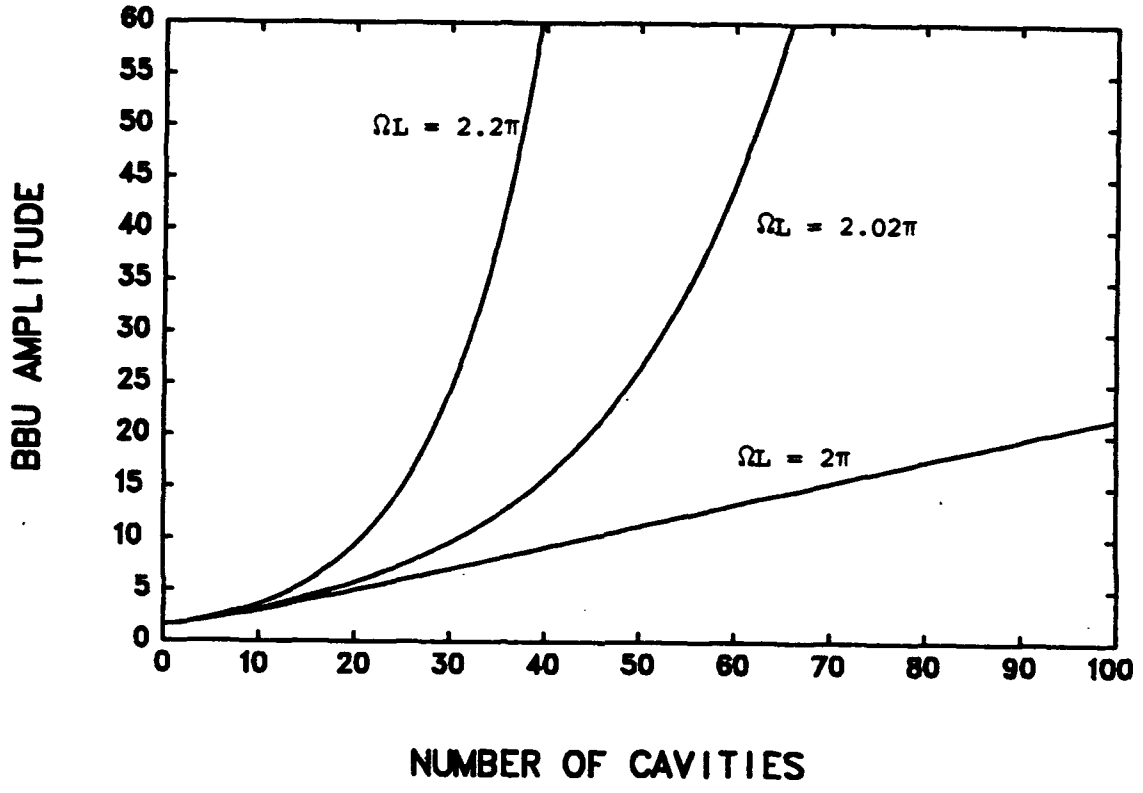

Figure 2. BBU amplitude growth for raw gain $g = 0.1$, with $|R| = |S|$ for three values of ΩL.

The resonant spacing of gaps [i.e., $\Omega L = 0, 2\pi, 4\pi, \ldots$] clearly provides a route to reduced BBU growth; however, significant reduction requires that the resonance condition be very precisely satisfied. It turns out that this resonance may be more easily exploited if a supplemental focusing scheme is employed.

RESONANT SPACING WITH SUPPLEMENTAL FOCUSING

The resonant gap-to-gap spacings just discussed may be made more practical by employing a supplemental strong solenoidal focusing element. If a solenoidal field of strength $\bar{B} >> B$ is applied within a short region of length $d << L$, then the effect on the particle trajectories may be described in the "thin-lens" limit by the transformation

$$\begin{bmatrix} p \\ q \end{bmatrix} = \begin{bmatrix} 1 - \frac{F}{i\Omega} & -\frac{F}{i\Omega} \\ \frac{F}{i\Omega} & 1 + \frac{F}{i\Omega} \end{bmatrix} \begin{bmatrix} p_o \\ q_o \end{bmatrix} \qquad (11)$$

where $F = \bar{\Omega}^2 d/2$, with $\bar{\Omega} \equiv e\bar{B}/\gamma mc \equiv \bar{\Omega}_o/\gamma$. If this focusing is applied halfway through the drift space (at distance L/2), then the total transformation is given by the matrix product

$$\begin{bmatrix} e^{i\Omega L/4} & 0 \\ 0 & e^{-i\Omega L/4} \end{bmatrix} \begin{bmatrix} 1 - \frac{F}{i\Omega} & -\frac{F}{i\Omega} \\ \frac{F}{i\Omega} & 1 + \frac{F}{i\Omega} \end{bmatrix} \begin{bmatrix} e^{i\Omega L/4} & 0 \\ 0 & e^{-i\Omega L/4} \end{bmatrix} \begin{bmatrix} 1+g & g \\ -g & 1-g \end{bmatrix},$$

(12)

where for simplicity we again consider the case $|R| = |S|$. The eigenvalues are given by

$$\lambda^2 - 2\lambda \{ \cos\chi - \hat{F}\chi \sin\chi + ig [\sin\chi - \hat{F}\chi (1 - \cos\chi)] \} + 1 = 0 \quad (13)$$

where $\chi \equiv \Omega L/2$ and $\hat{F} \equiv \bar{\Omega}^2 d/\Omega^2 L$ is the ratio of solenoidal magnetic field energy in the "thin lens" to that in the rest of the drift space of length L.

The unstable eigenvalue is plotted vs. ΩL in Figures 3, 4 and 5, for two nonzero values of $\hat{F}$, as well as for $\hat{F} = 0$ [part of the latter curve was seen in Figure 1(b)]. Two pronounced effects are obvious. First, the $\hat{F}$ focusing itself leads to instability for some values of ΩL. This is illustrated in Figure 6 for the case $g = 0$; unstable propagation occurs for $|\cos\chi - \hat{F}\chi \sin\chi| > 1$ (corresponding to $\chi = (\Omega L)/2 < n\pi$). Such unstable transport regimes are well known to the accelerator community, and operating parameters are easily chosen to avoid them.

A second, much more beneficial effect seen in Figures 4 and 5 is a reduction in BBU gain for certain values of ΩL. In Figure 4, the spikes of $\hat{F}$ transport instability noted in Figure 6 are visible at $\Omega L < 2\pi n$, while between these spikes the growth rate alternates between being enhanced ($\omega L > [2n + 1]\, 2\pi$) and reduced ($\Omega L > 4\pi n$) compared to the raw value $1 + g$. For stronger $\hat{F}$ focusing (Figure 5), the BBU gain in the windows $\Omega L > 4\pi n$ is significantly reduced, although the windows do become somewhat narrower.

Thus supplementary focusing essentially replaces the sharp resonant notches with finite regions, or "windows," of reduced BBU growth at $\Omega L \sim 4\pi n$. These regions provide multiple, easily accessible parameter regimes without the strict spacing requirements encountered for $\hat{F} = 0$ (Figure 3).

Of particular interest is the regime of the lowest window $\Omega L < 2\pi$, which corresponds to the substantial portion of accelerator operation at high γ. Operation in this regime is discussed in the next section.

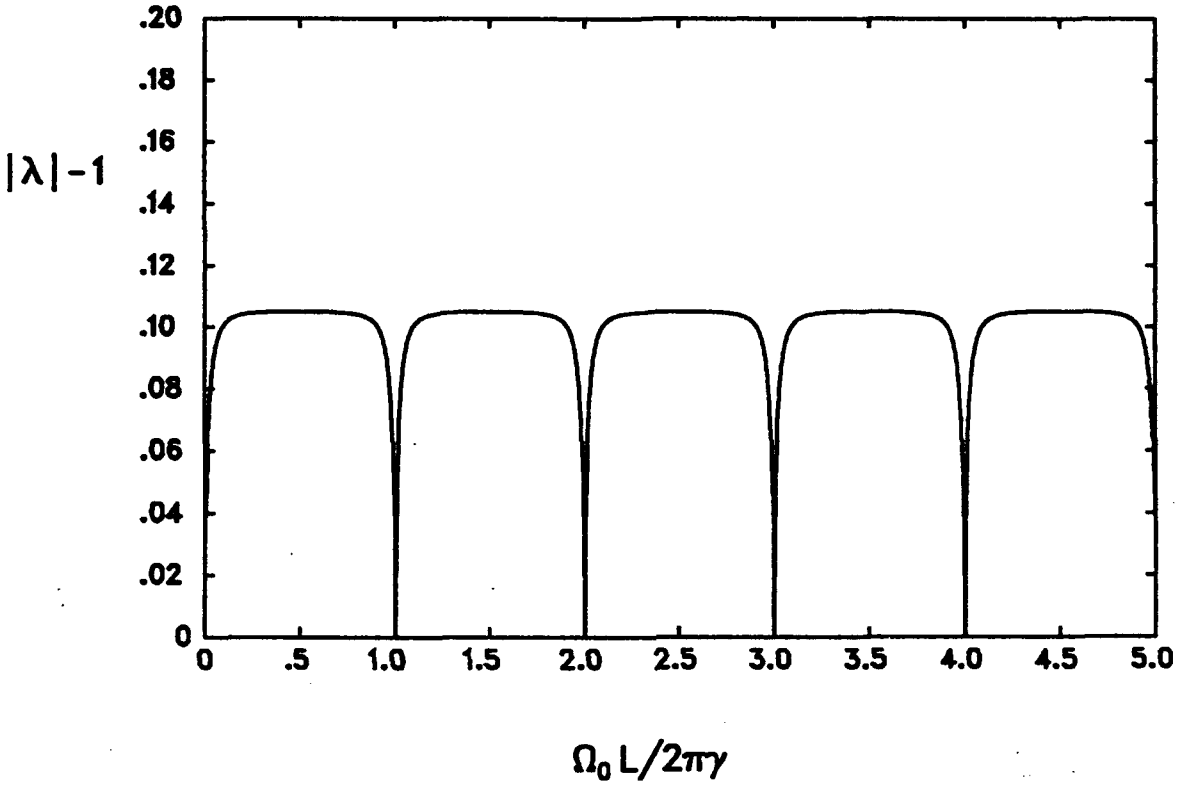

Figure 3. Unsable eigenvalue for raw BBU gain $g = 0.1$, with $|R| = |S|$, without supplemental focusing.

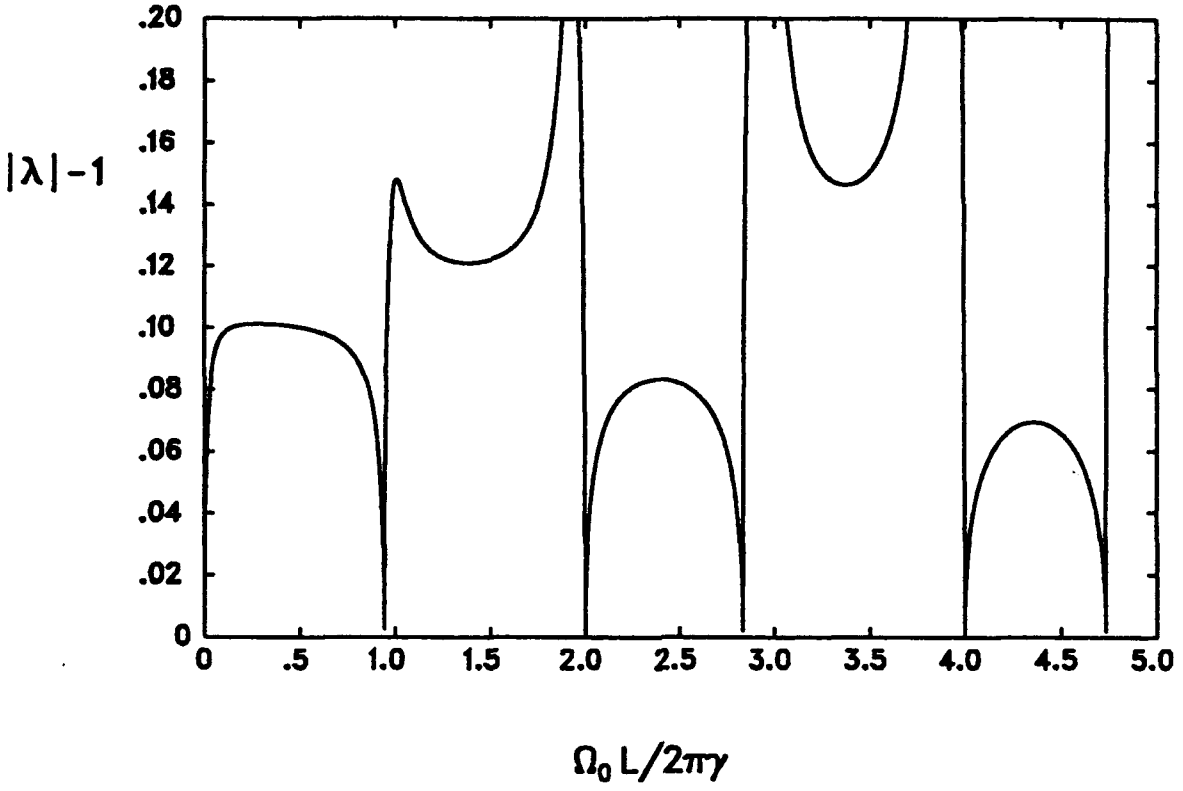

Figure 4. Unstable eigenvalue with raw BBU gain $g = 0.1$, $|R| = |S|$ and supplemental focusing $\hat{F} = 0.03$.

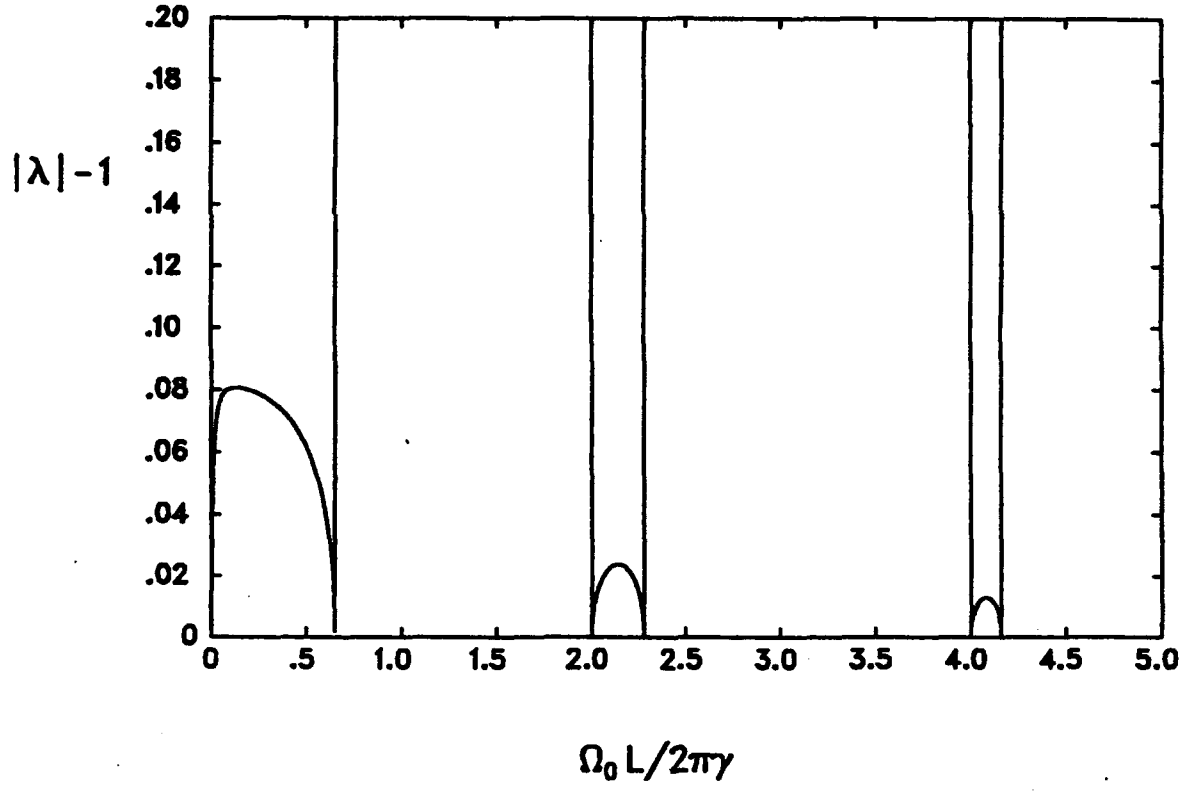

Figure 5. Unstable eigenvalue with raw BBU gain $g = 0.1$, $|R| = |S|$ and supplemental focusing $\hat{F} = 0.3$.

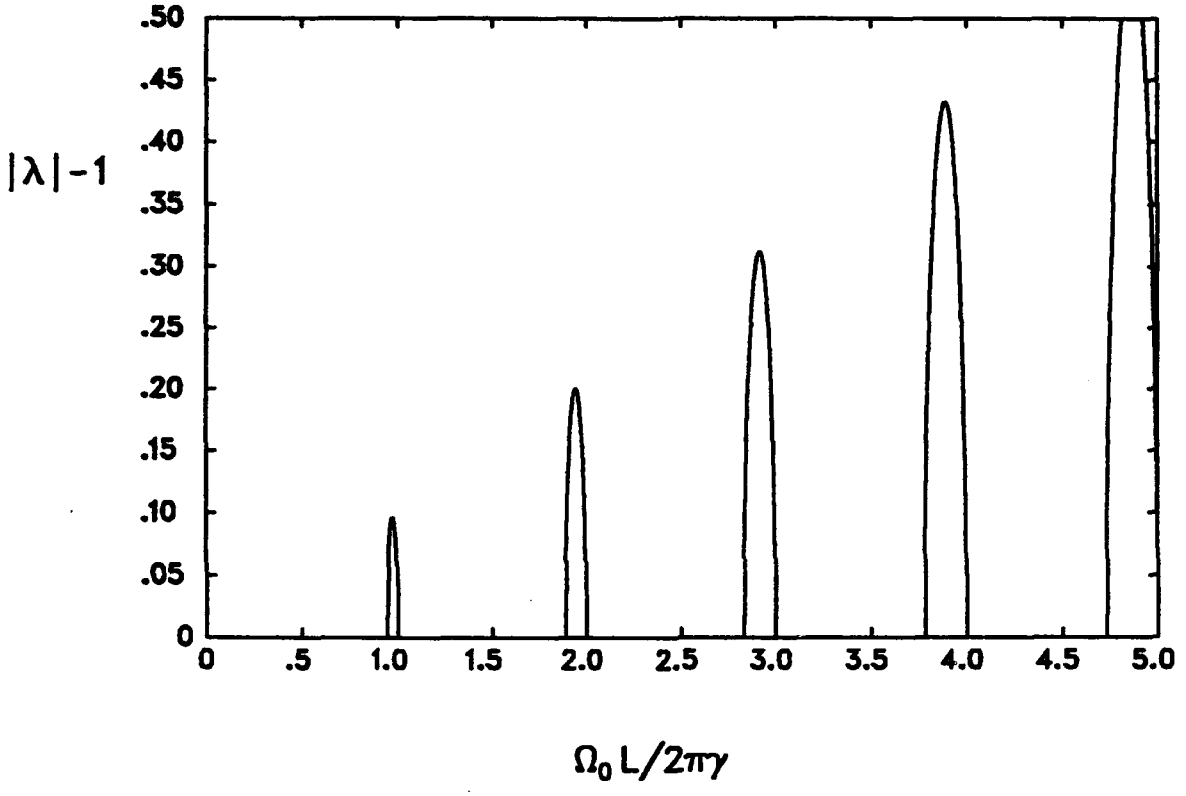

Figure 6. Unstable eigenvalue for supplemental focusing alone, with $\hat{F} = 0.03$; the raw BBU gain g is zero.

REDUCTION OF BBU GAIN FOR HIGH-γ OPERATION

As the beam is accelerated, γ increases and Ω decreases, so that for a substantial portion of the high-γ end of the machine the only window of reduced BBU growth available will be that at $\Omega L \sim 0$. As seen in Figures 4 and 5, the BBU reduction is most effective at higher ΩL, so that relatively stronger supplemental focusing will be used in the small-ΩL regime.

Figure 7 shows the unstable eigenvalue for small ΩL, for $g = 0.1$ and $\hat{F}$ ranging from 0.0 to 2.0. For $g \ll 1 + 2\hat{F} \sim O(1)$, $\Omega L \ll 1$, the eigenvalues are approximately

$$|\lambda| - 1 = \begin{cases} \sqrt{g \frac{\Omega L}{2}}, & 0 \le \Omega L < \frac{4g}{1+2\hat{F}} \\ \frac{g}{\sqrt{1+2\hat{F}}} \left[1 - \frac{1+3\hat{F}}{24} \Omega^2 L^2\right], & \frac{4g}{1+2\hat{F}} < \Omega L < 1 \end{cases} \qquad (14)$$

and the indicated scalings are consistent with Figure 7. Since the raw BBU gain $g \ll 1$, and $\Omega_0 L = \gamma \Omega L > 10^2$ typically, it is generally impractical to operate in the first regime where $|\lambda| - 1 \simeq \sqrt{g\,\Omega L/2}$ until the beam energy approaches the GeV level.

However, the second regime is generally accessible throughout the high energy range of the accelerator. In this regime, it may be seen that the gain per gap is only weakly dependent upon ΩL and is significantly reduced below the raw BBU gain g by the factor $\sqrt{1+2\hat{F}}$. Since $g \propto 1/B$ and $\hat{F} \propto 1/B^2$, where B is the overall solenoidal focusing field, the gain per gap of $g/\sqrt{1+2\hat{F}}$ is also relatively insensitive to the value of B for large enough $\hat{F}$.

The BBU values indicated in Figure 7 are for the particular value of raw growth rate $g = 0.1$. Such a value is not inconsistent with typical large induction accelerator parameters of the ATA class. It is seen that $\hat{F}$ in the range of 1-2 provides over 50% reduction in BBU gain per gap. For a 200- gap accelerator, this alone would reduce cumulative BBU gain by a factor of over 10^4, a very significant improvement.

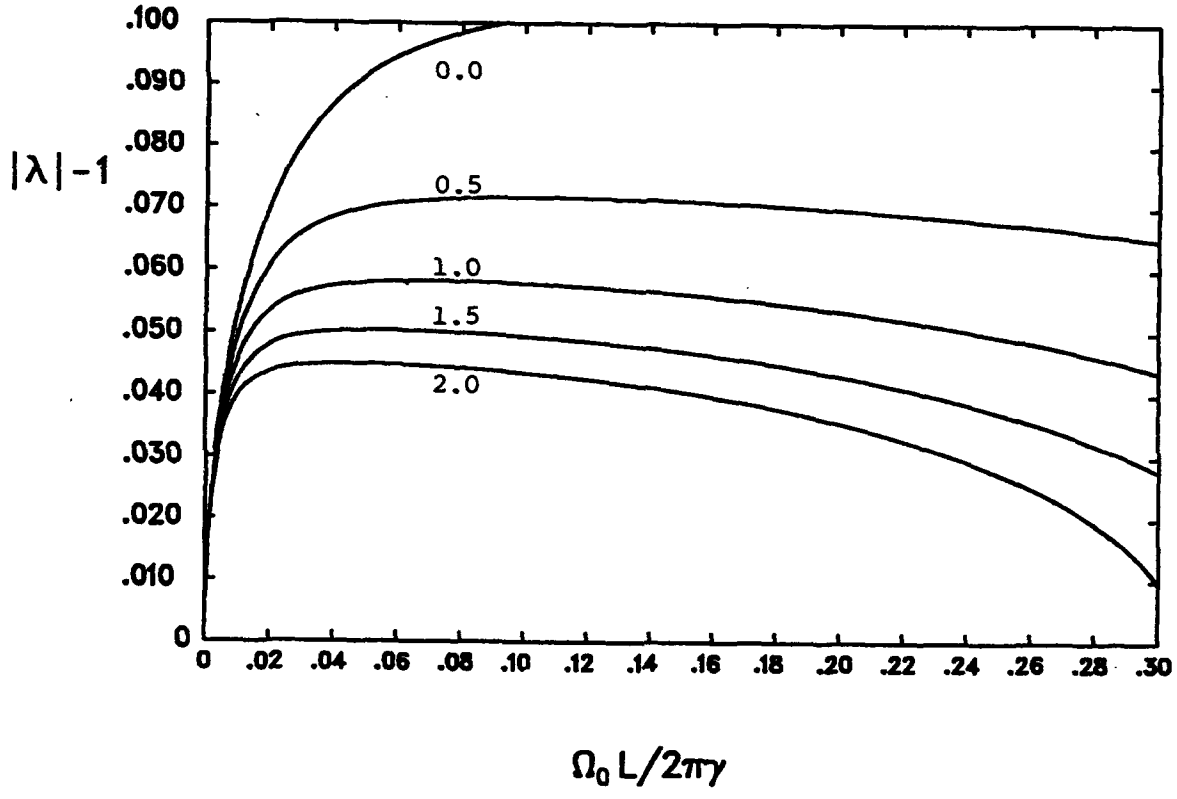

Figure 7. Unstable eigenvalue for raw BBU gain $g = 0.1$, and for supplemental focusing $\hat{F} = 0$, 0.5, 1.0, 1.5 and 2.0.